NASA CONTRACTOR REPORT

NASA CR-498

OPTICAL-INERTIA SPACE SEXTANT FOR AN ADVANCED SPACE NAVIGATION SYSTEM

PHASE B

by W. D. Foley, G. F. Auclair, J. J. Wilczynski, and R. M. Derby

Prepared by
GENERAL ELECTRIC COMPANY
Johnson City, N. Y.
for Ames Research Center

NATIONAL AERONAUTICS AND SPACE ADMINISTRATION • WASHINGTON, D. C. • JUNE 1966

NASA CR-498

OPTICAL-INERTIA SPACE SEXTANT FOR AN ADVANCED SPACE NAVIGATION SYSTEM

PHASE B

By W. D. Foley, G. F. Auclair, J. J. Wilczynski, and R. M. Derby

Prepared under Contract No. NAS 2-1087-III by
GENERAL ELECTRIC COMPANY
Johnson City, N.Y.

for Ames Research Center

NATIONAL AERONAUTICS AND SPACE ADMINISTRATION

For sale by the Clearinghouse for Federal Scientific and Technical Information
Springfield, Virginia 22151 – Price $4.00

FOREWORD

This report summarizes the work performed by the General Electric Co., Light Military Electronics Department, Armament and Control Products Section, Johnson City, New York, to fulfill the requirements of the National Aeronautics and Space Administration Contract NAS2-1087-III, "Optical-Inertial Space Sextant for an Advanced Space Navigation System." This contract was initiated under Control No. 37974001, and administered under the cognizance of Mr. D. Hegarty of the Ames Research Center, Moffett Field, California.

The work was performed by the Advance Engineering Component of the Armament and Control Products Section, under the direction of Mr. W. D. Foley as Project Engineer, in Johnson City, N. Y.

Principal contributors to the project were Messrs. G. F. Auclair, R. M. Derby, J. Dunckle, W. D. Foley and J. Wilczynski.

The results of this study have been published within the Armament and Control Products Section of the Light Military Electronics Department of the General Electric Company under publication number LMEJ 7459.

TABLE OF CONTENTS

SECTION		PAGE
1	INTRODUCTION	1
	GENERAL	1
	BACKGROUND	1
	SPACE SEXTANT TRACKER SYSTEM, PHASE A/B	2
	SUMMARY OF RESULTS	4
	RECOMMENDED FUTURE DEVELOPMENT	5
2	OPTICS	7
	GENERAL	7
	OPTICS SPECIFICATIONS	7
	OPTICAL TRANSFER FUNCTIONS	9
	General Transfer Functions	9
	Narrow Mode Off-Axis Transfer Function	10
	Intermediate Mode Off-Axis Transfer Function	11
	Wide Mode Off-Axis Transfer Functions	13
3	E/S VIDICON AND CAMERA ELECTRONICS	15
	INTRODUCTION	15
	VIDICON IMAGE TUBE	18
	VIDICON CAPSULE AND MOUNTING	19
	VIDEO CHAIN	22
	VIDEO PROCESSING	22
	CENTER PULSE DETECTION	27
	ORTHOGONAL SCAN GENERATORS	29
	RADIAL SCAN GENERATOR	30
	DEFLECTION AMPLIFIERS	34
	SYNCHRONIZATION	34
	FAIL SAFE CIRCUIT	36
	VIDICON BIAS SUPPLY	36
4	DATA PROCESSOR	38
	INTRODUCTION	38
	MODES OF OPERATION	40
	Star Mode	40
	Disc Edge Mode	46
	Omni Mode	47

TABLE OF CONTENTS (Cont'd)

SECTION		PAGE
	Extended Body Mode	49
	Calibrate Mode (Orthogonal and Radial)	49
	DATA DISPLAY	50
	SYSTEM CONTROL	51
	RETICULIZATION	51
	DATA PROCESSOR SPECIFICATIONS	55
5	SYSTEM CONSIDERATIONS	56
	CALCULATION OF TARGET COORDINATES	56
	DUAL MODE RETICLE PATTERN DESIGN	56
	General	56
	Orthogonal Pattern	59
	Circular Pattern	61
	Dual Mode Reticle Pattern	61
	Discrimination of Sub-Patterns by Logical Gating	63
	FRAME RATES	64
	General	64
	Orthogonal Scan Frame Rate	64
6	TESTS	69
	INTRODUCTION	69
	TEST FACILITIES	69
	Optics Laboratory	69
	Extended Body Simulator	74
	Intermediate Mode Optics	75
	Vidicon with Reticle	75
	Photometric Sensitivity - Actual Stars	79
	Slewing Rates	82
	Angular Accuracy Tests	86
	Multiple Star Tests	89
	Interangular Accuracy Tests	96
	Extended Disc Tests - Orthogonal Scan	102
	Extended Disc Tests - Radial Scan	105
APPENDIX A		
APPENDIX B		
REFERENCES		118

LIST OF ILLUSTRATIONS

FIGURE		PAGE
1	Space Sextant Phase B System Diagram	3
2	Electro-Optical Assembly	8
3	Transfer Function Evaluation - Narrow Mode Optics	12
4	Transfer Function Evaluation - Intermediate Mode Optics	12
5	Transfer Function Evaluation Wide Mode Optics	14
6	Vidicon Camera System	16
7	Vidicon Camera System Block Diagram	17
8	Vidicon Capsule	20
9	Assembly Rayxar 15^{0} Lens and Vidicon Capsule	21
10	Main Electronics Assembly	23
11	Video Chain Block Diagram	24
12	Shading Compensation	25
13	Shading Compensation Test Results	26
14	Radial Scan Dark Level Shading	27
15	Radial Scan Compensation	27
16	Pulse Center Detector Operation	28
17	Radial Scan Electronics	31
18	Radial Scan Block Diagram	32
19	Radial Scan Quadrant Selection	33
20	Deflection System Block Diagram	35
21	Power Supply	37
22a	Data Processor Assembly	39
22b	Data Processor Assembly	39
23 Sh. 1	Data Processor Block Diagram	41
23 Sh. 2	Data Processor Block Diagram	42
24	Sequencing Diagram Averaged Data Output	44
25	Sequencing Diagram Instantaneous Readings Output	48
26	Sequencing Diagram Vertical Reticulization	54
27	Direction Cosine Computation Flow Chart	57
28	Single-Mode Reticle Pattern Space Sextant - Phase A Vidicon	58
29	Orthogonal Sub-Pattern Dual-Mode Reticle	60
30	Raster Line Starting Sequence	61
31	Dual-Mode Reticle Pattern Space Sextant - Phase B Vidicon	62
32	Reticle Crossing Analysis	65
33	Electro-Optics Laboratory - General View	71
34	Layout-Star Pattern Simulator	73

LIST OF ILLUSTRATIONS (Cont'd)

FIGURE		PAGE
35	Mask Layout Extended Disc Simulator	76
36	Image Quality Intermediate Mode Optics	77
37	Optical Comparator Presentation of Dual Reticle Pattern	80
38	Dual Reticle Dimension Check	81
39	Photometric Test Results (sheet 1 of 2)	83
39	Photometric Test Results (sheet 2 of 2)	84
40	Peak Signal vs. Visual Magnitude	85
41	Signal Peak and Width vs. Angular Rate	87
42	Linearity Test Point Locations	88
43a	Deviations vs. Position X-Axis Test	90
43b	Deviations vs. Position X-Axis Test	91
44a	Deviations vs. Position Y-Axis Test	92
44b	Deviations vs. Position Y-Axis Test	93
45	Multiple Star Test Positions	95
46	Test Point Locations - Intermediate Mode Optics	98
47	Test Point Locations - Narrow Mode Optics	98
48	Extended Disc Test Locations	103
49	Radial Scan Test Positions	106

LIST OF TABLES

TABLE		PAGE
1	Tracking Modes	4
2	Potential Physical Parameters, Repackaged Tracker System	6
3	Optical Fields of View	7
4	Operational Modes	38
5	Gate Start Coordinates	50
6	Signals to Camera	51
7	Reticle Spacing vs k	63
8	Star Simulator Range	74
9	Disc Simulator Range	74
10	Reticle Measurement Results	79
11	Target Star List	82
12	Resolution Angular Rates	86
13	Multiple Star Test Results	94
14	Intermediate Mode Optics, Interangular Accuracy Test Data	99
15	Narrow Mode Optics, Interangular Accuracy Test Data	100
16	Interangular Accuracy Test Results	101
17	Extended Disc - Ortho Scan Test Results	104
18	Radial Scan Test Results	107

Section 1
INTRODUCTION

GENERAL

The National Aeronautics and Space Administration Contract NAS2-1087-III covering an "Optical - Inertial Space Sextant for an Advanced Space Navigation System Phase B" was placed with the Armament and Control Products Section of the Light Military Electronics Department, General Electric Company, in June 1964.

This is the final report, summarizing the work accomplished in both Phase A and B of the program and covering in detail the Phase B work. The report divides the effort into the following major areas, each of which is reported in detail in a separate section.

- o Optics
- o T. V. Camera
- o Data Processing
- o Systems Considerations
- o Test Results

The operating procedure, system schematics, and circuit functions are included in a separate manual.

BACKGROUND

The work accomplished on Phase A of this program was the logical first step in the development of a unique celestial navigation instrument, the Space Sextant. In this instrument a precision off-axis tracker was to be body-mounted with two free body electrostatic gyroscopes. The gyroscopes formed the reference frame for the tracker while the tracker's off-axis capability eliminated the need for precise target acquisition methods, thus, reducing the requirements on gimbal systems and in some applications eliminating these systems entirely. This concept is discussed in Reference No. 12.

Phase A concentrated on the tracker development and resulted in the development of a sweep correction technique for T.V. image tubes which provides substantial increases in position measurement accuracy. This technique employs reticles in a dynamic feedback loop. (Refer to Phase A Final Report-Reference No. 1)

Delays in the development of the electrostatic gyroscopes, which was not a part of this contract, in turn delayed the overall Space Sextant development. However, the results achieved in Phase A had demonstrated the feasibility

of the tracker which has potential applications independent of the gyroscopes and Phase B was undertaken to expand on these results.

SPACE SEXTANT TRACKER SYSTEM, PHASE A/B

At the end of Phase B of the program, a laboratory model of an off-axis tracker had been designed, fabricated and tested. This tracker system, shown in block diagram form in Figure 1 has the following components and characteristics:

- Optics - two interchangeable sets are provided with the following fields of view[1]:

Narrow	$0.63^{o} \times 0.63^{o}$
Inter	$8.3^{o} \times 8.3^{o}$
Wide	79^{o} to 155^{o}

- Vidicon - 1" electrostatic vidicon with special dual mode reticle pattern.
- Vidicon Camera Electronics - provides orthogonal sweeps for the vidicon and amplification, and processing for the target signals.
- Data Processor - operates on target signals to determine image plane coordinates of single and multiple targets. Its output is to a visual display and/or to the NASA/Ames SDS 920 Computer.
- Radial Scan Electronics - provides an alternative scanning technique for tracking extended body targets in a nulling mode operation.

The tracker is equipped with a wide range of operational modes making it ideally suited as a laboratory tool for tracker concept evaluation.

The system can operate in the tracking modes shown in Table 1.

a. Operating modes are indicated by an "x"

b. $\bar{N}$, $\bar{I}$, and $\bar{W}$ are the narrow, intermediate and wide mode optics respectively

c. Stars (single or multiple) are targets which can be treated as point sources

d. Extended bodies are targets larger than point sources but small enough to be encompassed by the field of view

e. Disc edges are edges of extended bodies larger than the field of view.

(1) Reference Section 2

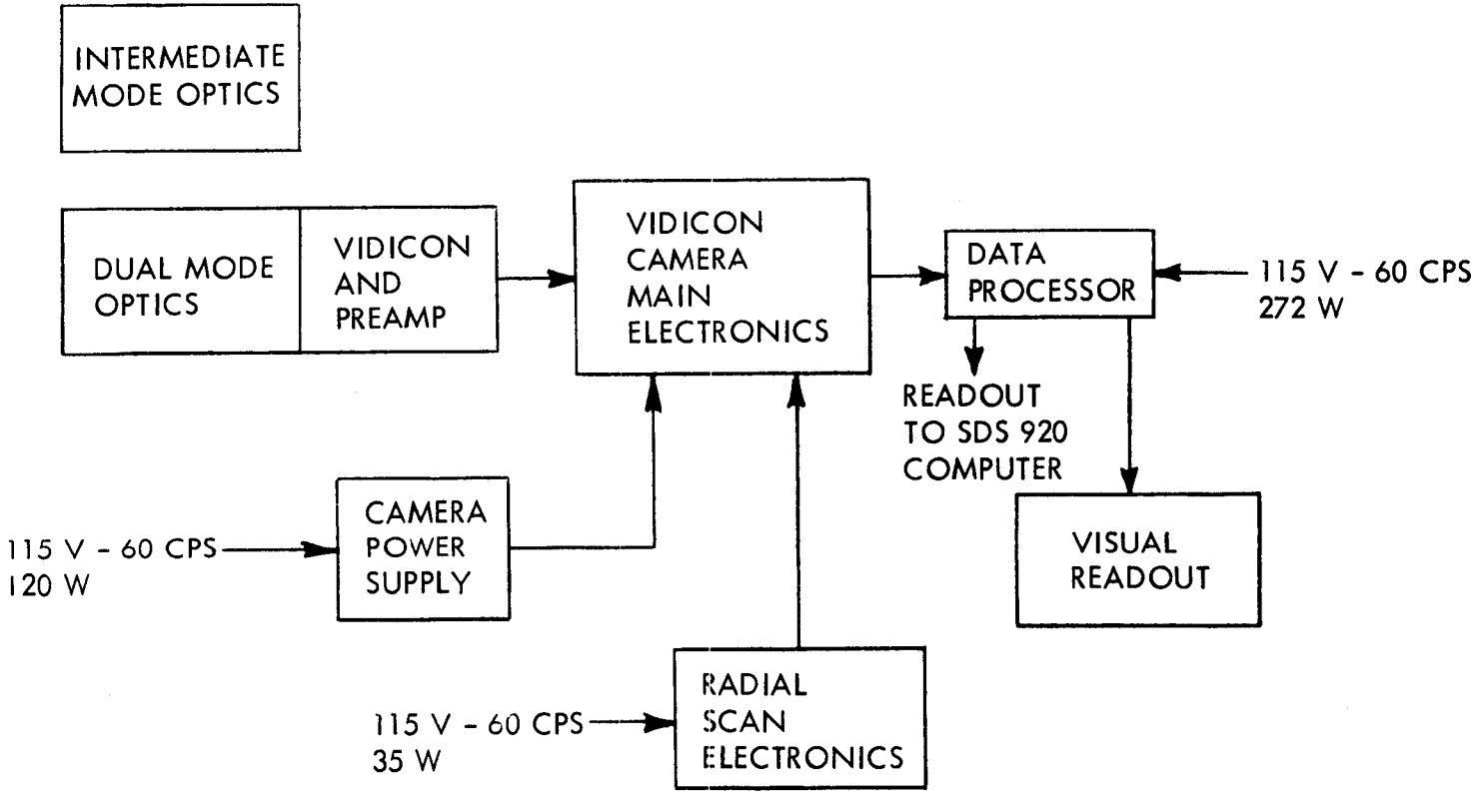

Figure 1. Space Sextant Phase B System Diagram

TABLE 1

TRACKING MODES

SCANNING MODES			TARGETS: SINGLE STAR N	SINGLE STAR I	SINGLE STAR W	MULTIPLE STARS N	MULTIPLE STARS I	MULTIPLE STARS W	EXTENDED BODY N	EXTENDED BODY I	EXTENDED BODY W	DISC EDGE N	DISC EDGE I	DISC EDGE W
	OPTICS →													
	ORTHO	NORMAL	X	X		X	X		X	X		X	X	
		REV	X	X		X	X		X	X		X	X	
	RADIAL	DIV.									X			
		CONV.							X	X				

SUMMARY OF RESULTS

At the end of Phase B the Space Sextant Tracker system had successfully demonstrated its ability to:

- Locate single stars (point source targets) within the field of view with an accuracy of:

  2.64 arc sec rms - Azimuth
  4.84 arc sec rms - Elevation
  } Narrow Mode Optics

  0.59 arc min rms - Azimuth
  1.09 arc min rms - Elevation
  } Intermediate Mode Optics

- Determine the interangular separation between multiple stars with an accuracy of:

  13.2 arc sec rms - Narrow Mode Optics
  2.1 arc min rms - Intermediate Mode Optics

- Detect actual stars with the Narrow and Intermediate Mode Optics down to 2.2 Visual Magnitude with a minimum peak signal to rms noise ratio of 10/1.

- Detect extended bodies in both orthogonal and radial scan modes
- Detect disc edges in orthogonal scan
- Operate with slewing rates up to

  0.15°/min - Narrow Mode Optics
  2.1 °/min - Intermediate Mode Optics
  13.1 °/min - Wide Mode Optics

These results represent a significant improvement in both performance and versatility over the results achieved in Phase A.

One unresolved problem remains in the use of the radial scan. The results achieved point up the undesirability of incorporating multiple scanning modes into a single vidicon. There is a noticeable change in the dark level when the radial scan passes into or out of the target area previously scanned by the orthogonal scan. This step made circular reticle detection difficult and the radial scan system was operated without reticle corrections. Otherwise, performance of the radial scan was good and in a future application where only radial scan would be employed, the system should perform satisfactorily with reticle corrections.

RECOMMENDED FUTURE DEVELOPMENT

The results of this program have pointed out certain areas which would be profitable to pursue to further enhance the application potential of the tracker:

- Improved Reticle Techniques. The reticles now employed cause a reduction in target signal in their immediate areas. This is not objectionable for bright targets (+1.0 visual magnitude and brighter) but for dimmer targets the effect is objectionable. Two approaches are feasible. The first would eliminate all reticles from the active field of view. A single starting reticle and a set of diagonal reticles placed outside the field of view would initialize each line correctly and allow line position determination to be made. Along the length of the line the tracker accuracy would depend upon sweep linearity. Further tests with the system are necessary to establish the accuracy levels attainable with this approach. The second method would incorporate striations all across the target material to produce a low level ripple in the dark level. This ripple could be counted to determine x position. Since the ripple reticle quantization can now approach the vidicons resolution limit no reliance on sweep linearity is necessary. The General Electric Company is now pursuing a small

independent development effort to test the feasibility of this approach.[1] A starting reticle and diagonal set would still be employed outside the field of view to initialize the lines and determine the line positions.

- Reduce Effects of Vidicons Non-Linearities. The vidicon has a characteristic geometric distortion which produces a pin cushioning in the raster. The diagonal reticle method of line position determination does not entirely correct for this since corrections are made only along one edge. Either a new method of vertical reticulization should be investigated or provisions made for easily introducing compensating non-linearities into the sweeps to produce a near-linear system.

- Reduce Size Weight and Power Requirements. In its present form the tracker is a laboratory model. No efforts were made to reduce size, weight and power. By applying present state-of-the-art packaging techniques, including micro-circuits in the camera and data processor, drastic improvements can be made. It is conservatively estimated that a complete system can be built up with the characteristics shown in Table 2.

TABLE 2

POTENTIAL PHYSICAL PARAMETERS
REPACKAGED TRACKER SYSTEM

	Size	Weight	Power
Tracker Head	4" dia x 10" long	4 lbs.	-
Camera Electronics	5" x 7" x 6"	9 lbs.	15 watts
Data Processor	7" x 6" x 3"	5 lbs.	5 watts
Totals	$<1/3$ ft^3	18 lbs.	20 watts

- Tailor the System to a Specific Mission. As it now exists, the tracker has considerable versatility. This is both a blessing and a curse, since while it allows a good deal of flexibility it also causes a good deal of unnecessary complexity. The requirements for dual scans and dual directions of scans required many parallel adjustments and switching, etc. With the present system tailored to a specific application, a considerable simplification of circuits and switching will result.

(1) Reference No. 13

Section 2
OPTICS

GENERAL

The Space Sextant tracker head is equipped with two, manually interchangeable, optical assemblies. When used with the reticulized vidicon, these assemblies provide the following fields of view:

TABLE 3

OPTICAL FIELDS OF VIEW

Assem. No.	Optical Mode	Field of View	
		Ortho Scan	Radial Scan
I	1. Narrow Field	0.63^{o}x0.63^{o}	1.00^{o}(1)
	2. Wide Field	—	79^{o}-155^{o}(2)
II	3. Intermediate Field	8.3^{o}x8.3^{o}	13.6^{o}(1)

(1) Total included angle
(2) Total included angle between two concentric cones. Presentation is radially inverted.

Selection between the narrow and wide modes of operation is by means of a manually operated shutter mechanism contained in assembly I.

When in use, the optical assemblies are bolted to the face of the vidicon capsule.

Figure 2 illustrates the two optical assemblies, the vidicon capsule and the spacer ring and mounting adapter used with assembly I and II, respectively. Also shown in this figure are the aperture plates for use with the intermediate optics. These will be discussed later under Optics Specifications.

OPTICS SPECIFICATIONS

Assembly I, the narrow and wide mode optics, was fully described in the Phase A report.[1]

(1) Reference No. 1, Section 2, pp. 9 thru 16 and Section 6, pp. 109, and pp. 112 thru 116.

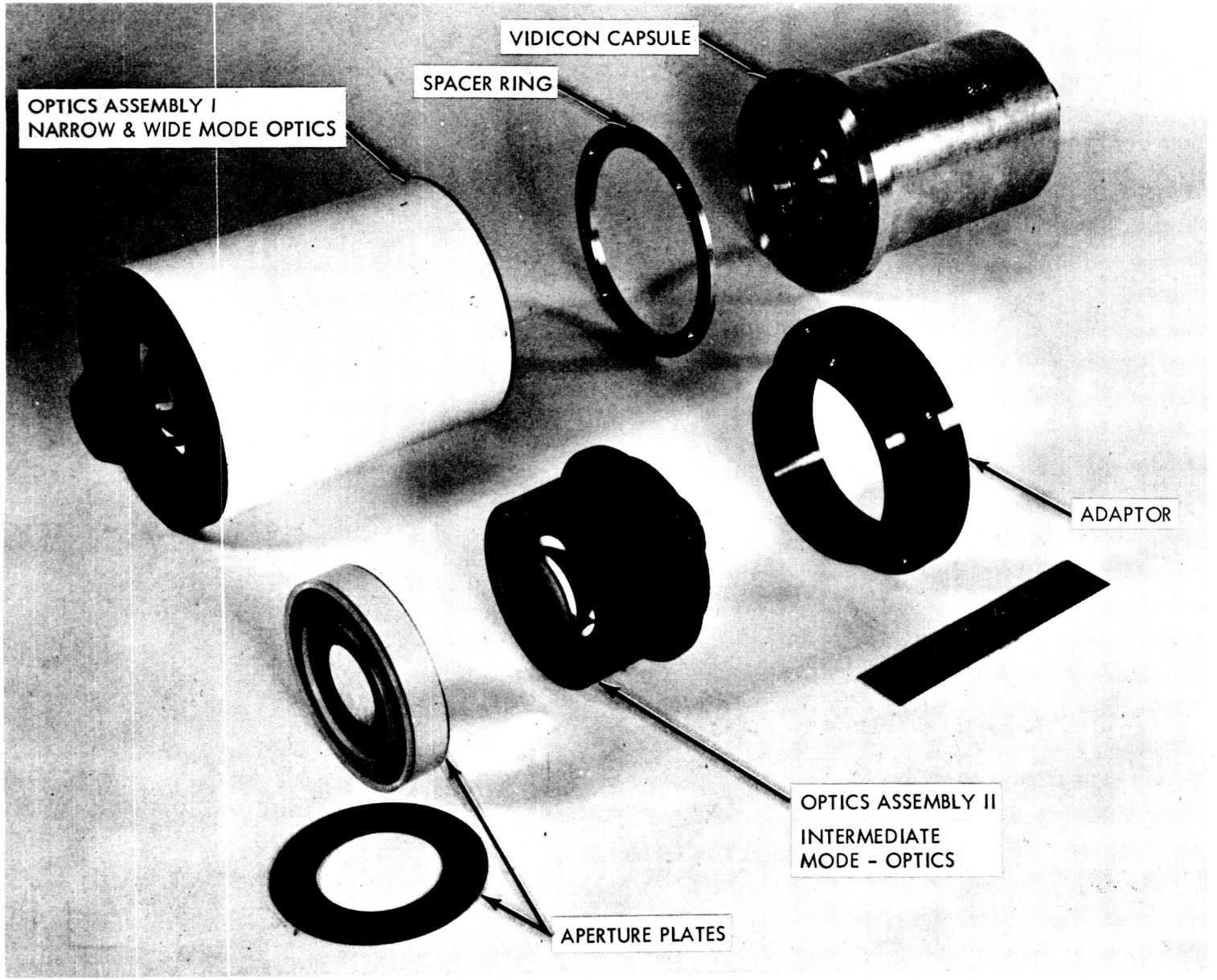

Figure 2. Electro-Optical Assembly

Assembly II, the intermediate mode optics is a high quality commercial lens produced by the Aerojet Delft Corporation for use with T.V. Camera tubes. This lens, a model Rayxar E 65/0.75, has the following specifications:

Equivalent focal length	65 mm (2.56")
Relative aperture	f/0.75
Image plane diameter	22 mm (0.87")
Light transmittance (visual light)	81%
T Stop for visual light	0.79
Field of view (half angle)	10.5^{o}
Back focal distance (visual light)	1.4 mm (.055")
Resolution (on-axis)	90 lines/mm (2286 lines/inch)

Five interchangeable diaphragm stop plates have been provided for use with the intermediate mode optics. The table below lists the resulting lens speeds:

Stop Plate	Aperture	Speed
None	3.41"	f/0.75
1	2.41"	f/1.0
2	1.71"	f/1.4
3	0.625"	f/4.1
4	0.213"	f/12.0
5	0.106"	f/24.2

Normally, the lens is used without a stop plate for star tracking. Plate 3 is designed for tracking Mars or Jupiter. Plate 4 is suitable for tracking the moon, while Plate 5 is designed for tracking Venus.

The dynamic range of the vidicon is sufficiently broad so that a precise match of aperture size to target brightness is not required.

OPTICAL TRANSFER FUNCTIONS

GENERAL TRANSFER FUNCTIONS

The optic assemblies can be considered as transducers which convert the direction of the target line of sight, with respect to the tracker frame, to a position in the image plane.

If x and y, are the image plane coordinate of the target, measured from the boresight position, the direction cosines for the target line of sight can be expressed as[1]:

$$A_x = \sin\gamma \ \frac{(-x_1)}{\sqrt{x_1^2 + y_1^2}}$$

$$A_y = \sin\gamma \ \frac{(-y_1)}{\sqrt{x_1^2 + y_1^2}}$$

$$A_z = \cos\gamma$$

Where γ is the off-boresight angle of the target line of sight. The negative signs account for the image inversion of the optics.

These general relationships are correct for all of the optical modes. $\gamma = \gamma$ (x, y), the off-axis transfer function of the optics will, of course, vary with each mode used.

In the discussion of these functions the following symbols are used:

γ_n = off-axis angle, narrow mode, in arc-sec.

γ_i = off-axis angle, intermediate mode, in arc-min.

γ_w = off-axis angle, wide mode, in degrees.

r_1 = off-center distance of image in milli-inches.

r_2 = off-center distance of image in data processor decimal counts.

NARROW MODE OFF-AXIS TRANSFER FUNCTION

The application of a first order least squares fit to laboratory data obtained for the optics alone resulted in:

$$\gamma_n = 6.0138 \ r_1 \text{ arc-sec}$$

(1) Reference: Appendix B for development

where, γ_n is the off-axis angle

and r_1 is the off-center distance of the image measured in milli-inches.

Since there are 128 decimal counts of the data processor readout for each 47 milli-inches [1], this relationship can be restated as

$$\gamma_n = 2.2082\ r_2 \text{ arc sec}$$

$$\text{or, } \gamma_n = 1.0706 \times 10^{-5}\ r_2 \text{ radians}$$

where, r_2 is the off-center distance of the image measured in counts.

The deviation of the test data from these linear relationships is shown in Figure 3. Since the quantization of the data processor is ±1 count which is equivalent to ±2.2 arc sec, the linear relationship is adequate.

INTERMEDIATE MODE OFF-AXIS TRANSFER FUNCTION

The intermediate mode optics are sufficiently non-linear that a second order transfer function is required. [2] Application of a second order least squares fit to the test data obtained from the optics alone resulted in:

$$\gamma_i = 1.3457\ r_1 - 7.63 \times 10^{-5}\ r_1^2 \text{ arc min}$$

where, γ_i is the off-axis angle

and r_1 is the off-center distance of the image measured in milli-inches.

In terms of data processor decimal counts, this becomes

$$\gamma_i = 0.4941\ r_2 - 1.0287 \times 10^{-5}\ r_2^2 \text{ arc min}$$

$$\text{or } \gamma_i = 1.4373 \times 10^{-4} r_2 - 2.9924 \times 10^{-9}\ r_2^2 \text{ radians}$$

where, r_2 is the off-center distance of the image measured in decimal counts.

(1) Reference Figure 31

(2) The best linear fit ($\gamma_i = 0.4898\ r_2$) results in errors of 2 to 3 arc minutes at the edges of the field.

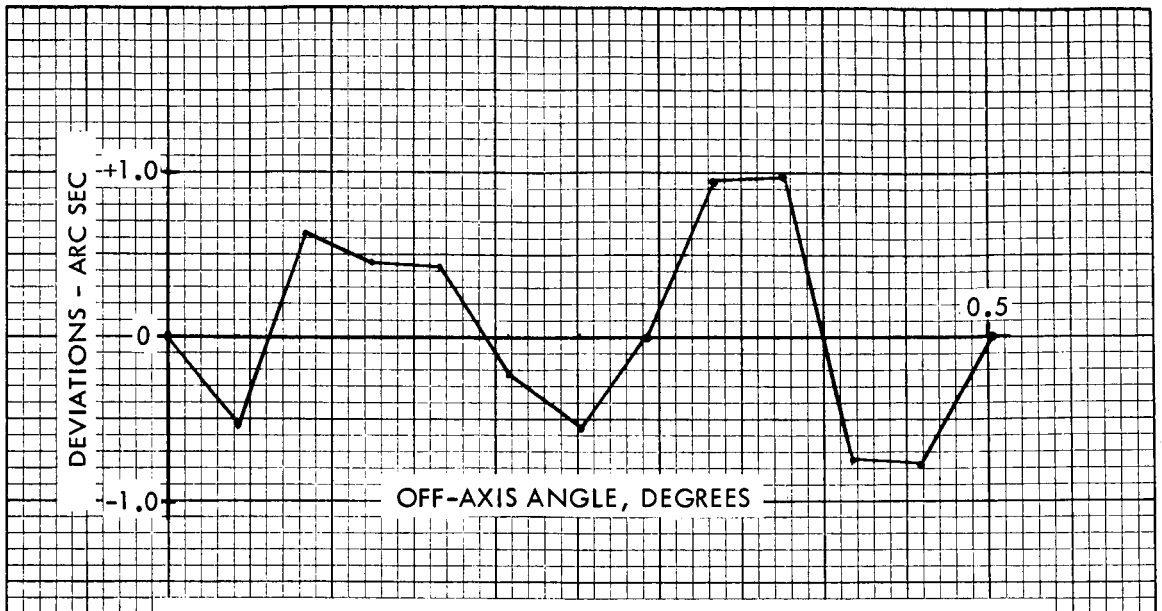

Figure 3. Transfer Function Evaluation Narrow Mode Optics

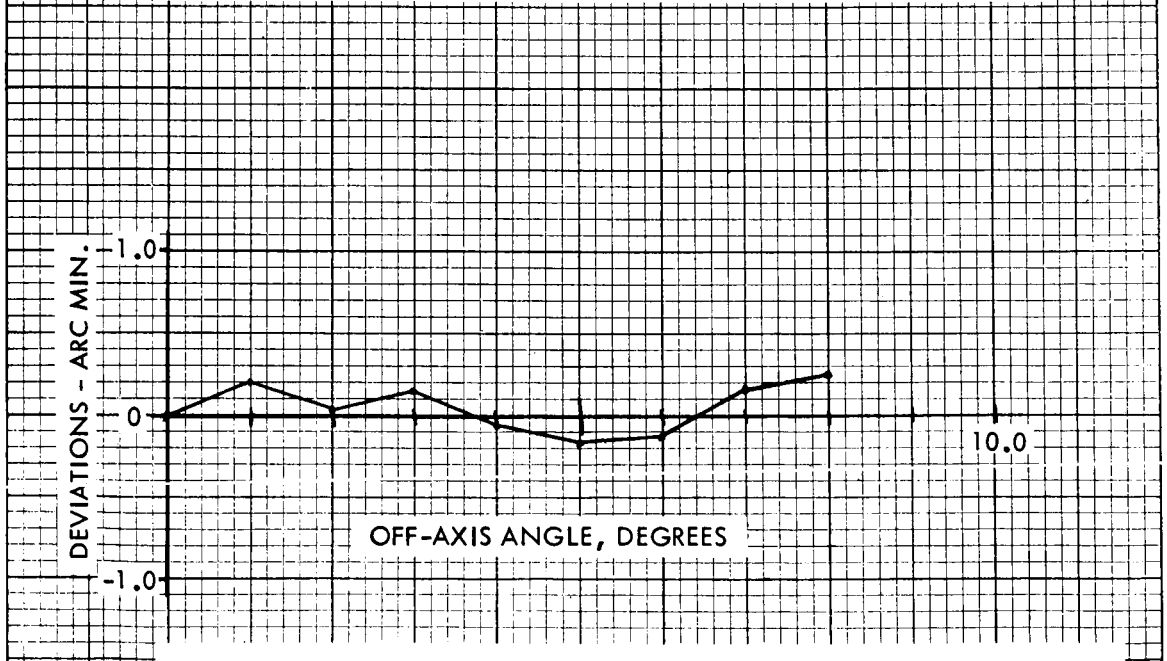

Figure 4. Transfer Function Evaluation Intermediate Mode Optics

The deviation of the test data from this relationship is shown in Figure 4. The quantization error of the data processor being ±1 count, or ±0.49 arc-min, the fit is adequate.

WIDE MODE OFF-AXIS TRANSFER FUNCTIONS

The application of a second order least squares fit to the laboratory test data obtained for the optics alone resulted in:

$$\gamma_\omega = 90.378 - 138.25 \times 10^{-3}\, r_1 - 81.836 \times 10^{-6}\, r_1^{\,2} \text{ degrees}$$

where, γ_ω is the off-axis angle

and r_1 is the off-center distance of the image measured in milli-inches.

In terms of the data processor decimal counts, this becomes:

$$\gamma_\omega = 90.378 - 50.764 \times 10^{-3}\, r_2 - 11.034 \times 10^{-6}\, r_2^{\,2} \text{ degrees}$$

$$\text{or } \gamma_\omega = 1.5774 - 2.4129 \times 10^{-3}\, r_2 - 1.4283 \times 10^{-6}\, r_2^{\,2} \text{ radians}$$

where, r_2 is the off-center distance of the image measured in decimal counts.

The deviation of the test data from this relationship is shown in Figure 5. In this mode the data processor's quantization is ±1 count = ±3.0 arc minutes. Therefore, the second order approximation, while marginal, appears to be adequate.

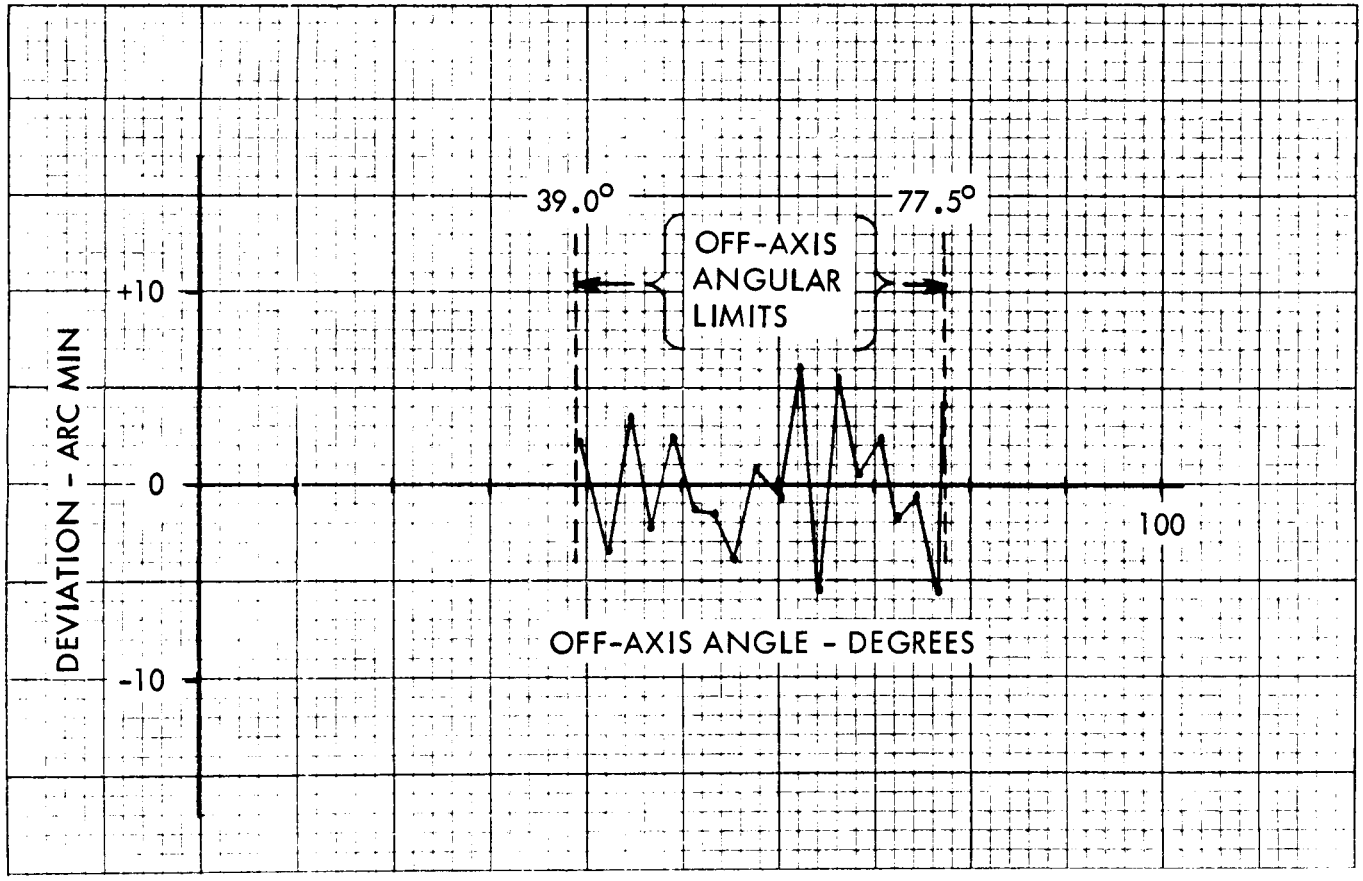

Figure 5. Transfer Function Evaluation Wide Mode Optics

Section 3
E/S VIDICON AND CAMERA ELECTRONICS

INTRODUCTION

The target detection system of the Space Sextant Tracker consists of a precision vidicon television system. This system converts the target images, presented by the optics, to precise electrical signals from which the Data Processor determines target location.

Functionally, the system consists of (1) the vidicon tube and its bias circuitry, (2) the video chain which amplifies the signals for processing, (3) the video processing and pulse center detection circuits which provide precise output signals and (4) the deflection circuits which sweep the electron beam across the vidicon target.

The complete camera system is illustrated in Figure 6 and the functional elements are shown in block diagram form in Figure 7.

The major changes to the camera electronics from those which existed at the end of Phase A of the program were directed to increase scanning versatility. In order to simplify the edge crossing detection circuits employed in disc edge and extended body tracking, it was decided to limit the problem to one of dark-to-light crossings. To avoid the need for reorienting the tracker head itself, provisions were made to reverse the scanning directions to suit the target orientation.

In addition, the radial scan system which was breadboarded in Phase A has been incorporated as an operating component of the system. Provisions were also made to reverse this scan.

The camera now has the following scanning modes:

Normal Orthogonal - Left to Right
Bottom to Top

Reverse Orthogonal - Right to Left
Top to Bottom

Diverging Radial - Center to Outside

Converging Radial - Outside to Center

The nominal frame rates for the two scanning systems, discussed in detail in the Analysis Section of this report are:

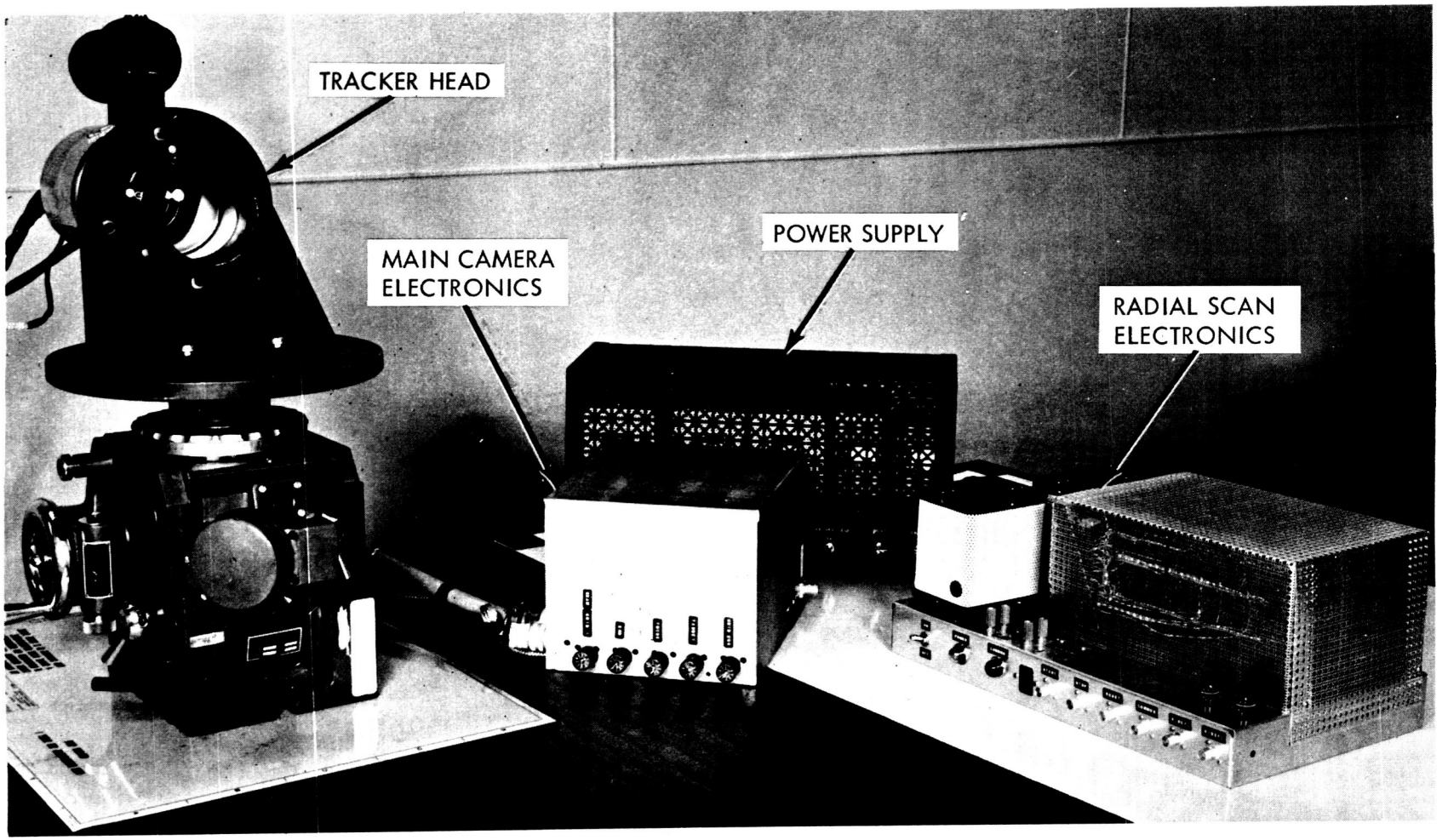

Figure 6. Vidicon Camera System

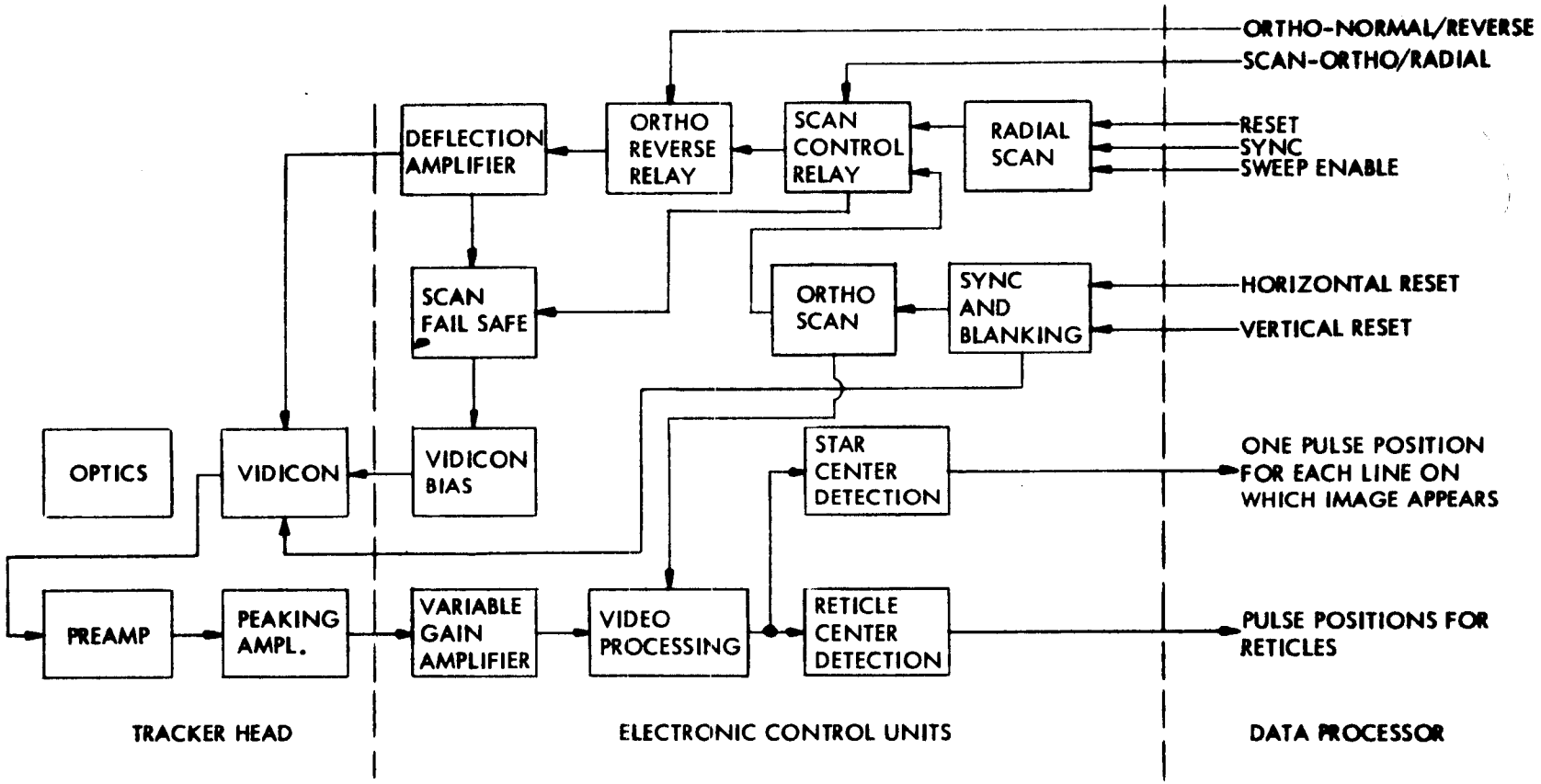

Figure 7. Vidicon Camera System Block Diagram

Orthogonal - 4.0 frames/second

Radial - 17.0 frames/second

Other operational improvements made to the camera are:

- o Increased bias voltages on the vidicon to improve the dark level shading.
- o Incorporation of compensation circuits to reduce the residual shading.
- o New pulse-center detection circuits.
- o Revised deflection circuits to accommodate the higher vidicon bias levels.
- o Improved vidicon capsule and mounting.

The various functional components of the system are discussed in the following sections.

VIDICON IMAGE TUBE

The primary sensor of the Space Sextant tracker is a fully electrostatic 1" vidicon image tube with an integral reticle pattern in the target.

The vidicon, a type 1347-014, serial number 4341364, was manufactured by the General Electrodynamics Corporation of Garland, Texas, to a specification prepared by the General Electric Company.

In physical dimensions and operating parameters, this tube is similar to the model GEC 7522 vidicon which is described in Appendix A.

This vidicon differs from the vidicons used in Phase A of this program only in the configuration of the reticle pattern employed.

The Phase A camera operated primarily with a one direction orthogonal scan while the Phase B camera employs dual direction scans in both orthogonal and radial modes of operation. It was, therefore, necessary to redesign the reticle pattern to accommodate this increased versatility.

The reticle is a pattern deposited between the target and the photo conductive material of the vidicon. In operation, it produces negative going pulses in the dark level of the vidicon and acts as a fixed mechanical reference for the scanning electron beam. The reticle requires no back lighting and its negative signals are readily distinguished from the positive signals produced by targets.

The design of the reticle pattern is discussed further in the Analysis Section of this report.

VIDICON CAPSULE AND MOUNTING

An aluminum capsule which supports and protects the vidicon has been provided and is shown in Figure 8. The assembly is shown in Figure 9.

The capsule consists of two concentric aluminum tubes. The outer tube, which is flanged, is the fixed member of the assembly and in use, bolts to the rear of the optics being used. Figure 9 shows it mounted with the Intermediate Mode Optics. The inner tube forms a housing for the vidicon and its preamplifier. This housing is axially adjustable for mechanical focus.

Electrical connections to the capsule are through two connectors. The Amphenol connector carries the vidicon bias voltages while the Cannon connector carries the video output and the preamplifier power.

The capsule was designed for laboratory use and no attempt was made to minimize physical size. The preamplifier occupies only a small portion of the available volume.

On a future model, it would be feasible to either reduce the capsule size significantly or to repackage the entire vidicon camera chain using microcircuits to fit within the present capsule size.

The vidicon itself is "potted" into a flanged aluminum tube. The potting compound employed was Sylgard 184 which provides a firm support and yet has sufficient resilience to cushion the vidicon from shock.

Connection to the target is by means of a wire welded to the target ring and brought out through a hole in the protective tube.

Connection to the vidicon's pins is through a short cable which prevents the application of transverse forces.

To replace the vidicon, it is necessary to replace the entire potted assembly. The accurately machined O.D. of the flange provides the necessary radial alignment.

This method of mounting the vidicons is an improvement over the Phase A assembly in that it provides accurate centering while providing maximum protection to the vidicon.

The two vidicons used in Phase A have been similarly potted and are available as interchangeable spare parts for the present system. The use of these vidicons will require modifications in the direction and rate of the sweeps and in the processing of the vertical (Y-axis) data due to the differences in the reticle pattern.

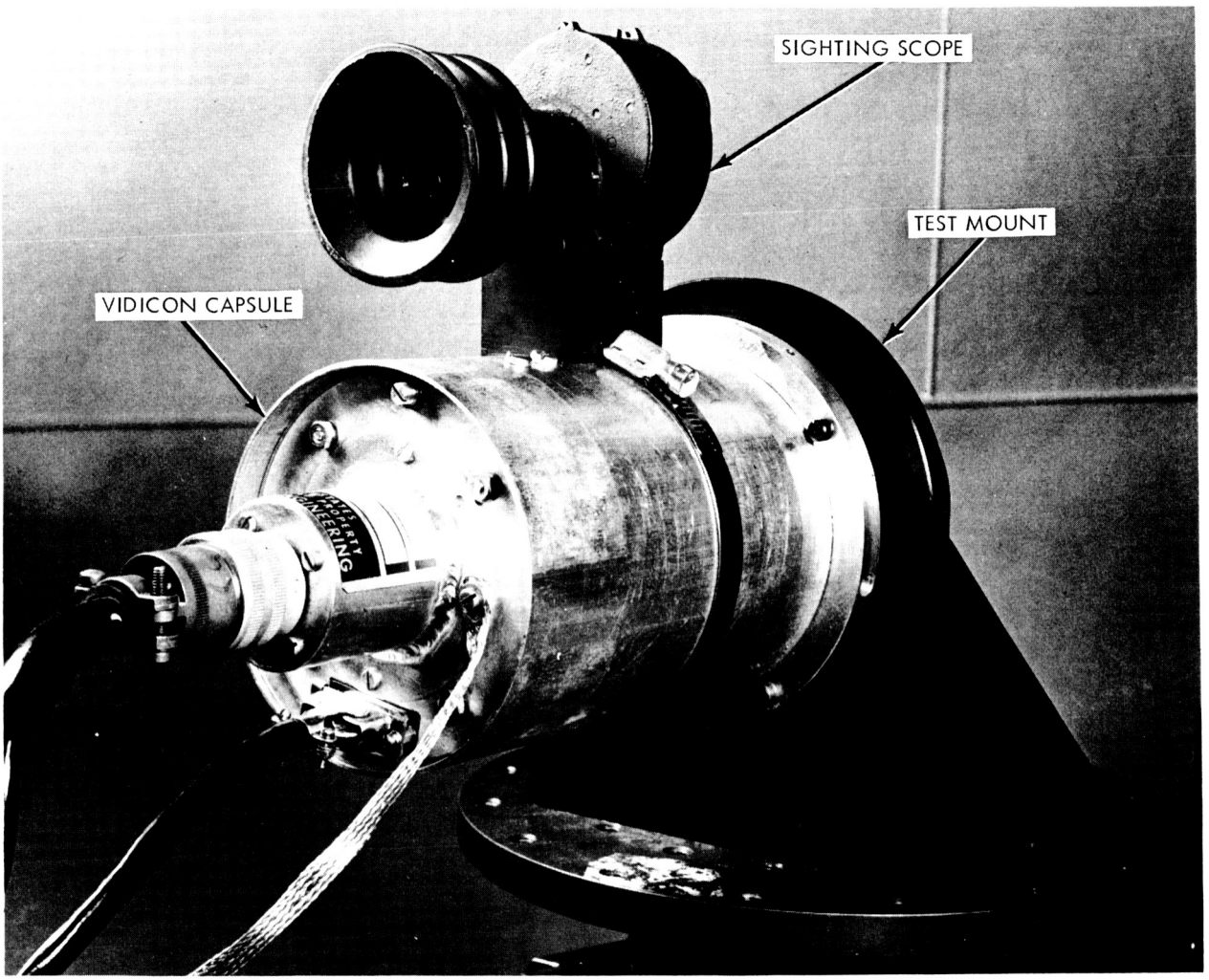

Figure 8. Vidicon Capsule

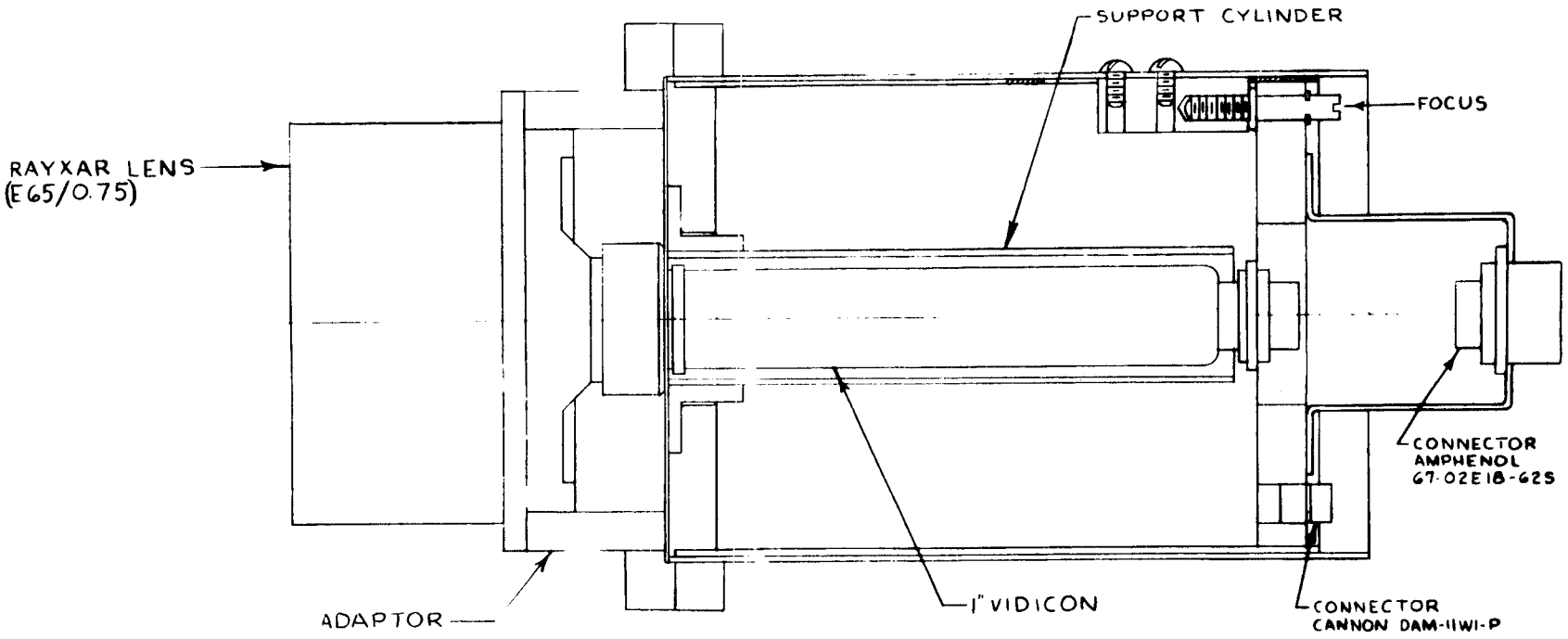

Figure 9. Assembly Rayxar 15° Lens and Vidicon Capsule

The O. D. of the flanged tube is wrapped with three staggered layers of Co-netic shielding to reduce magnetic field interference to a minimum. The flanged tube itself provides adequate electrostatic shielding.

VIDEO CHAIN

The video chain, along with the video processing, the pulse center detection circuits and the orthogonal sweep circuit is located in the compact Main Electronics Assembly shown in Figure 10.

The video amplification path is fundamentally the same as in Phase A, except that the aperture correction amplifier has been eliminated. Aperture correction is used in normal T.V. systems to enhance the high frequency response of the video signal, but it also amplifies the noise and degrades the signal-to-noise ratio. In tracker applications, where a visual presentation is of secondary importance, its use is not justified.

Figure 11 illustrates in block diagram form the functional elements of the video chain.

The preamplifier located in the vidicon housing uses a hybrid cascade arrangement of a "Nuvistor" vacuum tube and a transistor. This is used to minimize preamplifier noise and to present the vidicon target with a high input impedance buffer. A target load resistor of 50K is used to transform the current drawn by the target into a voltage for the vacuum tube input. Any shunt capacity at this point introduces a frequency lag which is compensated for by a peaking amplifier following the preamplifier. The peaking amplifier introduces a compensating lead into the frequency response, and has an emitter follower output driver for the coax cable to the main electronics chassis.

A variable gain amplifier in the main electronics chassis increases the signal from the preamplifier and supplies the amplified signal to the summing amplifier of the detection circuitry.

VIDEO PROCESSING

The higher vidicon mesh bias voltage incorporated in Phase B significantly reduced the warpage of the dark level due to beam landing error. However, compensation of this warpage is required so that a fixed bias level can be used in the detection circuitry. Since a lower signal appears around the edges than at the center, the form of compensation employed in Phase B is to generate a signal to enhance the edges. This generated signal is summed with the actual video resulting in a uniform dark level being presented to the threshold detectors.

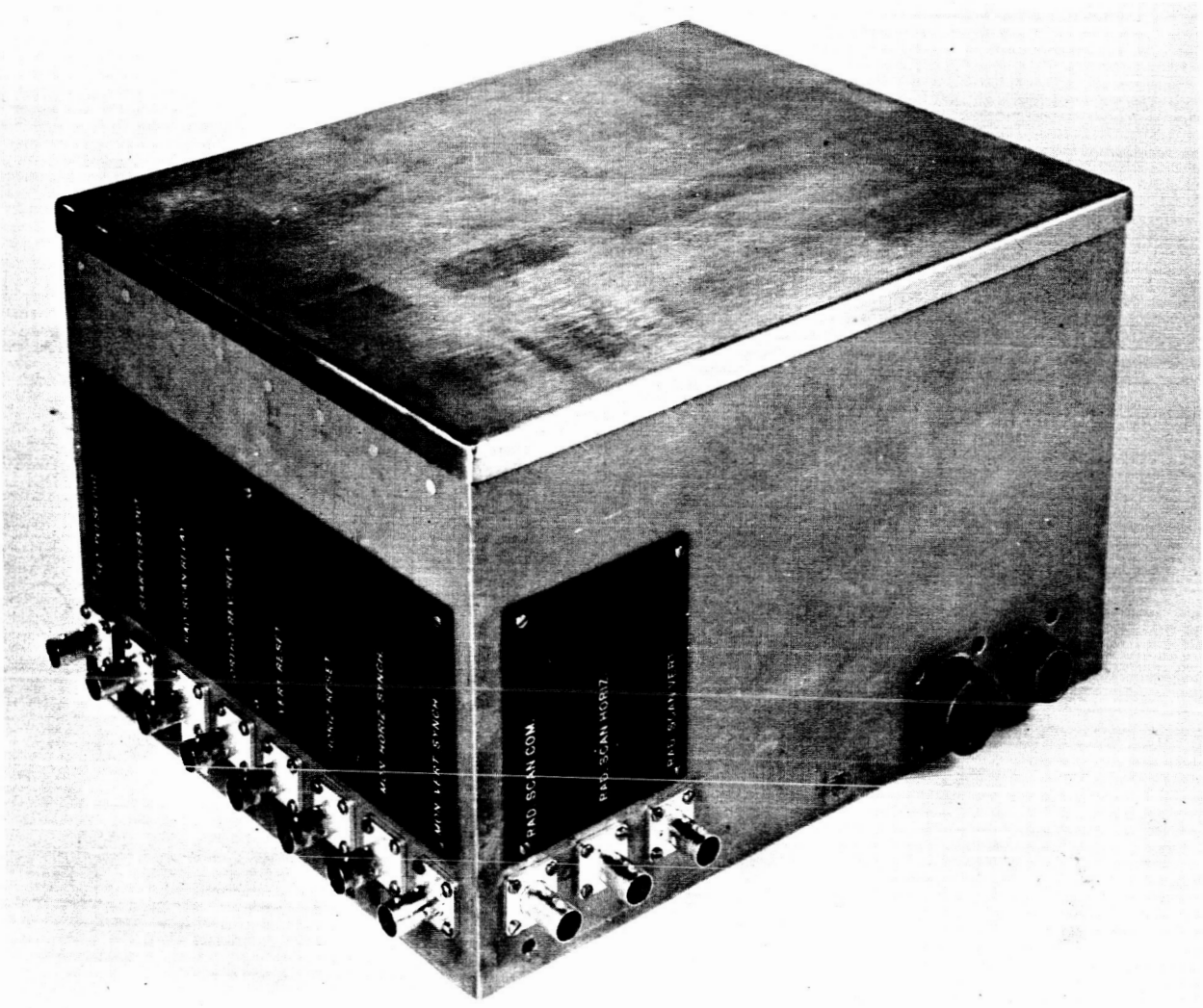

Figure 10. Main Electronics Assembly

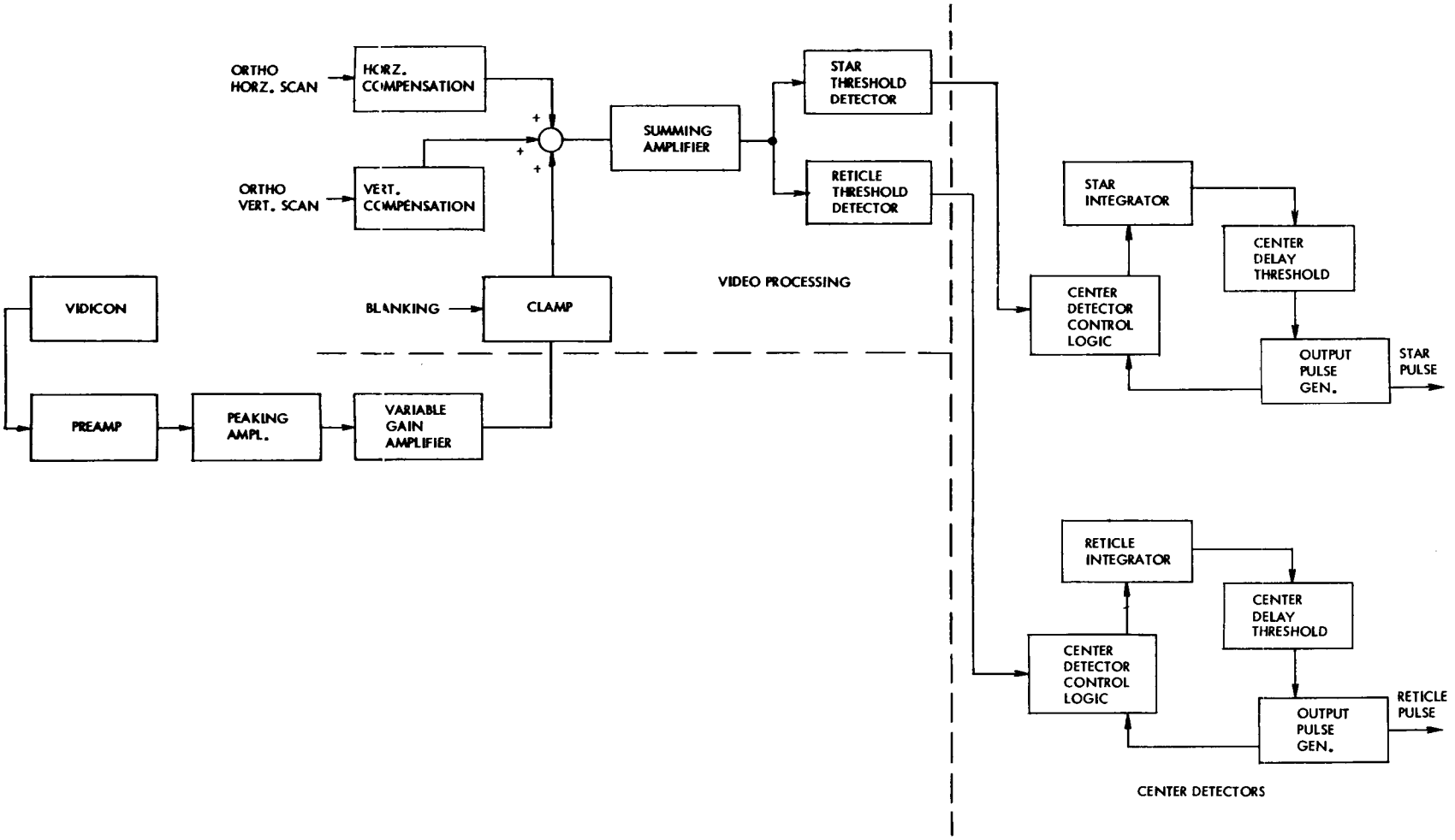

Figure 11. Video Chain Block Diagram

Since this compensation must be a two dimensional process both horizontal and vertical compensation signals, generated in the same fashion, are used. The sawtooth ramps from the scan generator are converted into triangular waveforms with the center clipped, as shown in Figure 12.

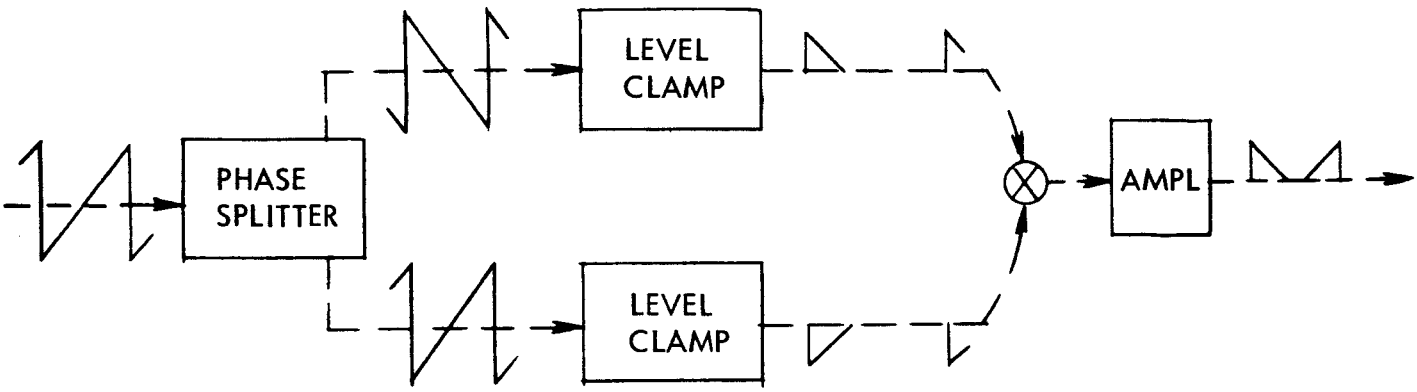

Figure 12. Shading Compensation

These signals are attenuated and summed with the video signal. The video signal prior to summing is clamped to ground during the blanking period referencing it to ground.

The results of this shading compensation are shown in the oscilloscope trace photos of Figure 13. Part "a" of this figure shows the uncompensated video signal from a horizontal line of the orthogonal raster. The negative pulses in this figure are the reticle signals. Part "b" shows the compensation waveform. Part "c" shows the results of summing the compensation and the video signal. The flattening achieved makes thresholding relatively simple.

The output of the summing amplifier is directed to the star threshold detector and to the inverter prior to the reticle center detector. The inverter is needed to present a positive pulse to the threshold detector. As long as the threshold levels are exceeded, a positive level at the output occurs. Therefore, for each star or reticle, a square pulse output occurs whose pulse width is dependent on the time the threshold level has been exceeded. Each output is directed to its respective center detector.

The compensation technique required for the radial scan differs from that used in orthogonal scan. In orthogonal scan, the shading is roughly symmetrical on each line so the same compensation can be used both for normal and reverse scanning directions. The radial shading is not symmetrical with the radii but is as shown in Figure 14.

Thus, the compensation used is not only different from the orthogonal compensation but must change depending on direction of radial scan.

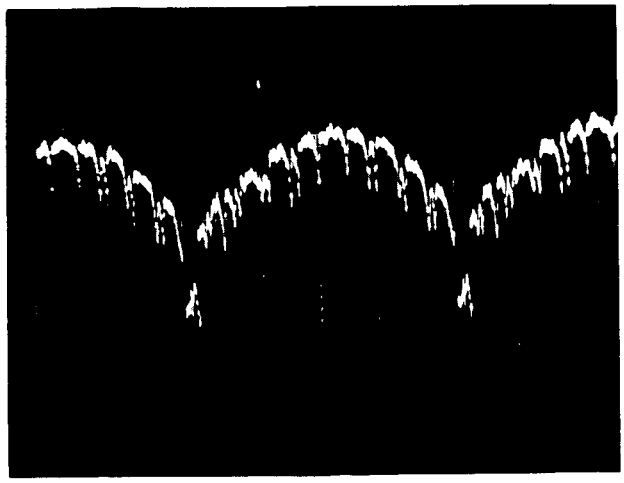

a) UNCOMPENSATED VIDEO
HORIZONTAL LINE
ORTHOGONAL SCAN

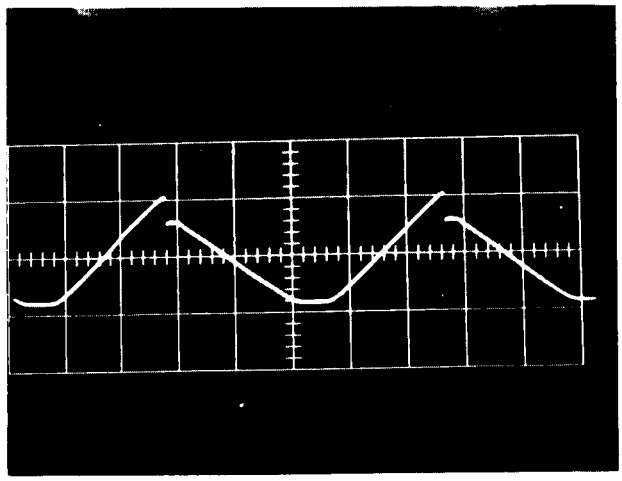

b) COMPENSATION WAVEFORM

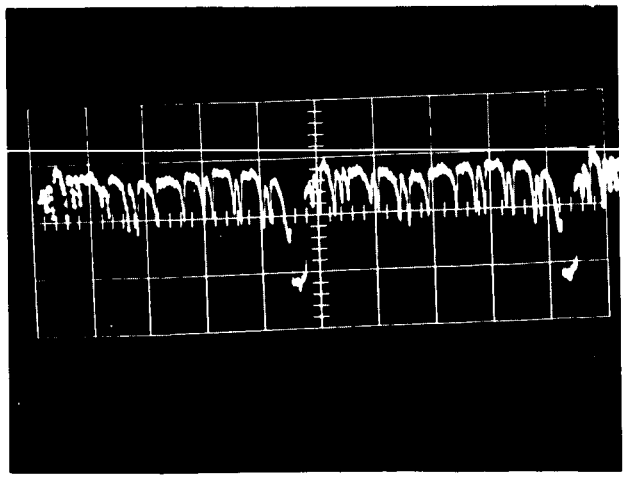

c) COMPENSATED VIDEO
AFTER SUMMING a) & b)

Figure 13. Shading Compensation Test Results

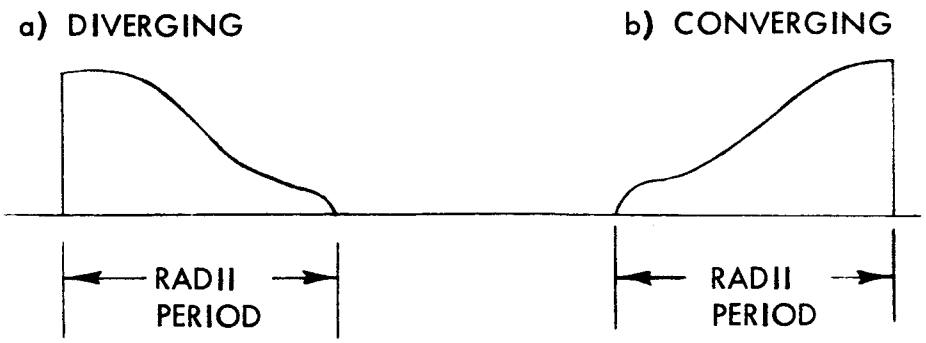

Figure 14. Radial Scan Dark Level Shading

The compensation waveforms are generated from the un-blanking pulse which has the time length of the radial lines. This pulse is differentiated for the diverging scan and integrated for the converging scan. The resulting wave shapes are shown in Figure 15.

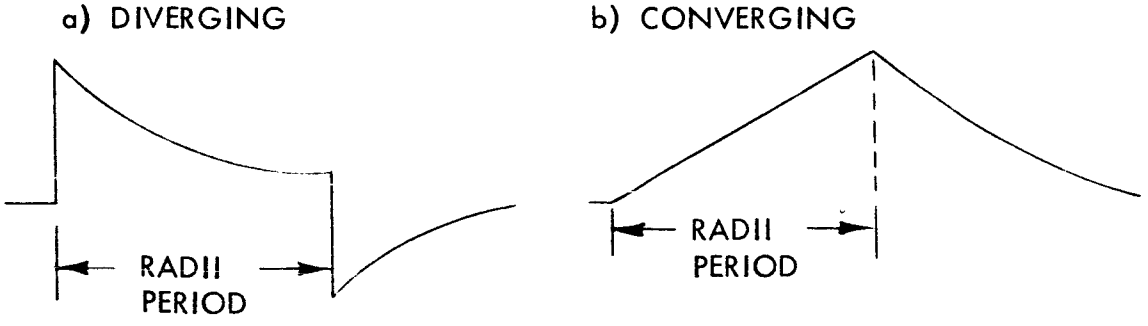

Figure 15. Radial Scan Compensation

The compensation waveform is subtracted from the video in the summing amplifier. This largely eliminates the variation in dark level from the center to the edges. The output of the summing amplifier is handled from this point as it is in the ortho scan.

CENTER PULSE DETECTION

The new pulse center detection method [1] is based on controlled rate integration to a reference threshold. Referring to Figure 16, the pulse width to be center detected, t_p, initiates a charge rate r_1 into an integrating capacitor at time t_0. At the end of t_p, the voltage on the capacitor is V_c such

(1) Reference No. 11

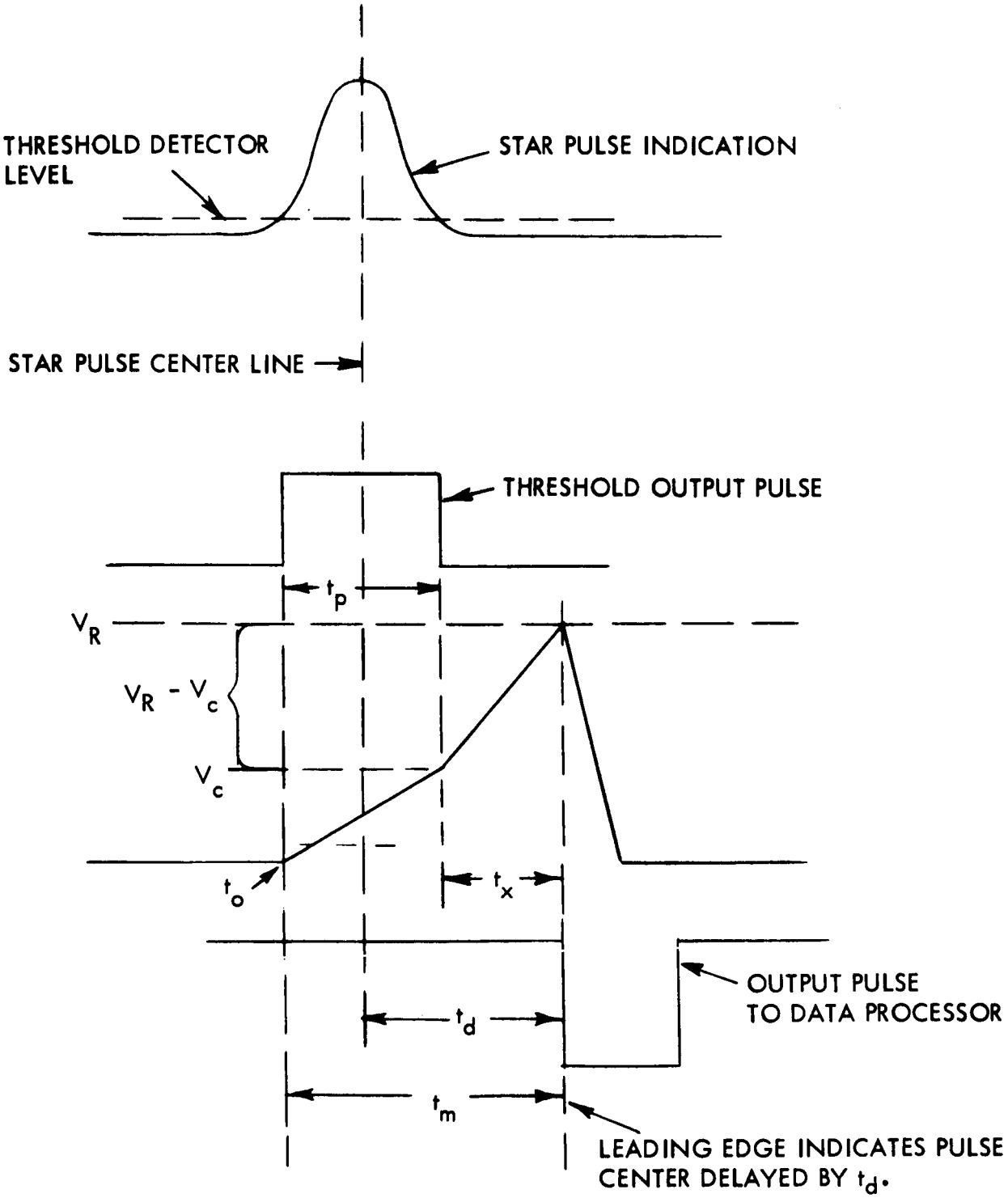

Figure 16. Pulse Center Detector Operation

that $V_c = r_1 t_p$. At this time the charge rate is doubled so that $V_R - V_c = 2r_1 t_x$ where V_R = reference threshold voltage. This can be rewritten

$$V_R - r_1 t_p = 2r_1 (t_m - t_p)$$

and by solving for t_m we have

$$t_m = \frac{V_R + r_1 t_p}{2r_1} = \frac{V_R}{2r_1} + \frac{t_p}{2} = t_d + \frac{t_p}{2}$$

The term $\frac{V_R}{2r_1} = t_d$ is the delay time from the center of the pulse width t_p to the crossing of the reference threshold. The circuit outputs a pulse at the crossing, the leading edge of which defines the center of the signal pulse delayed by t_d.

Since both V_R and r_1 are constant, t_d will be a constant regardless of pulse width. The maximum pulse width able to be handled by this arrangement is $2t_d$. The circuit values were chosen so that pulse widths up to 3.6 μ sec can be used. This is more than adequate for the range of targets used by the tracker.

A step response in the video due to a disc edge crossing will be differentiated by the hi-pass filter input to the threshold detector. The leading edge of the disc is then represented by a pulse which is handled identically as a star pulse from this point.

The mechanization of this center detection method is identical for both star and reticle pulses. The center detector control logic receives the pulse indication from the threshold detectors which in turn controls the integration rates. The output signals from the detectors are sent to the Data Processor.

ORTHOGONAL SCAN GENERATORS

The orthogonal scan generators are operational amplifiers used as integrators. A constant current source at the input provides linear ramp outputs. The integrators are reset to a negative reference voltage ($-V_R$) and allowed to charge to a $+V_R$, about deflection common, before being reset by the reset pulse. A match of integration rate and period of reset, therefore, determines the deflection voltage swing.

RADIAL SCAN GENERATOR

The radial scan generator is housed in a separate chassis (Figure 17). This system produces 32 equally spaced radii and can be operated in two modes -- diverging and converging. In the diverging mode, the radii start at the center and proceed to the outer edge. The converging mode has the radii starting at the outer edge and terminating at the center. A functional block diagram is shown in Figure 18.

The data processor provides three control pulses to the radial scan chassis. Two pulses are used to synchronize the radial scan sequence counter to the data processor's control counter. The third pulse enables the sweep period of the radii.

The sequence counter (5 stages) provides 32 discrete steps (or radii) for one full scanning cycle. The lower three stages of the counter control the sequencing of the sine and cosine multiplier switches. The last two stages control the quadrant and bias selection logic. The sequence counter counts the sweep enable pulses registering the count on the trailing edge of the pulse.

The sine and cosine multipliers are resistance ladder networks controlled by switches. These networks accurately divide a fixed reference voltage into 11.25° intervals of the sine and cosine function from 0° to 78.75°. The switches are sequenced by the first three stages of the sequence counter to continually generate these functions.

The outputs of the multipliers are presented to the sine and cosine sweep generators. These are operational integrators which are held in reset until a sweep enable pulse arrives from the data processor. The sweep period is fixed by the pulse width of the enable pulse. Therefore, the voltage from the multiplier circuits applied to the integrators' input resistor determines the sweep rate during the enabled period. As the multipliers are sequenced from 0° to $78\text{-}3/4^{\circ}$, the sine generator has increasing rates and the cosine, decreasing rates.

The quadrant switching selects the proper outputs of the sine and cosine generators so as to generate a full period (4 quadrants) cosine function for the horizontal deflection plates and a full period sine function for the vertical deflection plates during one complete counterclockwise rotation (all 32 radii). Figure 19 shows the two different sequences which are followed for the diverging and converging modes of operation. The converging mode requires the addition of a bias to place the sweep start at the outer edge. The proper bias is summed with the proper sweep generator to produce the converging scan. Control of the switching is done by logic controlled by the last two stages of the sequence counter. The diverge and converge command comes from the data processor and appropriately modifies the logic controlling the

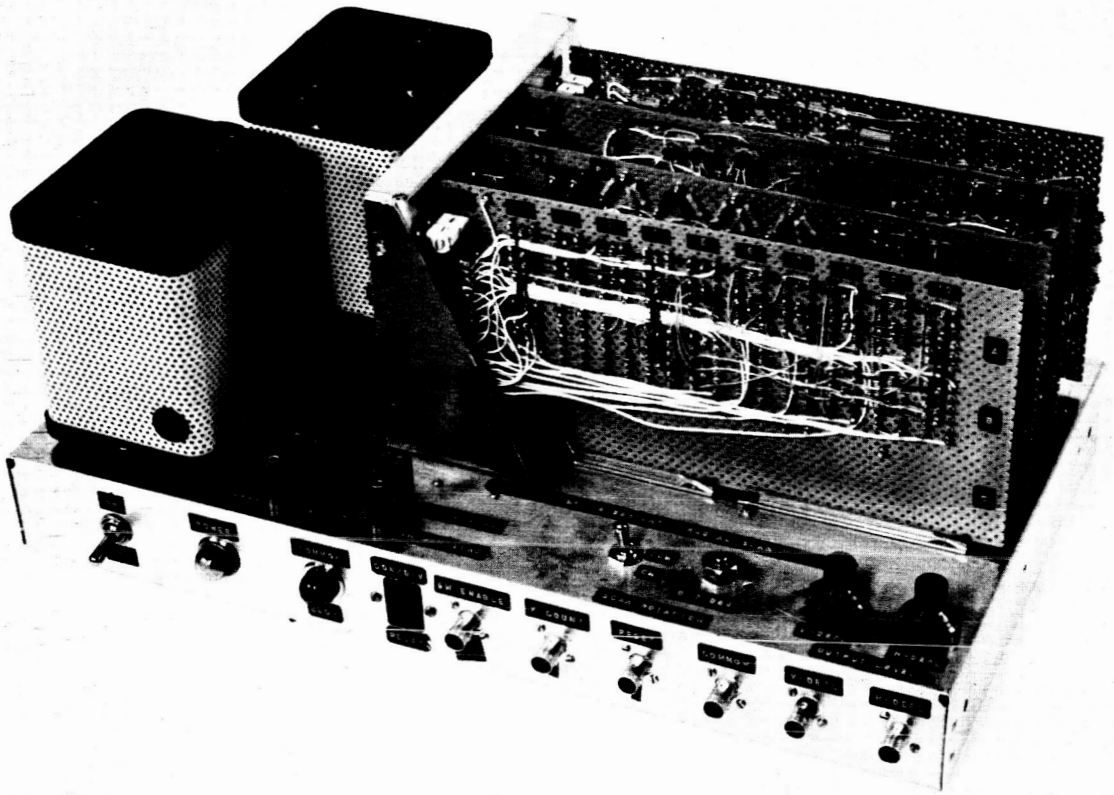

Figure 17. Radial Scan Electronics

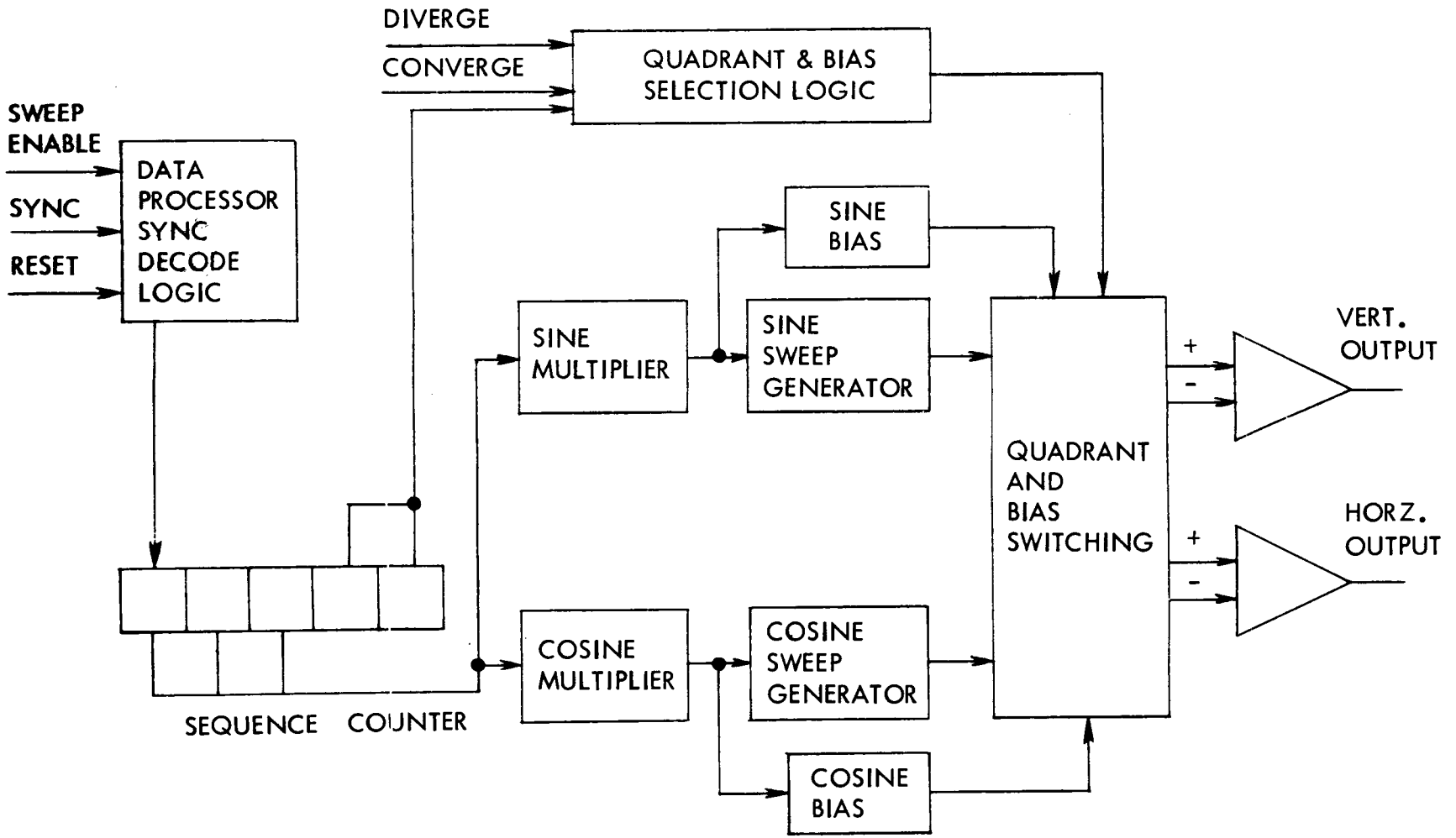

Figure 18. Radial Scan Block Diagram

b) DIVERGING SCAN

QUADRANT SELECTION
DIVERGING

QUADRANT	HORZ. DEFL.	VERT. DEFL.
FIRST	+COS	+SIN
SECOND	-SIN	+COS
THIRD	-COS	-SIN
FOURTH	+SIN	-COS

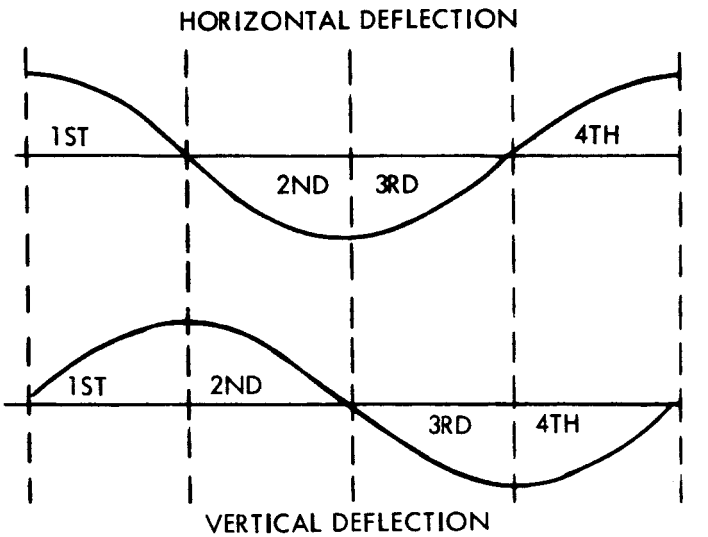

a) CONVERGING SCAN

QUADRANT SELECTION
CONVERGING

QUADRANT	HORZ. DEFL.	VERT. DEFL.
FIRST	-COS	-SIN
SECOND	+SIN	-COS
THIRD	+COS	+SIN
FOURTH	-SIN	+COS

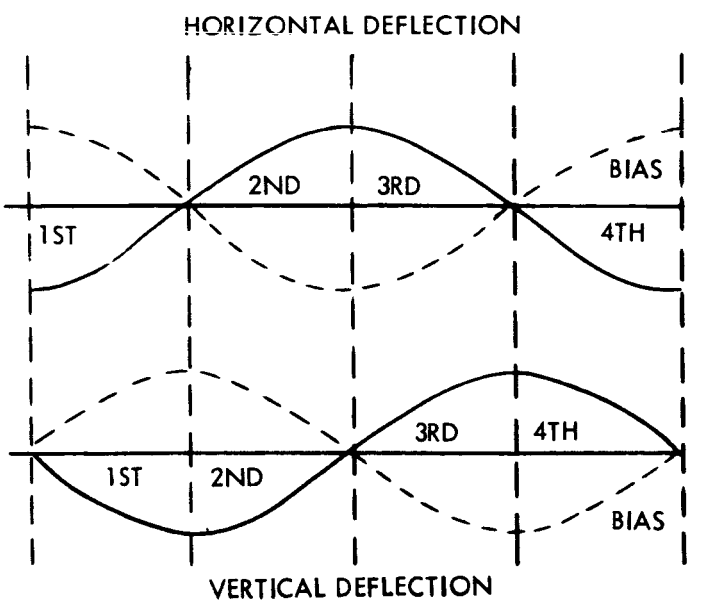

Figure 19. Radial Scan Quadrant Selection

switching. A pair of unity gain amplifiers buffer the switching process from the camera horizontal and vertical deflection amplifiers.

DEFLECTION AMPLIFIERS

The specially designed deflection plates of the electrostatic vidicon (Deflectron)[1] require a pair of deflection amplifiers for both the horizontal and vertical deflection. Each amplifier pair is used in a push-pull operation so as not to effect the axial field during deflection, thereby minimizing the lens action of the deflection field.

All deflection amplifiers are identical and each is associated with a particular deflection plate of the vidicon. In normal operation, Amplifier No. 1 provides voltage gain and load isolation from the scan generators, and provides an inverted ramp signal to its plate. It also drives Amplifier No. 2 which provides its plate with a noninverted ramp signal. In reverse operation, Amplifier No. 2 provides the load isolation and drives Amplifier No. 1. The switching of the scan generator to the proper amplifier and the position reversal of the amplifier is done by a 4PDT relay. A 2PDT relay connects either the radial scan or ortho scan to the amplifiers. Both relays are controlled by the data processor.

Each amplifier has its own zero bias and raster centering potentiometer. Also, there are provisions for a skewing adjustment on each amplifier where a portion of horizontal deflection voltage is fedback to the vertical, and vice versa. This provides a method of electronically rotating the raster to compensate for non-alignment of the raster with the reticle pattern. The complete deflection system is shown in block diagram form in Figure 20.

SYNCHRONIZATION

Synchronizing circuits provide timing to the orthogonal scan generators which determine the horizontal line frequency and the vertical frame rate. The synchronization is provided by reset pulse widths to both the horizontal and vertical scan generators. These same pulse widths are applied to the vidicon cathode for blanking during reset.

A toggle switch allows the selection of either internal reset sync or external reset sync. This allows operation of the camera independent from the data processor. When used with the data processor the switch should always be in the external position. In the case of the external sync from the data processor, the pulse widths are merely accepted by an OR circuit, level changed, and distributed to the appropriate reset and blanking switches. For internal sync, a variable horizontal rate oscillator determines the line frequency. Horizontal reset pulse width is generated by a single shot triggered by the rate oscillator. A counter counts down the horizontal rate to the proper vertical

(1) Appendix A

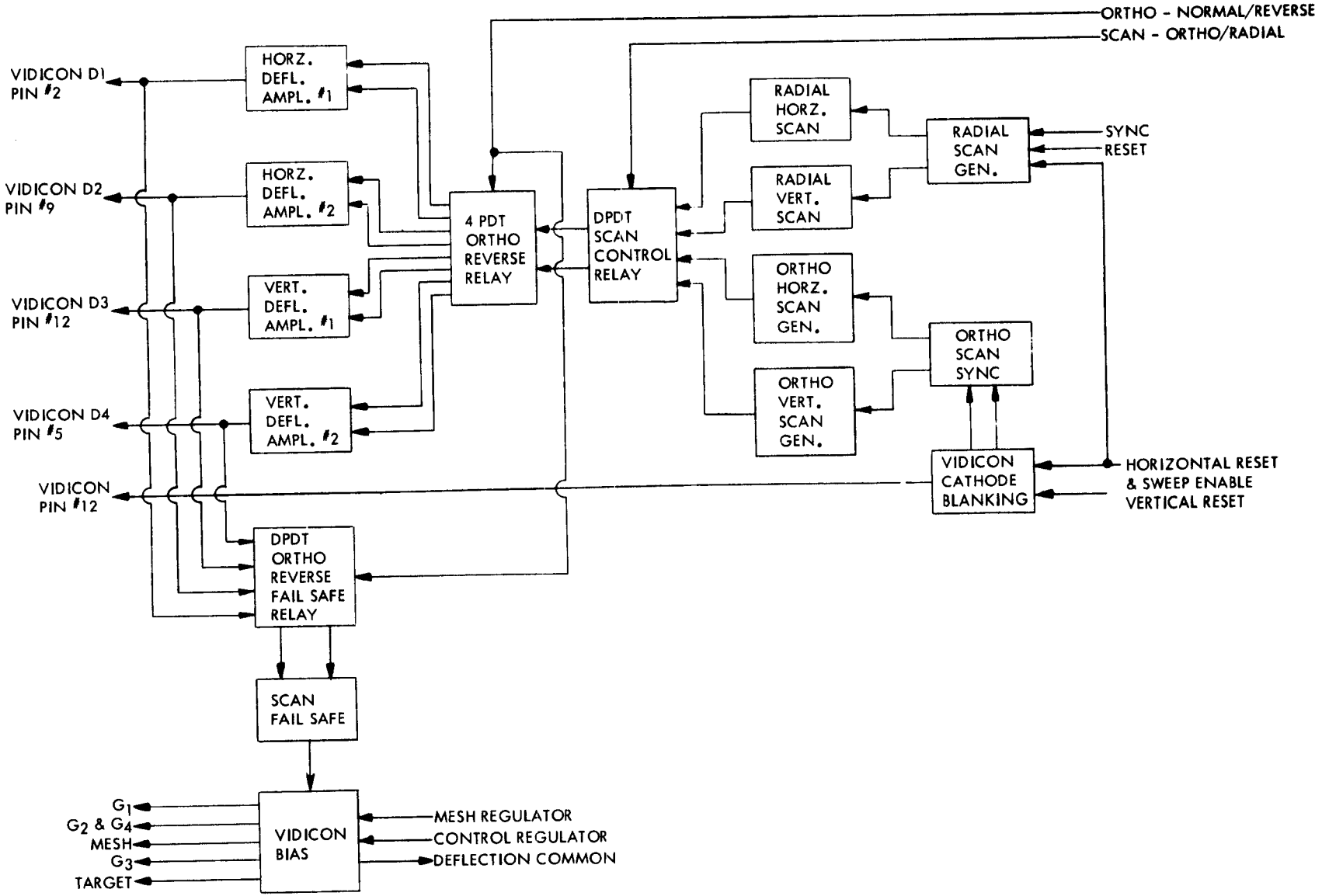

Figure 20. Deflection System Block Diagram

frame rate. The vertical reset pulse width is started by the proper count registered in the counter (1024) and ended when the counter is reset at count 1032. The Phase A preblanking and postblanking around the reset pulses in the camera has been eliminated. The data processor provides postblanking to the processed video it receives from the camera electronics.

FAIL SAFE CIRCUIT

A fail safe circuit is incorporated into the camera to protect the vidicon target from being damaged by prolonged operation without deflection voltages. This circuit monitors the deflection signals and blanks the vidicon control grid (G1) by de-energizing the blanking relay if a failure occurs. This circuit is operative only in the ortho mode of operation. An override circuit keeps the blanking relay energized when the system is switched into radial scan. This was an expedient to simplify circuit design and is justified by the fact that "fail safe" is far less critical in radial scan mode where the blanking periods take up approximately 98% of the frame time.

VIDICON BIAS SUPPLY

The vidicon bias supplies and the power supplies for the main camera electronics are housed in the separate enclosure shown in Figure 21. A separate meter box is provided to make set up and measurement of the primary voltages convenient. This box may be disconnected during operations.

Two precision voltage regulators supply the bias voltages for the vidicon. Bias settings are maintained at $\pm 0.1\%$ accuracies in order to avoid any degradation to the sensitivity of the vidicon. The mesh regulator supplies the mesh voltage directly and the fixed focus electrodes through a resistor potentiometer divider arrangement. The control regulator supplies, through resistor divider/potentiometer networks, the target, variable focus and deflection common biases. The beam current control voltage to the G1 electrode is supplied directly by an individual $\pm 2\%$ negative supply. Precision knob pots are provided in this bias arrangement to accurately and easily change bias settings.

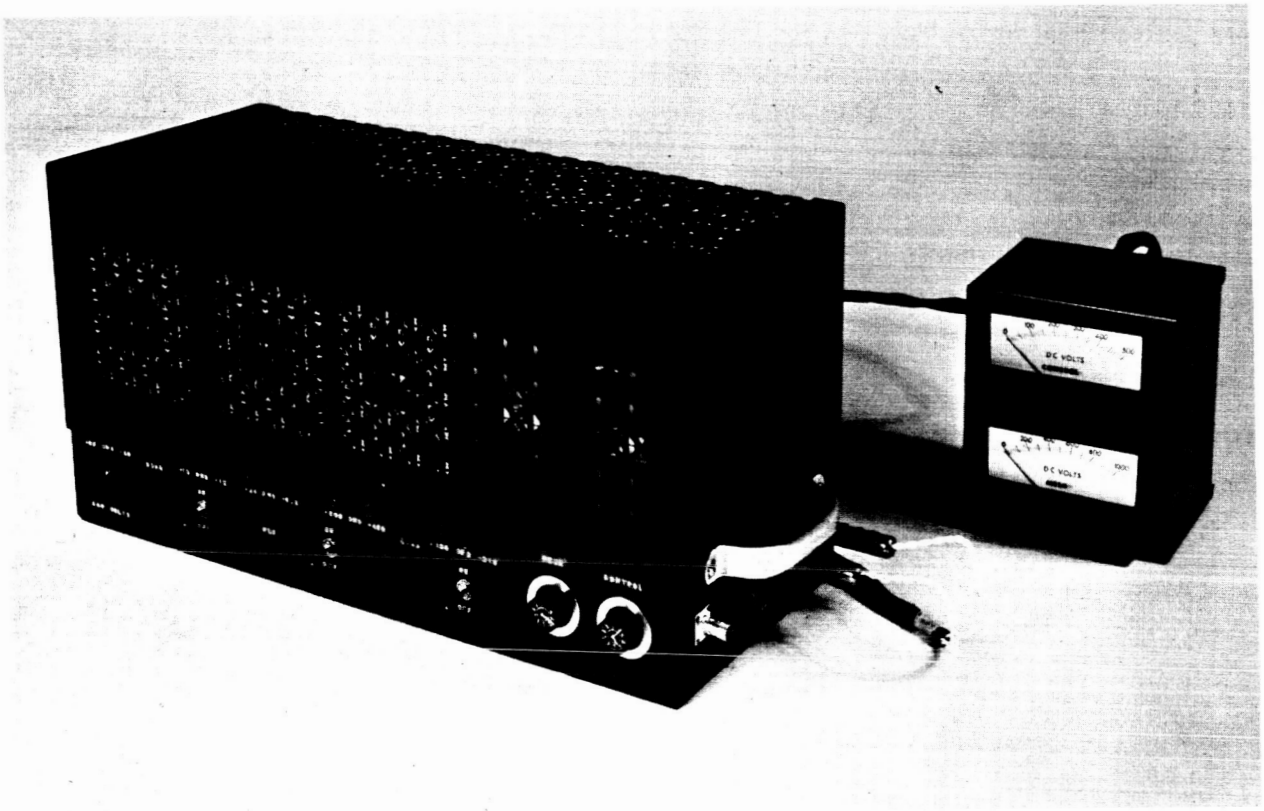

Figure 21. Power Supply

Section 4

DATA PROCESSOR

INTRODUCTION

The Data Processor for the Space Sextant tracker is a special purpose computer which operates on the target and reticle signals from the vidicon camera to produce image plane coordinates in digital form. The assembled unit is shown in Figure 22.

All considerations of size, weight, and appearance were regarded as secondary to system flexibility; the aim being to build a laboratory tool. Most signals are accessible on the front of the machine, the point-to-point wiring makes alterations simple, and the circuits used are relatively insensitive to loading, power supply variations, and ambient temperature. The variety of switch selected parameters makes evaluation of different modes of operation simple.

The data processor has six possible modes of operation. These modes, together with the data processor's function in each, are given in Table 4 below:

TABLE 4

OPERATIONAL MODES

				Data		
Mode	System Control	Ret. *	Gating	Avg.	Buffer Only	Display
OMNI	x	x			x	x
CAL-RAD	x	x	x		x	x
CAL-ORTHO	x	x	x		x	x
** EXT. BODY	x	x			x	x
** STAR	x	x	x	x		x
** DISC EDGE	x	x	x	x		x

*Ret.; Reticulization, or measuring the image location relative to the reticle pattern.

**For the definition of the target classes which correspond to these modes refer to Section 1 of this report.

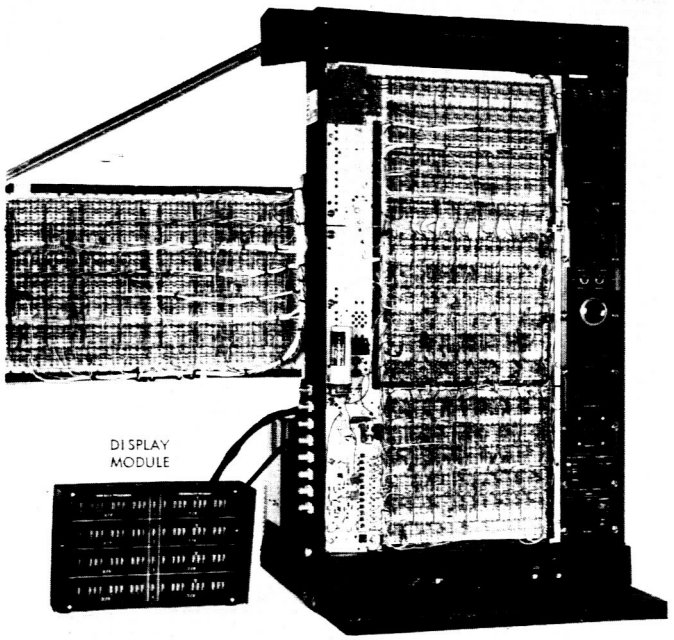

a) FRONT VIEW

Figure 22a. Data Processor Assembly

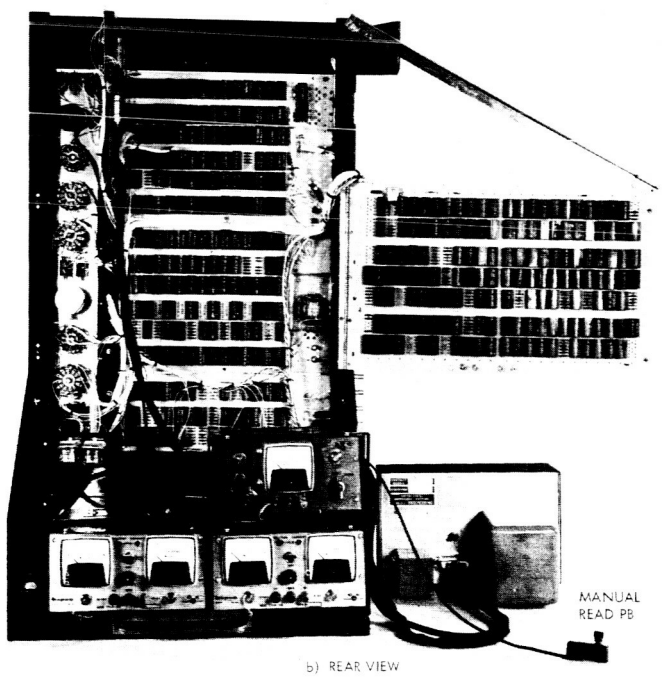

b) REAR VIEW

Figure 22b. Data Processor Assembly

These functions are performed by some five hundred and thirty logic packages organized into the following sections.

- o Horizontal - measures the image position along a single sweep relative to the reticle, controls each individual sweep start and stop.
- o Vertical - identifies each sweep with a number by reference to the reticle, controls frame start and stop.
- o Data Processing - averages and/or stores the image coordinates depending on the mode of operation.
- o Output Buffering - provides parallel outputs for the display and other external devices.
- o Display - accepts parallel outputs from data processor and presents the first four following its reset.
- o Sequencing and Timing - controls the other sections.

The Block Diagram of the data processor is shown in Figure 23. The various modes of operation are discussed in the following section.

The major differences between the Data Processor at the end of Phase A [1] and at the end of Phase B are:

- o Addition of the radial scan controls
- o Provisions for normal and reversed sweeps (previously discussed in Section 3)
- o Provisions for handling multiple stars in a single field of view
- o Provisions for inputing data to the NASA/Ames SDS 920 Computer

MODES OF OPERATION

The six modes can be broken down into two groups as far as sequencing and data processing are concerned. These groups are composed of the star and disc edge modes on the one hand and the omni, cal-ortho, cal-rad, and extended body modes on the other. Only one mode from each group will be discussed in detail; discussion of the remaining modes being limited to their differences.

(1) Ref. No. 1, Section 4

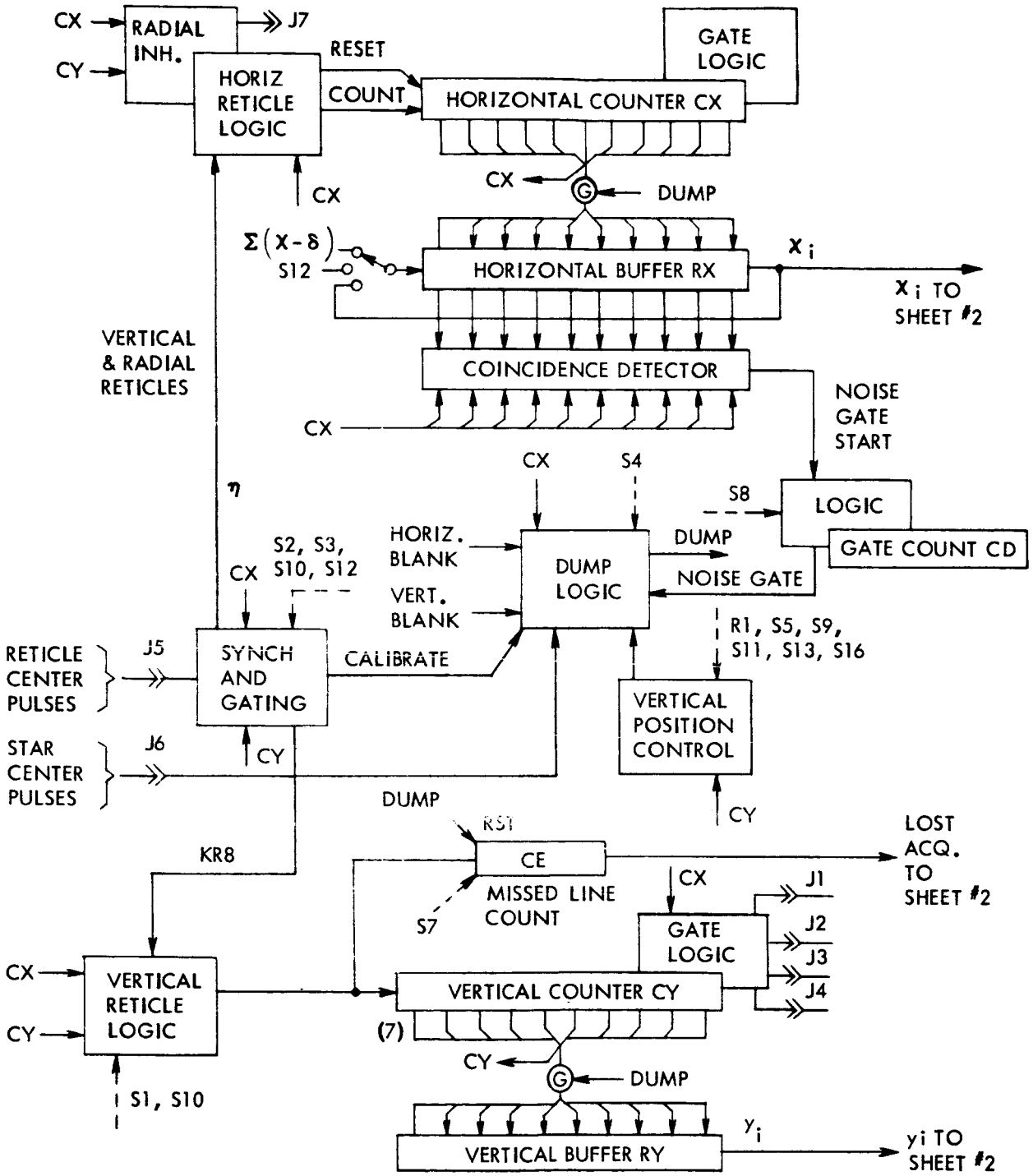

Figure 23, Sh. 1. Data Processor Block Diagram

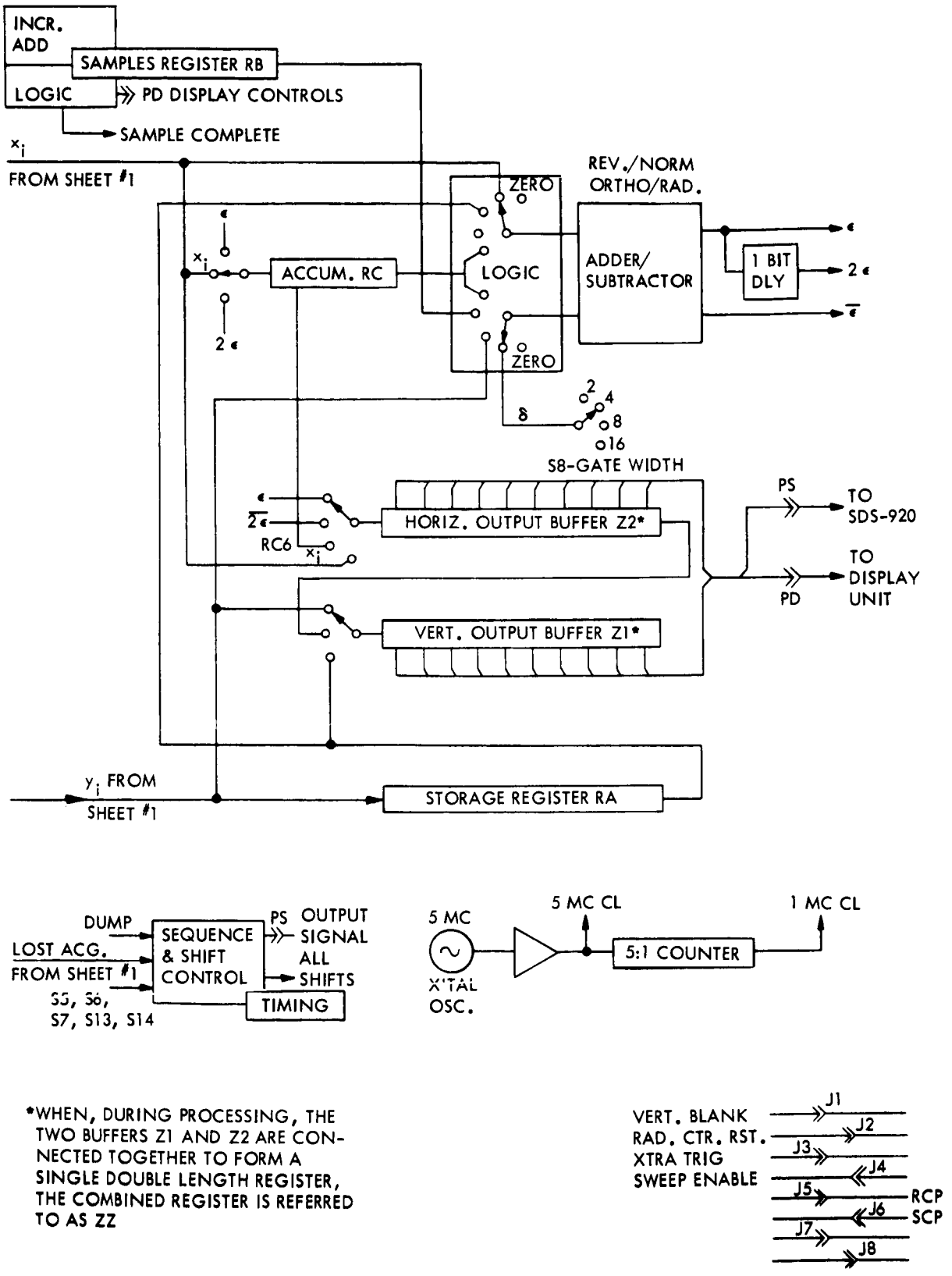

Figure 23, Sh. 2. Data Processor Block Diagram

.STAR MODE

As the vidicon camera proceeds through a complete frame the contents of the horizontal and vertical counters in the Data Processor (CX and CY) are an instantaneous measure of the position of the scanning electron beam in the vidicon. When a star image is encountered by this beam a star center pulse (SCP), (Refer to "Center Pulse Detection"- Section 3 of this report), is sent from the vidicon camera to the Data Processor. This SCP in turn triggers a data transfer pulse which has been given the descriptive title "DUMP." The DUMP pulse causes the contents of CX and CY to be transferred, in parallel fashion, to the horizontal and vertical registers respectively (RX and RY).

The contents of CX and CY are not destroyed by this transfer and these two counters continue their function of describing the scanning beam's position on the target of the vidicon.

The presence of a star image is detectable on several horizontal lines of the vidicon's raster so that, in general, several SCPs will be sent to the Data Processor for each star. An accurate single coordinate set is generated from this data by averaging. At the same time, the effects of noise are reduced by requiring that the SCPs occur on at least two successive lines with a horizontal deviation less than a switch selected constant (δ).

The last SCP of a set is identified as the pulse preceding a switch selected number of data free raster lines. The pulse signaling the end of a star signal set is called LOST ACQ. and is used to initiate the averaging and data output sequences.

After each DUMP a pair of numbers x_i and y_i are contained in RX and RY respectively. The subscript i describes from which SCP of the set the reading was obtained. The first SCP yields x_1 and y_1, the second x_2 and y_2, etc., until the last SCP yields x_n and y_n. The subscript n is the number of SCPs received for the one star image. It is required that $2 \leq n \leq 31$. The lower limit arises from the noise gate criteria while the upper limit is large enough to cover the practical "worst case" situation.

Operation of the star mode is best understood by referring to the sequencing diagram, Figure 24. The state numbers refer to flip-flop states in the sequencing logic. There are 6 flip-flops in the sequencer so that the number of possible states is $2^6=64$. Not all of these are used, however. State 00 is the normal "between stars" mode. When a DUMP moves the sequencer to state 20, the data processing registers RA, RB, and RC are cleared and $x_1 \rightarrow$ RC and $y_1 \rightarrow$ RA. The contents of RA are thereafter unchanged until

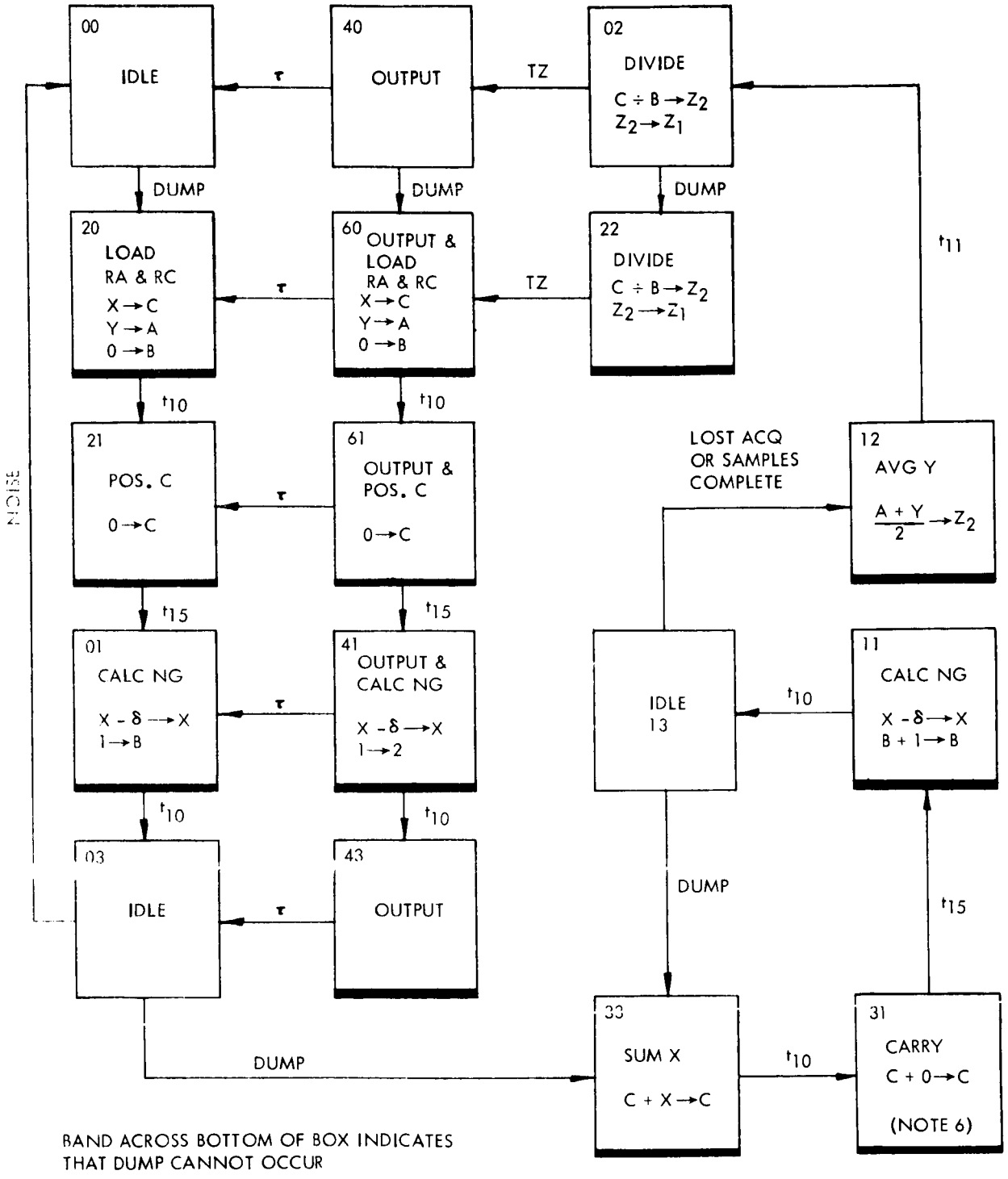

NOTE: a) t_{10} & t_{15} ARE PULSES FROM THE TIMING LOGIC WHICH TRIGGER THE SEQUENCER.

b) STATE 31 ALLOWS TIME FOR THE CARRY TO PROPOGATE IN C. THIS IS SYMBOLLICALLY INDICATED AS C + 0 C.

Figure 24. Sequencing Diagram Averaged Data Output

the data is averaged. State 21 finishes the clearing of the old RC contents and positions the new incoming contents. State 01 adds one to the cleared RB and places $x_1 - \delta$ in RX. Delta is a switch selected constant equivalent to half the noise gate width; i.e., the coordinate at which the gate will reopen is placed in RX. The sequencer then waits in state 03 for the next line. It will be noted from the sequence diagram that DUMPS are prohibited in states in which RX and RY are being shifted (e.g., states 11 and 41). This is to prevent loss of data.

When the noise gate opens at $x = N(RX)^{(1)}$ a dump becomes possible. The noise gate counter, CD, counts out the full width of the gate by recursive techniques; then closes the gate if no star were found. If the gate is closed in this manner, the sequencer will return to state zero. The first DUMP was caused by noise.

If a DUMP occurs within the gate on the second line, the gate is closed by it and the sequencer moves to state 33. It has now entered the loop which will be repeated n-1 times (n was the number of readings taken). In state 33, x_i is added to N (RC) and in 31 the carry is propagated through the most significant five digits of RC. In state 11, one is added to N (RB) and a new coordinate is calculated for the noise gate start. State 13 is the "between readings" idle condition. In state 13, if the noise gate closes without a dump, one is added to N (CE), the lost acquisition count. CE the lost acquisition counter is cleared to zero by each dump. If the contents of CE reach the number set on the LOST ACQ. switch, the sequencer moves to state 12 to prepare for output. The star is completed or lost. Marginal stars (low magnitude) will exhibit holes (that is, intermediate lines do not show a signal). By setting the LOST ACQuisition criterion high enough, useable readings can be made. Possible LOST ACQ settings are 1, 2, 3, 4, and 7.

State 12 forms the average vertical coordinate by taking half the sum of the first and last y readings. y_n is found in RY having replaced y_{n-1} during the last dump. The division by two is accomplished by shifting the sum one bit too far, the shift being least significant bit first, into the output buffers. The horizontal and vertical output buffers (Z2 and Z1) are initially tied together to form one long buffer identified as ZZ. The average is temporarily stored in the half of ZZ which will output $\bar{x}$ (Z2), then moves to its own half (Z1) when $\bar{x}$ is shifted in.

States 02 and 22 are occupied with dividing the contents of RC by the contents of RB, thus forming $\bar{x}$ according to the equation:

$$\bar{x} = \frac{1}{n} \sum_{i=1}^{n} x_i$$

(1) N (RX) is defined as the number in RX. Similarly N (RC) is the number in RC, etc.

The quotient accumulates in RC and is outputed at the end of the division. Since the quotient bits are formed most significant bit first, this accumulation is necessary in order that they can shift into ZZ least significant bit first. When the quotient is correctly positioned in ZZ the timing pulse TZ is emitted which moves the sequencer into either state 40 or 60 depending upon whether this pulse occurs before or after the occurence of the first DUMP from a second star.

In state 40 the contents of the output buffers are steady on the output lines going to the SDS computer and to the display. The duration of this state is determined by a single-shot of approximately 55 microseconds duration. In the sequence diagram τ indicates the single-shot's timing out.

States 22, 60, 61, 41 and 43 duplicate states 02, 20, 21, 01, and 03 as far as the data processing is concerned. Their purpose is to permit starting a second star before finishing the first, thus reducing by one the vertical separation required between stars. In state 22 the division for the first star is completed while x_1 and y_1 of the second star are held in RX and RY. In the other states, the only difference is that ZZ is outputting while the normal initial processing proceeds. The horizontal PRF is low enough that x_2 y_2 of the second star will not occur until after the output is complete.

The display requires only one microsecond for its input and is thus independent of any output duration adjustment. The 55 microseconds is a requirement of the SDS 920 Computer.

DISC EDGE MODE

The disc edge mode differs from the star mode in the fact that the target extends across the full field of view in elevation (Y axis) rather than being a point. Thus,a signal will occur on every line and it is necessary to specify in advance the general Y coordinates at which edge crossing measurements will be made. Therefore,a gate is set up such that four horizontal bands beginning at vertical coordinates y_1, y_2, y_3 and y_4 are used. The width of these bands, which is the number of lines used to compute the set of average coordinates is set by the SAMPLE SIZE switch.

The position of y_1 can be set by the VERTICAL POSITION controls at any point between 0 and 1024. The spacing of the four bands is either 256, 64, or 1, depending on the settings of S8 and S16, VIEW control switches. The positions of y_2, y_3, and y_4 depend upon the position of y, and the selected spacing.

If y_1 is set high enough that insufficient room is left for the others, they fold around and start up the bottom of the frame. The spacing is somewhat different in this event due to the time required for vertical retrace.

In the Disc Edge the transition between state 13, IDLE, and state 12, AVG Y is effected by comparing the number of readings taken, N (RB), with the setting of the SAMPLE SIZE switch. When they are equal, processing for output begins and the vertical gate is closed until the next band.

The wide spacing of the bands, 256 lines, would normally be used in Disc Edge tracking. The narrower spacing, 65 lines would be used in Extended Body tracking with orthogonal scan. The one line spacing is provided as a fine grain analysis tool for use during initial set up. Extended Body tracking with radial scan is handled by the EXTENDED BODY MODE of the Data Processor which is described later in this section.

OMNI MODE

The omni mode is typical of the second group of modes. In these, the data output are the raw coordinates of the star pulse center detector's outputs. The data processor buffers this data so that readings can be taken at smaller intervals than would otherwise be permitted by the outputs' destination; e.g., the SDS 920 requires 55 μsec. between readings while with buffering the data processor permits some readings to be taken at intervals of 10 μsec. as long as the average interval is within the SDS's capabilities. Operation of the Omni Mode is best understood by reference to the sequencing diagram for instantaneous readings, Figure 25.

Each frame is begun in state 00, idle. The first SCP (star center pulse) causes a DUMP which transfers x_1 and y_1 into RX and RY, and moves the sequencer to state 24. In state 24 the data is shifted from RX and RY into the output registers, a process requiring ten microseconds. At the end of the shift the timing logic emits pulse t_{10} which moves the sequencer to state 40. State 40, like the other states having corresponding numbers, is identical to state 40 of the Star and Disc Edge modes; i.e., the contents of the output buffers are steady on the lines going to the SDS computer and to the display. The duration is determined by a single shot whose "timing out" is indicated by τ on the sequence diagram.

If no new SCP occurs within this period, the sequencer returns to state 00. If, however, a second SCP occurs, the resulting DUMP puts x_2 and y_2 in RX and RY and moves the sequencer to state 60.

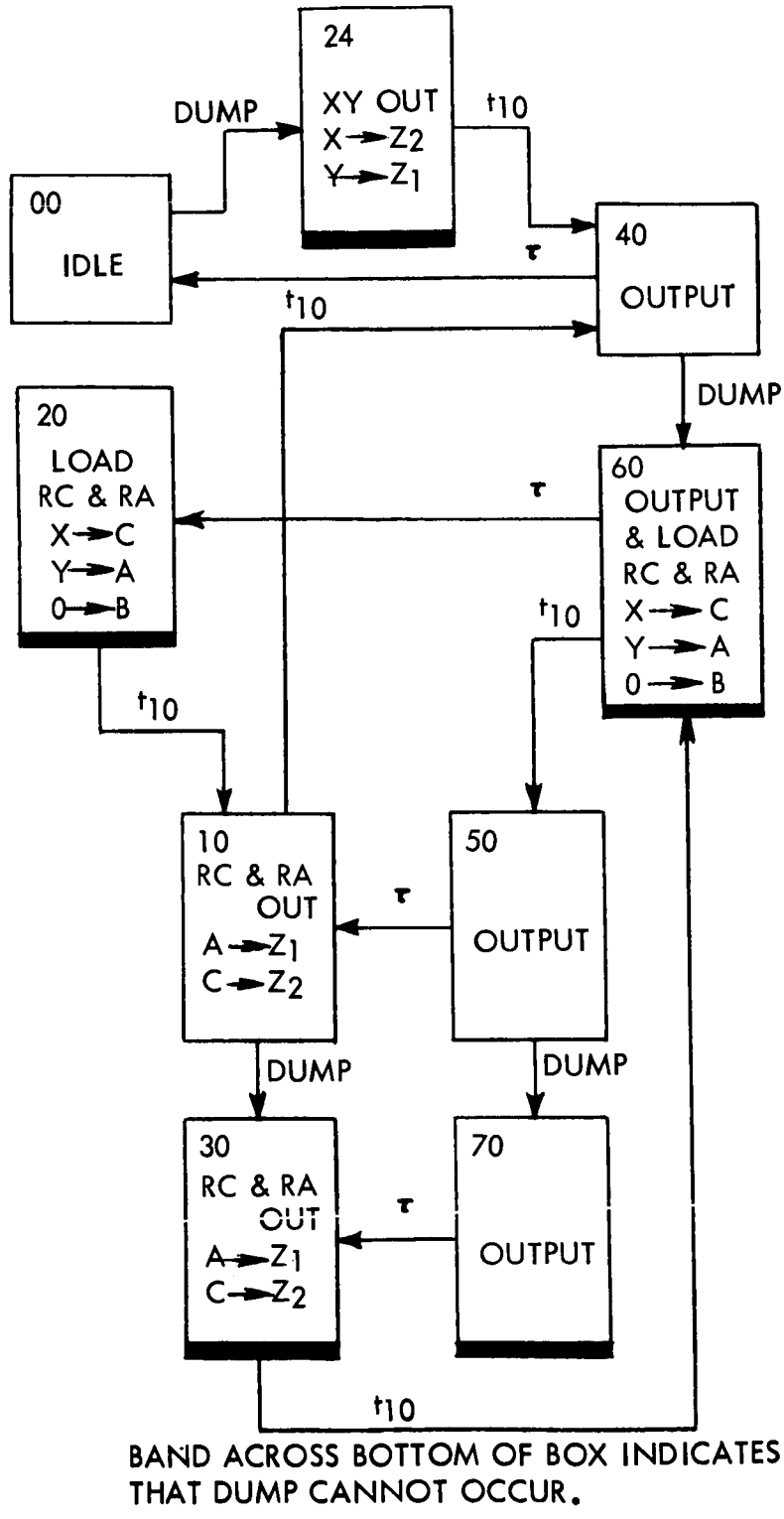

Figure 25. Sequencing Diagram Instantaneous Readings Output

In state 60, x_2 and y_2 are shifted to RC and RA respectively where they are held pending the completion of the output period. If τ occurs while this shift is in progress, the only effect is to move the sequencer to state 20 and end the output strobe. The shift is not interrrupted. Completion of the shift before τ is signaled by t_{10} and the sequencer moves to state 50.

It will be noted from the sequence diagram that DUMPs are prohibited by states in which RX and RY are being shifted. (e.g.: states 30 and 70) This is to prevent loss of the data therein.

A third SCP, occurring before the completion of the output of x_1 and y_1, dumps x_3 and y_3 into RX and RY where they are held. Further DUMPS are inhibited in the resultant state 70.

When the output of x_1 and y_1 is completed the sequencer moves from state 50 (70) to state 10 (30). In these states x_2 and y_2 are shifted into the output buffers Z2 and Z1 and the second output begins in state 40 (60). State 40 continues the open door policy toward a third DUMP, while state 60 shifts x_3 and y_3 into RC and RA as before. Completion of this shift allows a fourth DUMP, etc.

EXTENDED BODY MODE

The Extended Body Mode is identical to the Omni Mode except for the use of radial scan instead of orthogonal scan in the vidicon. (Tracking of Extended Bodies with orthogonal scan is handled in the Disc Edge Mode previously described). In this mode the x_i's are the radial locations of the edge crossings while the y_i's identify the radii which are numbered consecutively 0 through 31. Since there are only 32 such radii only the most significant five bits of the y output are used. The lease significant five bits are meaningless.

CALIBRATE MODE (ORTHOGONAL AND RADIAL)

With one exception, these modes are also identical to the omni mode. The exception lies in the use of the noise gate. The noise gate, which was described in the star mode, is used in calibrate to select which vertical or circular reticle will be examined. The gate start coordinate is set by the HORIZONTAL POSITION switch and is not a function of the coordinate of the data. This allows the operator to limit his field of interest to the reticle in question. The gate width is selected by S12 which should be set to 32. The gate start coordinates corresponding to the various settings are given in Table 5.

TABLE 5
GATE START COORDINATES

S12	Coordinate (Minimum x)
0	0
1	114
2	242
3	370
4	498
5	626
6	754
7	882
D	930
8	1010

DATA DISPLAY MODULE

The Data Display Module provides direct readout in octal grouped binary form of the coordinate sets for up to four targets. This allows for operation of the system completely independent of the SDS 920 and also serves as an instantaneous tracking monitor when required. This module requires twenty-two inputs plus 110VAC, 60 cps power. Twenty of these inputs are the parallel outputs of the buffer registers Z1 and Z2, the remaining two are for the "interlock reset" and the "display strobe" pulses. The minimum input pulse width is one microsecond.

Internal to the module are eighty-four flip flops which supply storage for four twenty-bit words and their associated interlocks. Following an "interlock reset" the four registers are loaded by the next four strobe pulses which occur. Strobe pulses following the first four in any one frame are ignored.

The data processor provides the same data to the display as to the SDS. The interlock reset is provided during the vertical retrace either on every frame, as directed by the pushbutton S30, or as directed by some external device; depending upon the setting of S5, READ CONTROL.

The strobe pulse sequence for the display depends on the mode and upon the settings of various switches. In Star and Disc Edge modes, the first four outputs to the SDS are displayed. In the remaining modes, provision is made for taking adjacent outputs, outputs spaced 64 lines apart, and outputs spaced 256 lines apart. Where these latter outputs begin depends on the setting of the VERTICAL POSITION controls; and are thus variable from top to bottom of the frame.

SYSTEM CONTROL

System Control is effected by furnishing to the camera the signals shown in Table 6.

TABLE 6
SIGNALS TO CAMERA

Signal	Description
Vertical Reset	- ground for 2.0 milliseconds per frame (effects vertical retrace)
$\overline{\text{(Sweep Enable)}}$ (Ortho)	- gnd for 12.8 microseconds per line (orthogonal) (effects horizontal retrace)
$\overline{\text{(Sweep Enable)}}$ (Radial)	- gnd for 1.79 milliseconds per radius (effects radial retrace and advances sin/cos generator)
Radial Scan Reset	- positive for 1.0 μ sec per radial frame (synchronizes sin/cos generator with CY)
Extra Count To Radial Scan	- positive for the 1.0 μ sec following the radial scan reset -- (part of synch procedure)
Rev/Normal	- sets relays in camera to determine sweep direction
Ortho/Radial	- sets relays in camera to determine type of sweep

RETICULIZATION

Reticulization is the process of imposing the vidicon's reticle pattern onto the coordinate system defined by the Horizontal and Vertical counters. For the nominal or zero error case, each sweep should encounter reticle center pulses at intervals of 128 counts. Deviations from 128 are measured and applied to CX, the Horizontal Counter, thus compensating for varying sweep rates and linearity. In addition, zero for the counter is defined by the first reticle, thus compensating for centering errors and incomplete retrace.

In the orthogonal sweep vertical error is detected by comparing the contents of the Horizontal and Vertical counters when a diagonal reticle is crossed. The diagonal reticle could have been a single line at 45^{o} to the vertical lines and extended across the full width of the vidicon force. However, since the maximum sweep errors will not exceed one or two percent the contents of the Horizontal and Vertical counters always agree in the four most significant

bits. It was therefore possible to break up the diagonal reticle into 17 segments placed at the edge of the field and compare only the six least significant bits of the two counters when the lines are crossed. This simplified the identification of reticles (vertical lines versus diagonal lines) and reduced the clutter in the active target area. Corrections dictated by a vertical error are applied to the input of CY, the vertical counter.

Completely different philosophies are used in handling corrections to the horizontal and vertical counters.

When an error is detected, the horizontal counter, CX, has its contents corrected by the exact amount of the error up to a design limit. The vertical counter, however, is merely incremented or decremented by one count in the direction required. Thus, N (CX) is inherently more accurate, as it must be, since the corrections to N (CY) are based on N (CX).

When the train of RCPs (Reticle Center Pulses) are received from the camera the pulses are identified as coming from either vertical or diagonal reticles by gating. Those pulses occurring at $1248 \leq N\ (CX) \leq 1280$ and at $120 \leq N\ (CX) \bmod 128 \leq 135$* are from the vertical reticles and are sent to the horizontal reticulization circuits. To allow for missing a reticle, which reduces the position accuracy and requires a wider gate, the lower limit of 120 is reduced to 112 if prior reticles were not present.

Those pulses occurring at $928 \leq N\ (CX) \leq 992$ for normal sweep or at $32 \leq N\ (CX) \leq 96$ for reversed sweep, are from the diagonal reticles and are sent to the vertical reticulization. If vertical reticle pulses have not been received just prior to the diagonal pulses, the transfer to the vertical reticulization circuits is inhibited since N (CX) will be in error.

V_o, the RCP occurring for $1248 \leq N\ (CX) \leq 1280$ is special in that it causes the entire CX counter to be reset to zero. If no RCP occurs in this interval, CX is reset automatically at x=1280. The miss is stored and results in a widened gate for subsequent reticles, inhibition of vertical corrections, and if S20 is ON, in inhibition of dumps. These restrictions are removed by any subsequent RCP's within CX's gate.

Subsequent RCP's gated into CX's circuits are further divided into those occurring before 0 mod 128 and those after 0 mod 128. Those before cause the least significant seven bits of CX to be reset to zero and a carry is propagated through the most significant stages. Thus, the counter is yanked up to the correct reading.

*C = A mod B is read "C equals A modulo B" and indicates that $C = A \pm Bn$ where n may be any integer including zero; e.g., x = 125 mod 128 implies x = -131 or -3 or 125 or 253 or 381 or 509 or 637 or 765 or 893 or 1021 or ...

. If the RCP to CX comes after 0 mod 128, CX is stopped and an auxiliary counter, CA, is started. This counter counts out the error and CX is restarted when it has missed the proper number of counts. Since the gate restricts errors to less than seven counts, the process requires 1.4 microseconds maximum. DUMPS during this period will read the same x regardless of where in the interval they occur. While this introduces some ambiguity, the error is less than or equal to that present in N (CX) when the RCP occurred.

The vertical counter is corrected by comparing its reading with N (CX) when a 45^{o} diagonal is crossed. Since these should be equal in the 6 least significant bits assuming that N (CX) is correct, the interval between the RCP representing the diagonal and the point of equality, π is a function of the error in N (CY).

When the reticles "turn the corner"; i.e., when transition from one diagonal segment to the next occurs, it is possible to get π at the end of the interval and RCP at the beginning or vice versa. This would indicate an error of nearly 64 counts and in some conditions could stop CY completely. The sequence diagram in Figure 26 shows how this is avoided by making no correction unless the indicated error is less than thirty-two counts.

Starting in the (0) IDLE condition, one of the following five events will occur first as the vidicon beam sweeps across the diagonal area of the reticle pattern:

1. RCP• π
2. RCP• $\overline{\pi}$ a
3. RCP• $\overline{\pi}\,\overline{a}$
4. $\overline{\text{RCP}}$• π a
5. $\overline{\text{RCP}}$• $\pi\,\overline{a}$

The first of these is the normal case with RCP and π, the pulse indicating coincidence between CX and CY (6 least significant bits), occurring simultaneously. The system moves to (7) NORMAL, the number in the Y counter, N (CY), is incremented +1 and the system returns to (0) IDLE.

As an example of a non-normal situation consider the fourth case. Here the pulse π is received in the first quarter of the diagonal area prior to receiving RCP. The system moves to (3) MAYBE ADD. The term MAYBE ADD is used here to indicate that the decision to add cannot be made until the next event occurs. If the next event is the receipt of the M pulse, indicating that the beam has crossed the center of the diagonal area, later RCP's are disregarded since they would yield erroneous corrections, the system moves to

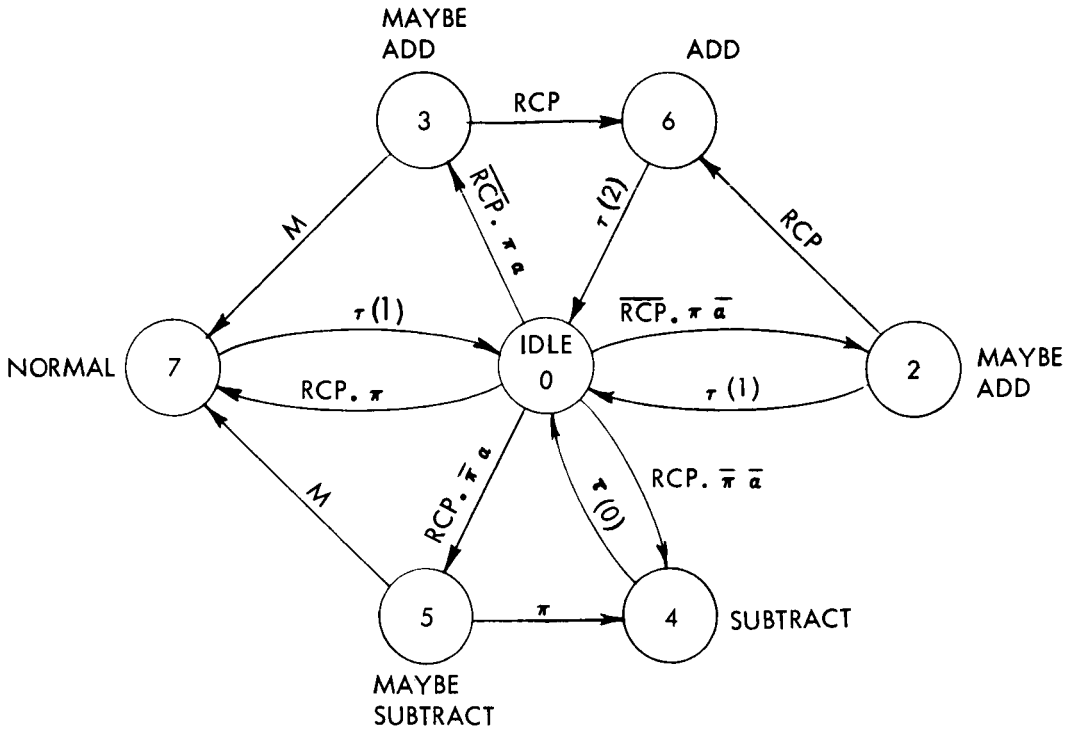

RCP - DIAGONAL RETICLE CENTER PULSE

π - COINCIDENCE BETWEEN CX AND CY

a - FIRST QUARTER OF DIAGONAL GATED AREA,
$928 \leq N\,(CX) \leq 944$ NORMAL SCAN OR $32 \leq N\,(CX) \leq 48$ REVERSED SCAN

M - MIDDILE OF DIAGONAL AREA, N (CX) = 960 NORMAL SCAN OR 64 REVERSE SCAN

$\tau(i)$ - PERIOD IN WHICH N (CY) IS INCREMENTED &
i = NUMBER OF COUNTS ADDED TO N (CY)
DURING τ

STATE	TITLE	WHY ENTERED
0	IDLE	STARTING POSITION.
2	MAYBE ADD	COINCIDENCE W/O RCP, RETICLE MISSED OR N (CY) LOW.
3	MAYBE ADD	COINCIDENCE W/O RCP, RET. MISSED, N (CY) LOW, OR N (CY) HIGH ENOUGH THAT TURNING CORNER LOST RCP.
4	SUBTRACT	N (CY) HIGH.
5	MAYBE SUB	RCP BEFORE π ; N (CY) HIGH OR N (CY) SO LOW THAT TURNING CORNER LOST π .
6	ADD	N (CY) LOW.
7	NORMAL	RCP AT π OR TURNING CORNER LOST EITHER π OR RCP.

Figure 26. Sequencing Diagram Vertical Reticulization

(7) NORMAL, CY is incremented +1 and the system returns to (0) IDLE that RCP occurs first the system moves to (6) ADD, the number in the Y counter N (CY) is incremented +2 and the system returns to (0) IDLE.

Vertical reticulization is inhibited if prior horizontal reticles were missed; if S1, S2, or S3 is on; or if the mode selected is either CAL-ORTHO, CAL-RAD, or EXT. BODY. The latter two utilize the radial sweep in which no equivalent to the diagonals exists.

Reticulization of CX is inhibited in the calibrate modes to the extent that only V_o is used. S2 also causes this effect. If the HORIZONTAL POSITION switch is placed in position 0 while in calibrate, no reticles are used, CX being reset a fixed interval after the sweep start.

DATA PROCESSOR SPECIFICATIONS

Count Rates

horizontal - 5 megacycles

vertical - 3.95 KC ± 0.05 KC

Frame Rates

orthogonal - 4.01 ± 0.12 fps (242.1 ms ≤T ≤257.1 ms)

radial - 16.98 ± 0.04 fps (58.8 ms ≤T ≤ 59.0 ms)

fps = frames/sec

T = frame time

Data Rate - 1.0 megacycle, SYNCHRONOUS

Control - Decision Making Sequential Logic

Inputs - Reticle Center Pulses, Star Center Pulses

Outputs - Data (21 bits parallel, ((10 bits for X, 10 bits of Y, 1 bit for "READ" signal)), 55 μsec* duration)

VERT RESET, SWEEP ENABLE, RADIAL COUNTER RESET,

EXTRA TRIGGER, ORTHO/RADIAL SWEEP, REVERSE/NORMAL

Modes - OMNI, DISC EDGE, STAR, CAL-ORTHO, CAL-RAD, EXTENDED BODY

Transistors- APPROXIMATELY 1100

*Adjustable duration - set to SDS 920 requirements.

Section 5

SYSTEM CONSIDERATIONS

CALCULATION OF TARGET COORDINATES

Relating a target's direction to the tracker can be done in several ways. For navigational purposes, where angular differences are to be calculated, directions cosines are particularly convenient and will be used here.

On page 10, the basic direction cosine relationships were presented. Figure 27 shows the steps required in orthogonal scan operations to get from the output of the data processor to the direction cosines. The illustrated procedure takes into account the optical transfer functions [1] and the compensation required for the Y data [2].

The optical transfer functions are the same as previously presented in Section 2 but converted to radians.

Both the optical transfer functions and the Y correction function, as given, assume that the image coordinates are in decimal form. If the binary output of the data processor is to be used directly appropriate changes must be made to these functions.

The NORM and REV notes on the figure refer to the normal and reverse modes of operations of the orthogonal sweep.

No comparable computational procedure was set up for the radial scan mode since this was primarily intended for nulling type operations.

DUAL MODE RETICLE PATTERN DESIGN

GENERAL

During Phase A of the contract, a single-mode reticle pattern was designed, procured (as part of a GEC vidicon) and tested. This pattern, which consisted of eight vertical lines and nine diagonal lines, was only suitable for orthogonal rasters with a single scanning direction. This pattern is shown in Figure 28.

To increase the versatility of the system, as an operating experimental model, Phase B of the contract incorporates a 32 radii, equally spaced, scanning pattern in addition to the orthogonal pattern.

(1) Reference Section 2, pages 10, 11 and 13
(2) Reference Section 6, page 86

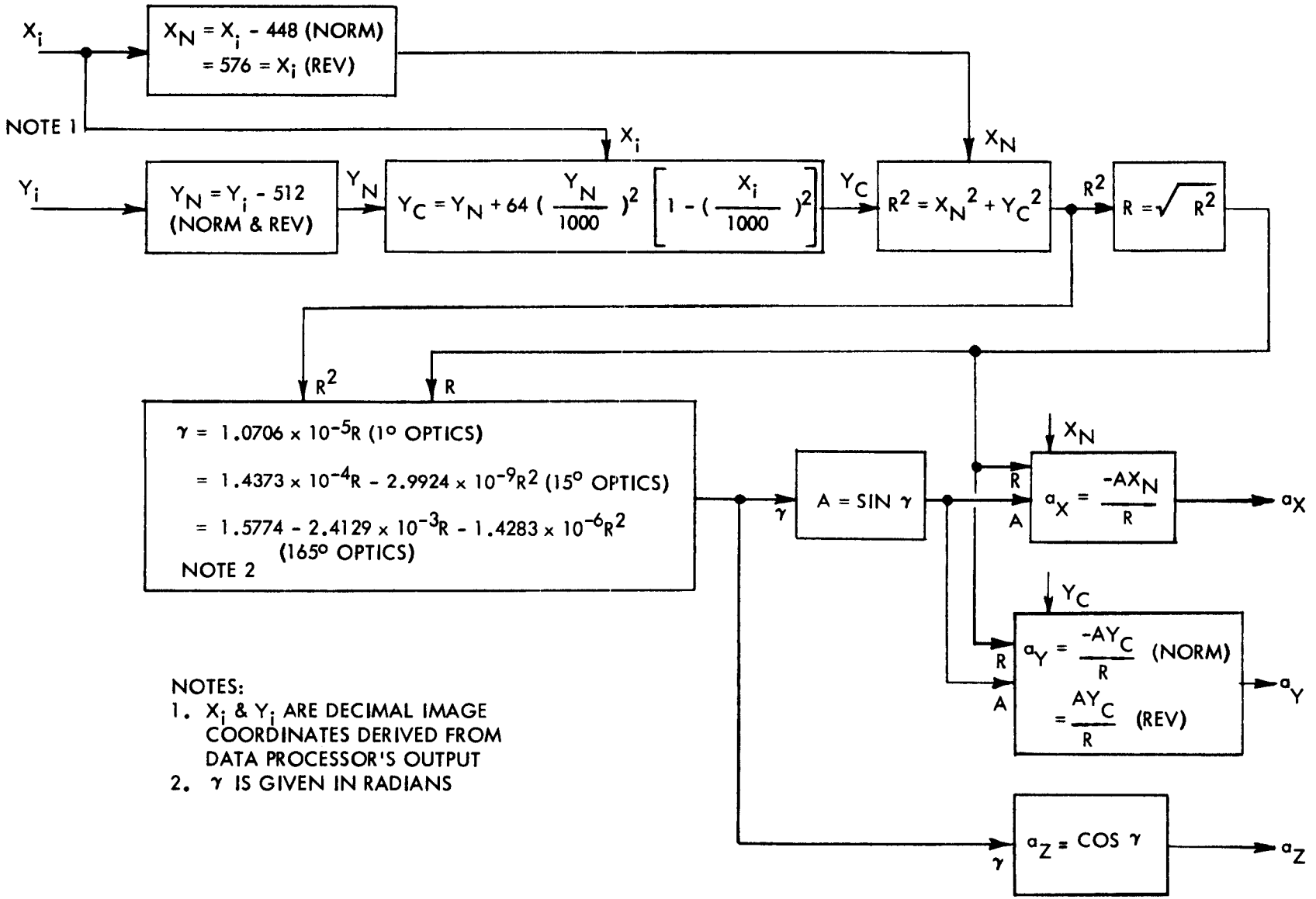

Figure 27. Direction Cosine Computation Flow Chart

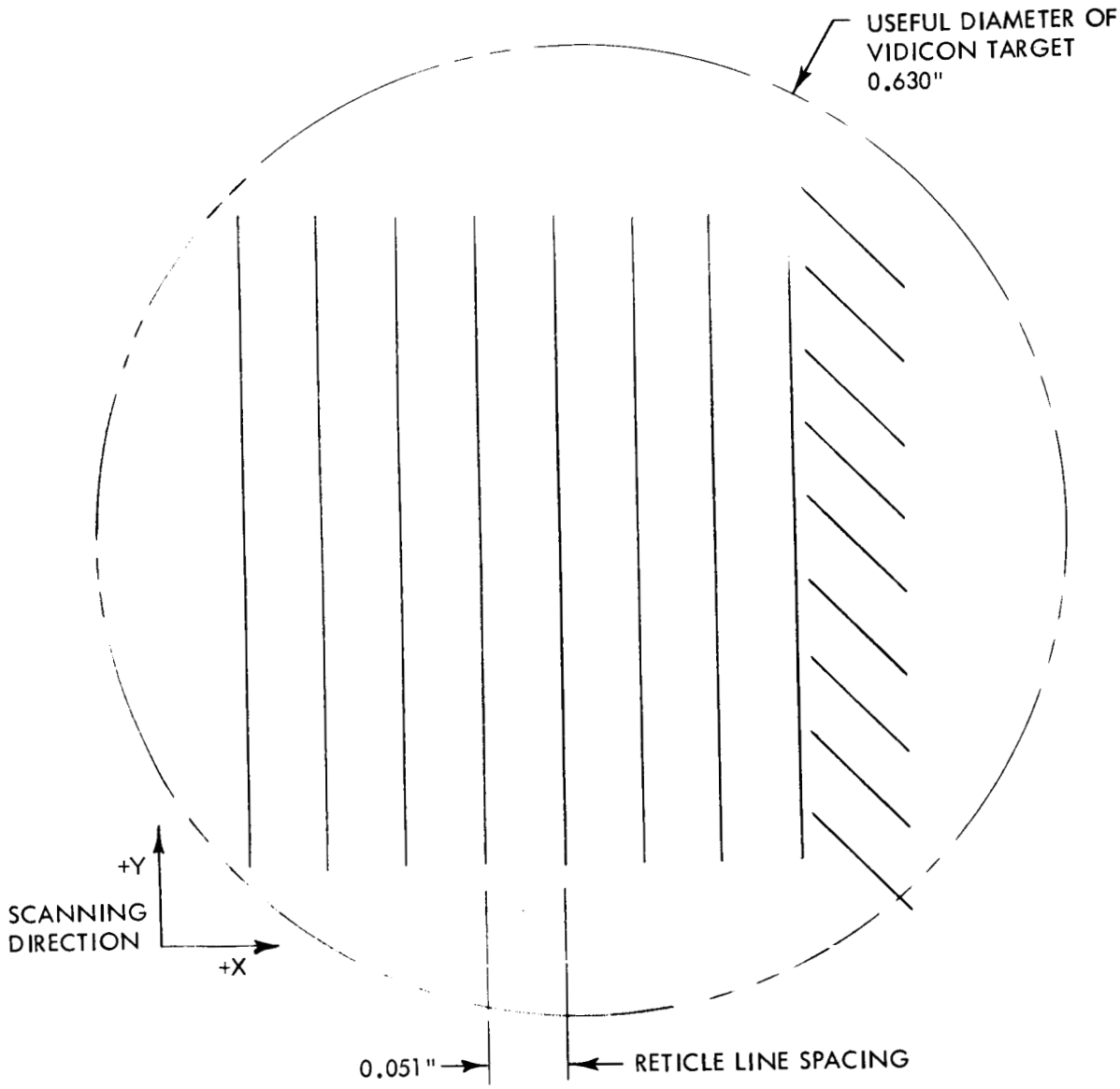

Figure 28. Single-Mode Reticle Pattern Space Sextant - Phase A Vidicon

A selection of scanning directions was also incorporated providing for:

a. Orthogonal Scan, Left to Right and Bottom to Top
b. Orthogonal Scan, Right to Left and Top to Bottom
c. Radial Scan, Center to Outside
d. Radial Scan, Outside to Center

These additional requirements necessitated a dual-mode reticle pattern which could be used for all modes of operation.

It should be stressed that this pattern was designed for purposes of experimental versatility. For a specific mission, much of the flexibility would be unnecessary and a simpler reticle pattern would suffice.

The basic horizontal correction interval of the Data Processor is 128 counts. This corresponds to the spacing between adjacent reticle lines. In the Phase A pattern, this spacing was chosen to be 0.051 inch which allowed efficient coverage of the vidicon target area with eight spacings (8 x 128 = 1024 which is the quantization of the raster in both the X and Y directions).

An attempt was made to retain this basic spacing in the new reticle pattern, but this proved impractical.

A second and more serious consideration was that the spacing intervals of the orthogonal and radial portions of the dual mode pattern be identical, otherwise the scanning rate would have had to be altered as modes were changed.

A third consideration was that the orthogonal and radial portions of the pattern have a minimum of interference with each other so that simple logical gating could be used to select between them as the modes of operation are changed.

ORTHOGONAL PATTERN

To retain the basic Data Processor Correction philosophy, developed in Phase A, eight intervals of 128 counts are again employed in both the horizontal and vertical directions. To provide for a reversal of sweep directions, however, it was necessary to add a ninth vertical line to act as a starting point in the right to left direction of scanning. Since the diagonal lines must fit inside this last interval, they cannot be as long as in Phase A. To provide for the gaps required during the manufacturing process and the horizontal overlap required by the data-processor, 16 shorter diagonals were used. (Actually 15 full length plus two shorter diagonals.) The layout of the orthogonal pattern is shown in Figure 29.

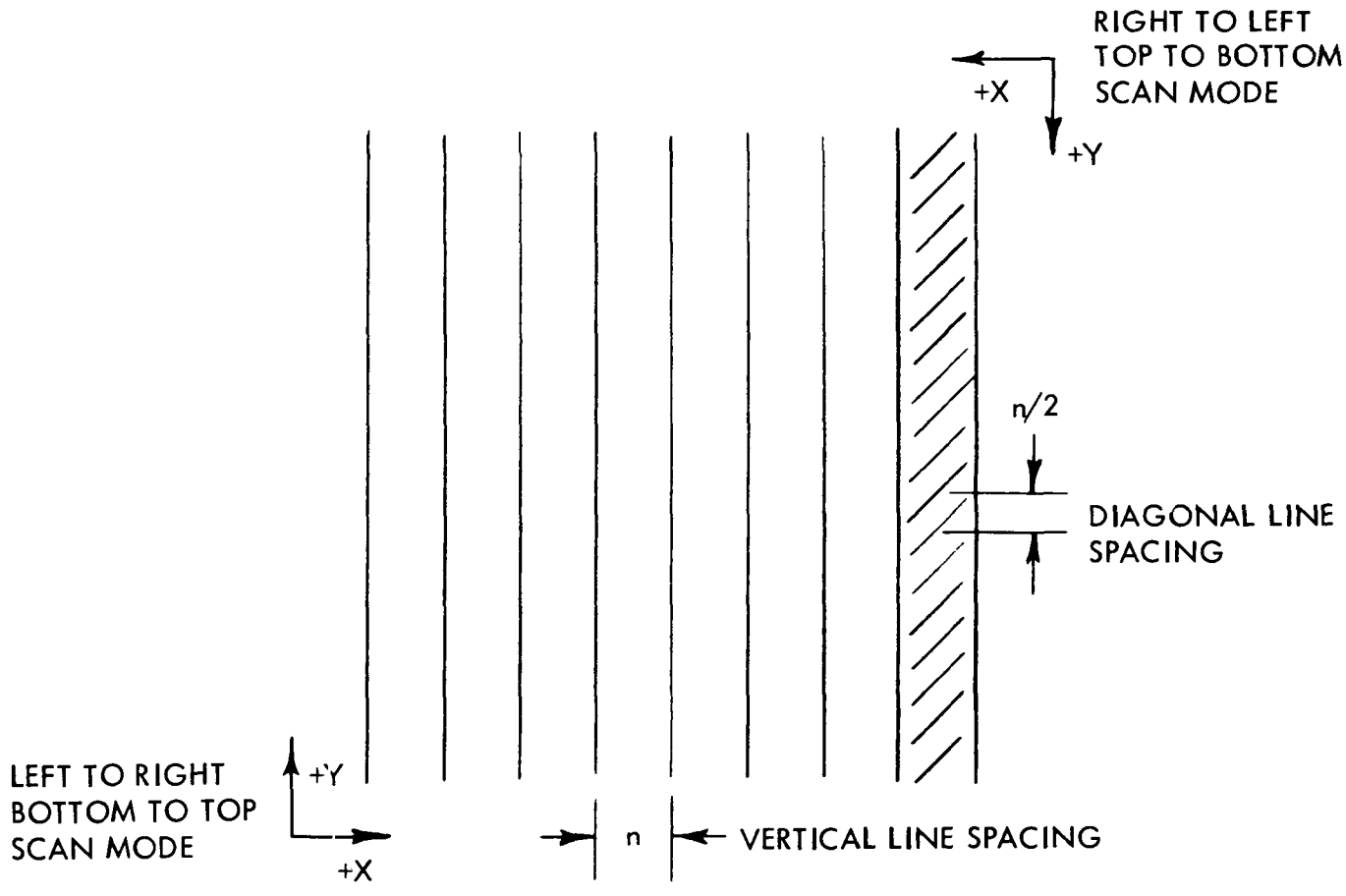

Figure 29. Orthogonal Sub-Pattern Dual-Mode Reticle

CIRCULAR PATTERN

The starting sequence for a raster line, in all modes of operation, is shown in Figure 30 below:

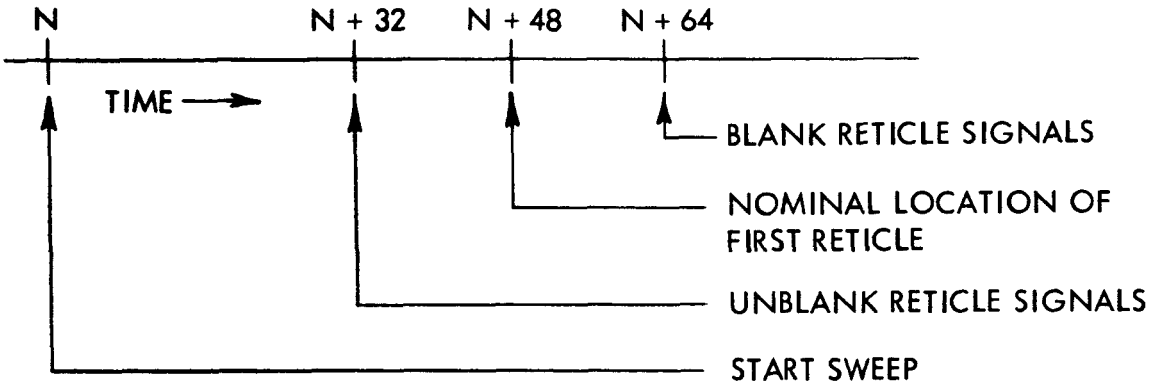

Figure 30. Raster Line Starting Sequence

This is of immediate concern in the circular pattern since it fixes the radius of the innermost circular reticle at a distance equivalent to 48 counts for the center-to-outside sweep direction.

Since the same sequence applies in the outside-to-center sweep direction, the radius of the largest circular reticle is set at 0.315 inch (radius of usable vidicon target area) less a distance equivalent to 48 counts.

This radius can also be expressed as:

$$[\ 2(48) + k(128)\ ] \quad \text{counts} \propto 0.315 \text{ inch}$$

where k = number of reticle spaces used. Table 7 lists the possible choices of k.

DUAL MODE RETICLE PATTERN

The combined orthogonal and circular pattern is shown in Figure 31.

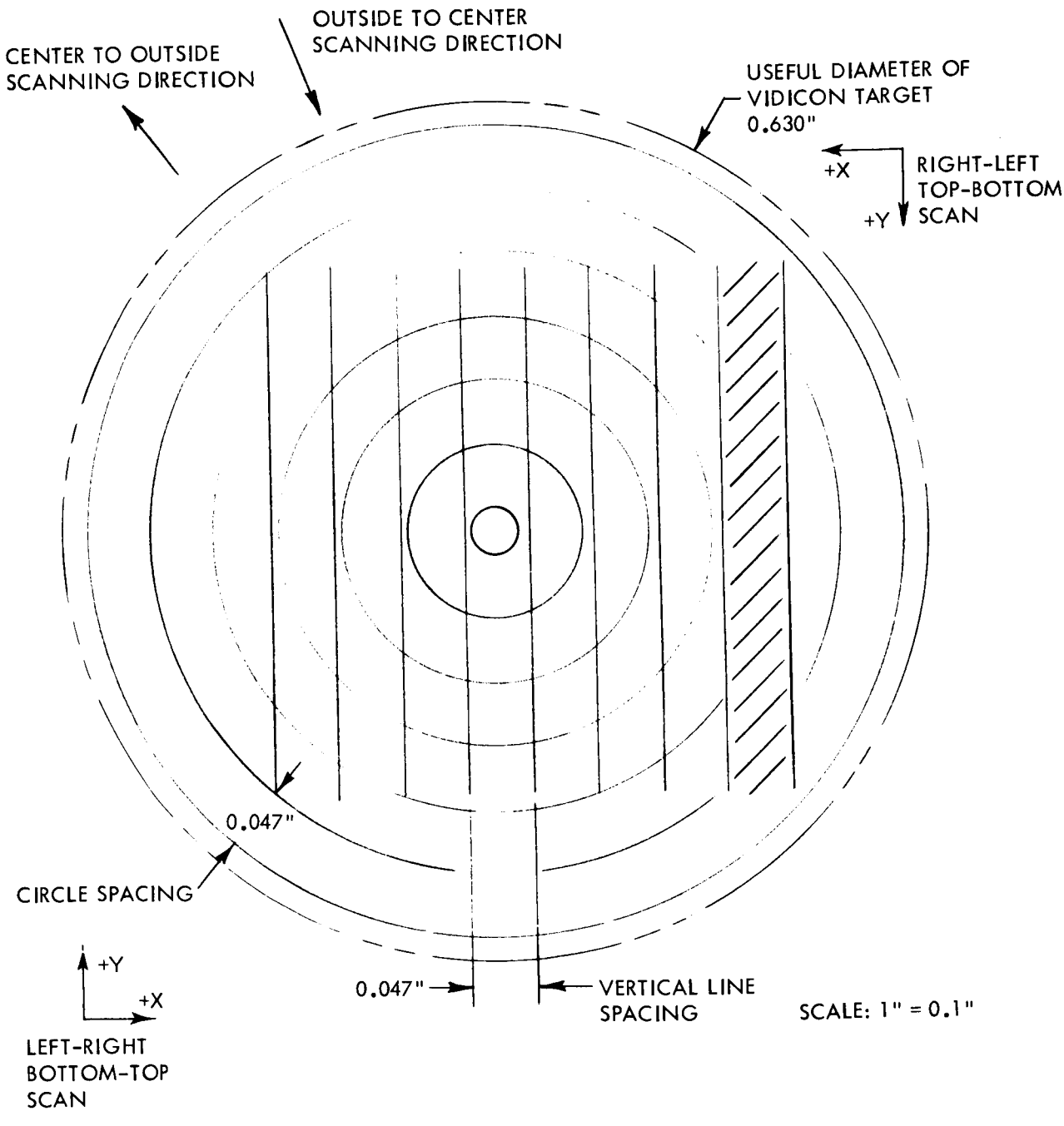

Figure 31. Dual-Mode Reticle Pattern Space Sextant - Phase B Vidicon

TABLE 7
RETICLE SPACING VS k

k	R Counts	Inches/Count x 10^{-4}	Inches/128 Counts
3	480	6.5625	0.084
4	608	5.1809	0.066
5	736	4.2799	0.055
6	864	3.6458	0.047
7	992	3.1754	0.041

A six space reticle was chosen since it allows the largest circle to fall outside the orthogonal pattern and in addition keeps the orthogonal pattern as large as possible.

DISCRIMINATION OF SUB-PATTERNS BY LOGICAL GATING

In order to provide a means of selecting the sub-patterns, certain accuracy limits were placed on the raster locations produced by the orthogonal and radial sweep circuits.

- The starting points for both types of sweeps must be repeatable within ±10 counts of true position. For the orthogonal scan, this means ±10 counts out of 1024 or ±1.0%. For the radial scan, this means ±10 counts out of 768 or ±1.3%.

- The angular accuracy of the radii of the radial pattern must be ±1 degree from true position.

In the orthogonal mode, the Data Processor provides ±16 count gating around the nominal position of the first reticle and ±8 count gating for the remainder. By providing ±0.010 inch clear area on each side of every vertical line in the pattern, the chance of picking up a circular reticle while in the orthogonal mode is eliminated (0.010 inch corresponds to 27.2 counts).

An analysis was then made of the possible areas where the orthogonal reticles could be detected in the radial mode. By providing eight selectively located gaps in the orthogonal pattern, these areas were eliminated.

In addition to these gaps, six additional gaps were required for fabrication purposes. The effect of these gaps is to permit the orthogonal scan to run uncorrected over two spaces rather than one. When the Data Processor fails to receive a reticle pulse within the gating period, it assumes one at the nominally correct location. Thus, these gaps do not produce gross errors in position locations.

Figure 37 in Section 6 is an actual photo of the finished reticle pattern and clearly shows the gaps mentioned above.

Figure 32 presents, in matrix form, the analysis of the special gating requirements for the final circular reticle pattern. The orthogonal sweep requires no special provision since it still employs the original gating around the nominal vertical reticle positions. The circular pattern never appears within these periods.

Radii 0 runs from the center of the tube to the right in Figure 37, toward the diagonals. Radii 8 is 90^{0} counter clockwise from it, Radii 16, 180^{0} from it, etc.

FRAME RATES

GENERAL

The frame period of the Space Sextant's digital readout tracker is the sum of the line scan times and reset times. Since both of these are effected by analog type variables such as sweep linearity and drift, the tracker's frame rate is not synchronized precisely with the Data Processor's clock.

A detailed discussion of the frame rate calculations will not only pin down the expected ranges for these rates, but will also give an insight to the operation of the Data Processor using the reticles for corrections.

Since these variables enter into the frame period differently for the Orthogonal and Radial scanning modes, it is necessary to consider these cases separately.

ORTHOGONAL SCAN FRAME RATE

The basic timing increment of the system is $t_c = 0.2$ μsec. corresponding to one count of the Data Processor's 5 mc clock.

There are nominally 1024 horizontal lines each corresponding to 1024 clock pulses. The Data Processor's horizontal counter is set to zero when the first reticle line is crossed. At each succeeding reticle line, the counter will have increased its content by 128 counts assuming perfect sweep linearity. If the sweep rate deviates from nominal, this is accounted for by adding or subtracting counts from the horizontal counter. Thus, each reticle crossing will correspond to a count of multiple of 128, but the time between reticles is a variable.

CIRCULAR RETICLE NUMBER

RADIAL RASTER RADII NUMBER	0	1	2	3	4	5	6
0					G		
1					G		
2					G		
3					G	G	
4			P	P		G	
5		P*	P		P		
6		NR		P*	P		
7		P*	NR	P	P*		
8							
9		P*	NR	P	P*		
10		NR		P*	P		
11		P	P		P		
12			P	P		P*	
13					G		
14							
15							
16							
17							
18							
19					G		
20			P	P		P*	
21		P	P		P		
22		NR		P*	P		
23		P*	NR	P	P*		
24							
25		P*	NR	P	P*		
26		NR		P*	P		
27		P*	P		P		
28			P	P		G	
29					G	G	
30					G		
31					G		

LEGEND:
G = LOGICAL GATING REQUIRED
P = LESS THAN 1/2 THE GATE IS OCCUPIED BY RETICLE
P* = MORE THAN 1/2 THE GATE IS OCCUPIED BY RETICLE
NR = NO RETICLE

Figure 32. Reticle Crossing Analysis

Conservatively assuming a ± 1% sweep rate linearity for the full line, and considering that there are eight reticle intervals, the linearity effect to be considered is the • 1/8% = ± 0.125%. In the nominal 128 count reticle interval, this corresponds to ± 1.56 counts ≈ ± 2 counts.

Under worst case conditions, the total line time, in terms of clock pulses, can vary as much as ± 8 x 2 = ± 16 counts. However, considering the fact that rate errors all in one direction can be corrected by an adjustment in the nominal sweep rate, a more reasonable variation will be ± 8 counts for a full line.

After crossing the last reticle, the sweep continues for an additional 64 counts to discharge the nearby area of the target and reduce geometric distortions in the vidicon. Thus, the basic horizontal line time, $t_{h\ell}$, in terms of clock pulses, is:

$$t_{h\ell} = 1024 + 64 \pm 8 = 1088 \pm 8 \text{ clock pulses}$$

At the end of each line, a blanking period, t_{hb} is generated by the processor during which time the electron beam is returned to its horizontal starting point. This period, in clock pulses is:

$$t_{hb} = 96 \text{ clock pulses}$$

At the end of the period, the system begins to look for the first reticle line, which is nominally 16 clock pulses away. Uncertainties in the starting point due to circuit drifts, etc., allow this time to the encounter to vary by as much as ± 16 counts so that the search interval, t_{hs} in clock pulses is:

$$t_{hs} = 16 \bullet 16 \text{ clock pulses}$$

At the completion of the 1024th line, the processor initiates a vertical blanking period during which time the beam is returned to both its vertical and horizontal starting points.

This vertical blanking period, t_{vb} in clock pulses is:

$$t_{vb} = 16\,(1088 + t_{hb} + 32) + 5$$

- 1088 is nominal value of $t_{h\ell}$
- 32 is max. value for t_{hs}
- 5 is a nominal value of additional counts required to restart sweep.

$$= 16\,(1216) + 5$$

$$= 19456 \text{ clock pulses}$$

The total number of lines in a frame, due to uncertainties in vertical starting position is:

$$N = 1024 \pm 10 \text{ lines}$$

The total orthogonal frame time, T_o, can now be expressed, in clock pulses, as:

$$T_o = N [t_{h\ell} + t_{hb} + t_{hs}] + t_{vb}$$

$$= (1024 \pm 10) [(1088 \pm 8) + 96 + (16 \pm 16)] + 19456 \text{ clock pulses}$$

Each clock pulse corresponds to 0.2 μsec so the orthogonal frame rate is:

$$F_o = 4.01 \pm 0.12 \text{ frames/sec}$$

RADIAL SCAN FRAME RATE

In the radial scan 32 equally spaced active radii are used. The same Data Processor clock rate (5 mc) is used here as is used in the orthogonal scan. Each of these radii has an active length corresponding to six reticle spaces of nominally 128 counts each. However, the Data Processor continues to count up to 1024 (the basic orthogonal scan line length) before considering the line complete. No corrections are made after crossing the sixth reticle. Allowing for sweep non-linearities, the basic radial line time, $t_{r\ell}$ in terms of clock pulses, is:

$$t_{r\ell} = 6 (128) \pm 6 + 2 (128)$$

$$= 1024 \pm 6 \text{ clock pulses}$$

Each line has associated with it a blanking period t_{vb} which is the same as for the orthogonal horizontal blanking:

$$t_{vb} = t_{hb} = 96 \text{ clock pulses}$$

Similarly, the search period for the first reticle t_{vs} is the same as in orthogonal scan so that:

$$t_{vs} = t_{hs} = 16 \pm 16 \text{ clock pulses}$$

For every active radii produced, the processor goes thru the motion of counting out 7 blanked radii which are not used. The length of time of these

radii is the same as for the active radii except that:

t_{vs} = 32 clock pulses

$t_{r\ell}$ = 1024 clock pulses

Once each frame, an additional blanking period of five counts is employed to allow for data handling.

A total radial frame period can now be expressed as:

$$T_R = N \left[t_{r\ell} + t_{vb} + t_{vs} + 7 \left(t_{r\ell}\,(\text{nom}) + t_{rb} + t_{vs}\,(\text{max}) \right) \right]$$

$$T_R = 32 \left[(1024 \pm 6) + 96 + (16 \pm 16) + 7\,(1024 + 96 + 32) \right] \text{ clock pulses}$$

Each clock pulse is equivalent to 0.2μ sec so the radial frame rate is

$$F_R = 16.98 \pm .04 \text{ frames/sec}$$

Section 6

TESTS

INTRODUCTION

The great versatility of the Space Sextant tracker system called for a wide variety of tests to establish acceptable performance. The tests fell into two basic categories: component tests and system tests. The tests performed are listed below:

- Component Tests
  1. 15^{o} Optics Evaluation
  2. Mechanical Evaluation of Vidicon Reticle
- System Tests

Optics	Target	Test	Comments
Narrow Mode	Single Simulated Star	Angular Accuracy	Ortho Scan
Intermediate Mode	Single Simulated Star	Slewing	Ortho Scan
	Multiple Simulated Stars	Interangle Accuracy	Ortho Scan
	Simulated Ext. Disc.	Disc Center Accuracy	Ortho and Radial Scan
	Real Stars	S/N Ratios	Ortho Scan

The tests performed were by no means exhaustive, primary stress being placed on determination of the angular measurement accuracy of the system on point source targets. However, sufficient data was taken in the other areas to establish overall feasibility of the tracking concepts and satisfactory performance of the system in all modes of operation was demonstrated.

TEST FACILITIES

OPTICS LABORATORY

With the exception of the photometric tests on actual stars, all of the component and system tests were conducted in the Optics Laboratory at General

Electric's plant in Johnson City. A general view of the laboratory is shown in Figure 33.

The large steel slab table shown in this figure, which is mounted on an isolated foundation, formed the test bed for all of the angular measurements.

ANGULAR MEASUREMENTS

For all angular tests the tracker head was mounted, as shown in Figure 33, on a Griswold Model OPL dividing head.

For tests using the intermediate mode optics, the dividing head's azimuth readout was used directly as an angular measurement. This readout is good to ±5 arc sec, or about 1/60 of the resolution limit of the tracker with these optics.

The elevation axis of the dividing head was used for coarse positioning only and its readout, accurate to perhaps 15 arc min, was not used to measure angular accuracy.

For tests using the narrow mode optics, an auto-collimator was used to measure angular motions. This device is described below:

Ernst Leitz GMBH Wetzlar
(Opto-Metric Tools Inc.)
List 85-5a/Engl. R
20 arc min range both azimuth and elevation
0.5 arc sec gradation
0.1 arc sec accuracy and readibility

The auto-collimator was used with a Kollmorgen Model K22-3.5" mirror mounted on the dividing head.

STAR SIMULATORS

The collimated, single-star simulator consists of a tungsten arc and pin hole assembly placed at the prime focus of a 8" f/8.0 parabolic mirror. This setup is the same as used in Phase A of the program[1].

An uncollimated, multiple star simulator was constructed for use on the Space Sextant contract[2]. The method of simulating the stars was to illuminate one side of a sheet of vellum with a projector, and to cover the other

(1) Reference 1, Pg. 99
(2) Reference 4

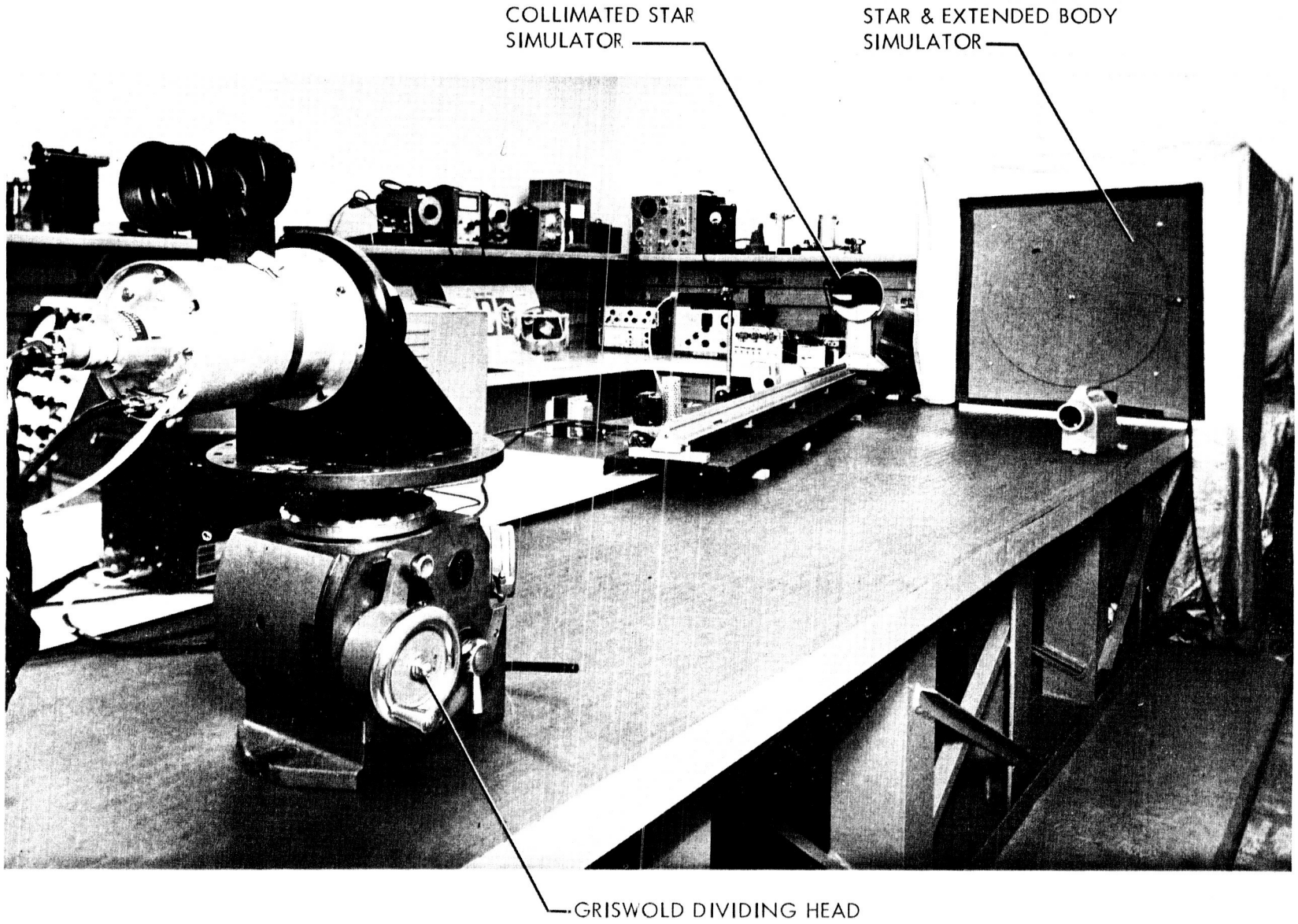

Figure 33. Electro-Optics Laboratory - General View

side with a sheet of non-transparent material in which there are several pinholes representing the stars.

The star simulator assembly consisted of a 3 ft. x 3 1/2 ft. background with a rotatable pattern of five stars. Star magnitudes from about -1 to +2 MV could be simulated at a color temperature of about 3250^{O}K.

The entire assembly including the projector was covered with an opaque canvas sheet to keep the stray light level in the laboratory down to an acceptable level. The complete assembly is shown in Figure 33.

These uncollimated targets were used only with the intermediate mode optics. Tests confirmed that the image quality of these optics was not detectably different for target distances of 11' - 0" than it was for infinitely distant (collimated) targets. There was, of course, a scale factor change in the optical transfer functions which must be accounted for in evaluating the resulting test data.

The pinholes simulating the stars were made in aluminum foil about 0.019 inch in diameter and were centered in larger 1/8 inch diameter holes in the textolite cover. This pinhole size was sufficiently small to provide an accurate point source, yet large enough to give sufficient light for the desired maximum magnitude star.

The approximate visual magnitude of the simulated stars was determined by measuring the brightness of the vellum screen with the pinholes removed and then multiplying this brightness by the area of the pinhole to establish the intensity of the "point" source. Using the measured distance from the pinhole plane to the optics entrance pupil (11' -0") the equivalent visual magnitude was then calculated. Screen brightnesses were measured using a Spectra Brightness Spot Meter, Model VB.

The visual magnitudes were varied by means of neutral density filters in the projector. Table 8 lists the ranges available.

The simple star pattern used is shown in Figure 34. The dimensions given are actual measurements made between star centers and are accurate to ±0.015".

By covering up selected pinholes and rotating the entire pattern, a wide choice of target arrays was available.

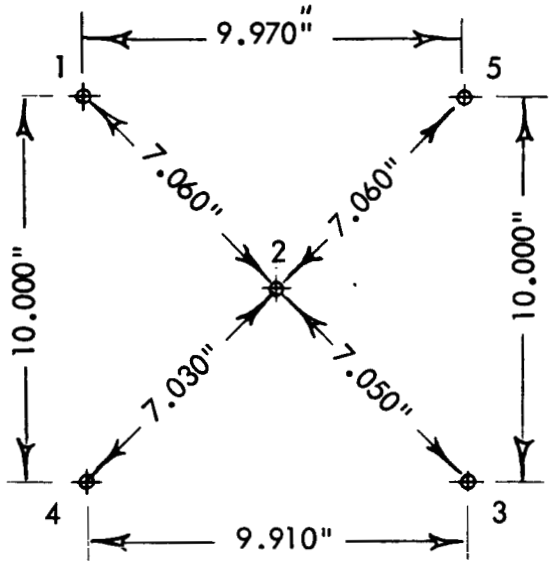

Figure 34. Layout-Star Pattern Simulator

TABLE 8

STAR SIMULATOR RANGE

Filter Density	Approx. Star * Magnitude
No filter	- 1.0 MV
0.3	- 0.2
0.6	+ 0.5
0.9	+ 1.3
1.2	+ 2.2

* At 11' -0" from the pinhole screen

EXTENDED BODY SIMULATOR

Extended bodies were simulated in a manner similar to that used for the uncollimated star patterns[1]. The same projector, vellum screen setup was employed with the pinhole patterns replaced by two interchangeable semicircular masks.

The brightness of the screen was varied by means of neutral density filters in the projector. Table 9 lists the available brightness values.

TABLE 9

DISC SIMULATOR RANGE

Filter		Normalized	Brightness
Density	Transparency	Brightness	ft-lamberts
No filter	1.00	1.00	86.0
0.3	0.50	0.46	40.0
0.6	0.25	0.25	21.5
0.9	0.126	0.12	10.3
1.2	0.063	0.052	4.5
1.2 + 0.3	0.0316	0.026	2.2
1.2 + 0.6	0.0158	0.013	1.1
1.2 + 0.9	0.0079	0.0062	0.54

(1) Reference 9

The layout of the masks is shown in Figure 35. Tolerance on the radii is ±0.01" and on roundness of the openings is ±0.002".

In use, the optics entrance pupil was located 11' -0" from the plane of the masks.

INTERMEDIATE MODE OPTICS

In checking the image quality and transfer function characteristics of the intermediate mode optics essentially the same procedure was used as for the narrow mode optics in Phase A[1].

The collimated simulated star was used as a target. The optics were mounted on the dividing head which served as the angular measurement device. A microscope mounted on a precision cross slide was used to study image quality and displacement. Cross motion of the microscope was measured with a dial indicator[2].

The effects of displacement on image quality are shown in Figure 36. Out to the limits used by the vidicon (±6.8° max.) the image suffered negligible degradation. Theoretically, the size of the image should be the size of the pinhole in the collimated star simulator (7×10^{-4}" diameter) reduced by the ratio of the optics focal length (2.56") to that of the collimator (64") or approximately 3.5×10^{-5}" diameter. The optical resolution is such that the image produced is 2×10^{-4}" diameter. This is still well under the resolution limit of the vidicon which is approximately 10^{-3}".

The results of the transfer function test have already been presented on page 11, (Figure 4).

VIDICON WITH RETICLE

The original specification submitted to General Electrodynamics for the dual-reticle vidicon is outlined below:

o Vidicon Characteristics

The vidicon was to be a 1" E/S deflected and focused unit with an S-18 response optimized for a 5 frames/sec, 1024 line scanning system with low light level operation (0.01 to 0.05 ft. candles at the vidicon target).

(1) Reference 1, pp. 109
(2) See Reference 2 for complete details

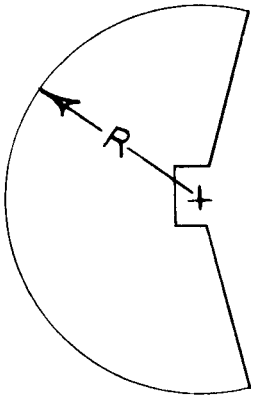

MASK	R
1	3.00"
2	6.00"

Figure 35. Mask Layout Extended Disc Simulator

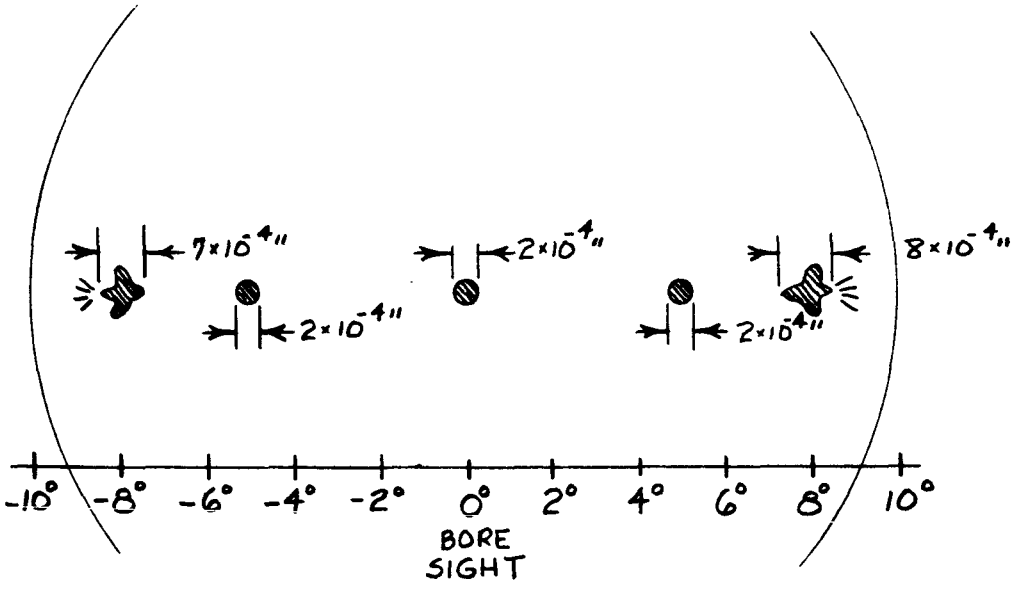

Figure 36. Image Quality Intermediate Mode Optics

The usable target area was to be the standard 0.63" diameter.

In all respects, except for the new reticle design, this tube was similar to the GEC Vidicon Type 1351-50 with the type 1 surface previously furnished to the General Electric Company (Phase A).

o Reticle Pattern

The reticle pattern was to be as shown in Figure 31.

The following paragraphs supplement this figure:

o Positioning of the Reticle

The pattern was to be positioned on the vidicon target so that the center of the concentric circles coincides with the zero deflection point of the vidicon.

The pattern was to be oriented so that the vertical lines are perpendicular to the vidicon's scan lines to within ±15 arc min.

o Reticle Signals

The reticle was to produce "blacker-than-black" pulses in the video signal under zero target illumination conditions (the vidicon face is covered). Under normal operating conditions, the reticle should produce a minimum of -33% modulation in a 3.0 nano-ampere dark level.

o Gaps in Reticle Lines

Due to the operating characteristics of our system, it is necessary that the inner circular reticle (0.017" Radius) and the first and last vertical reticle be continuous (unbroken).

Gaps are permissible in the remaining reticle lines.

General Electrodynamics Corporation took exception to the paragraph on positioning the reticle as it was agreed that fine centering of the pattern would be done by offset biasing of the sweeps and that a $\pm 3^{o}$ orientation tolerance would be acceptable.

The electrical performance of the vidicon was checked both by General Electrodynamics Corporation and General Electric and found to be acceptable. Reticle modulation up to 70% was observed and adequate signals from low level star images were achieved.

The overall reticle pattern was checked using an optical comparator which projected a magnified image of the reticle (50X) on a screen where it was photographed. The resulting picture is shown in Figure 37. In this figure, the white lines are the reticle. The black lines are the grid pattern in the comparator.

A dimensional check was then made of the reticle pattern using a microscope on a cross-slide with the slide movement measured by a dial indicator[1]. The results of these measurements are shown in Figure 38.

Additional tests were also made to determine line width and pattern orientation. The summary of results is shown in Table 10.

TABLE 10

RETICLE MEASUREMENT RESULTS

	Specified	Measured
Ortho Reticle Spacing	.0470"	.0470" + .0004" - .0003"
Radial Reticle Spacing	.0470"	.0470" + .0006" - .0003"
Reticle Line Width	.0010"	.0010" + .0007" - .0000"
Reticle Pattern Orientation[2]	$\pm 3.0^{o}$	$+ 3.0^{o}$

PHOTOMETRIC SENSITIVITY - ACTUAL STARS

The sensitivity of the vidicon camera was demonstrated with the intermediate mode optics and using actual stars as targets.

The tests were conducted on the night of 1/14/65 between the hours of 9:00PM and 12:00PM at General Electric, Johnson City.

Viewing conditions were good with some small evidence of sky glow from the city and haze from industrial plants in the area.

The stellar target of opportunity was the constellation Orion. This constellation is easily recognized and provides a fine range of magnitudes.

(1) Reference No. 6
(2) Measured with respect to orthogonal raster lines

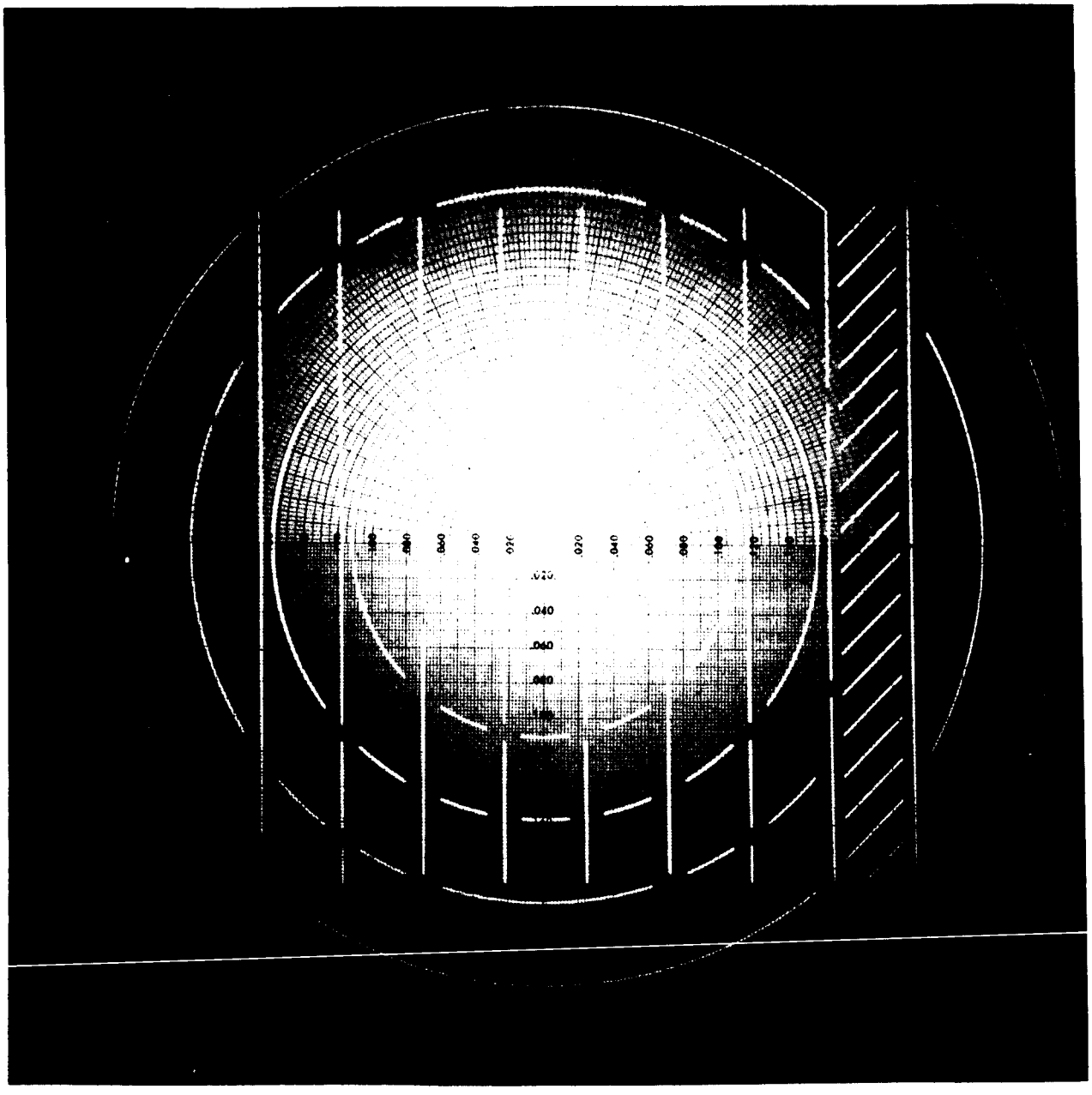

Figure 37. Optical Comparator Presentation of Dual Reticle Pattern

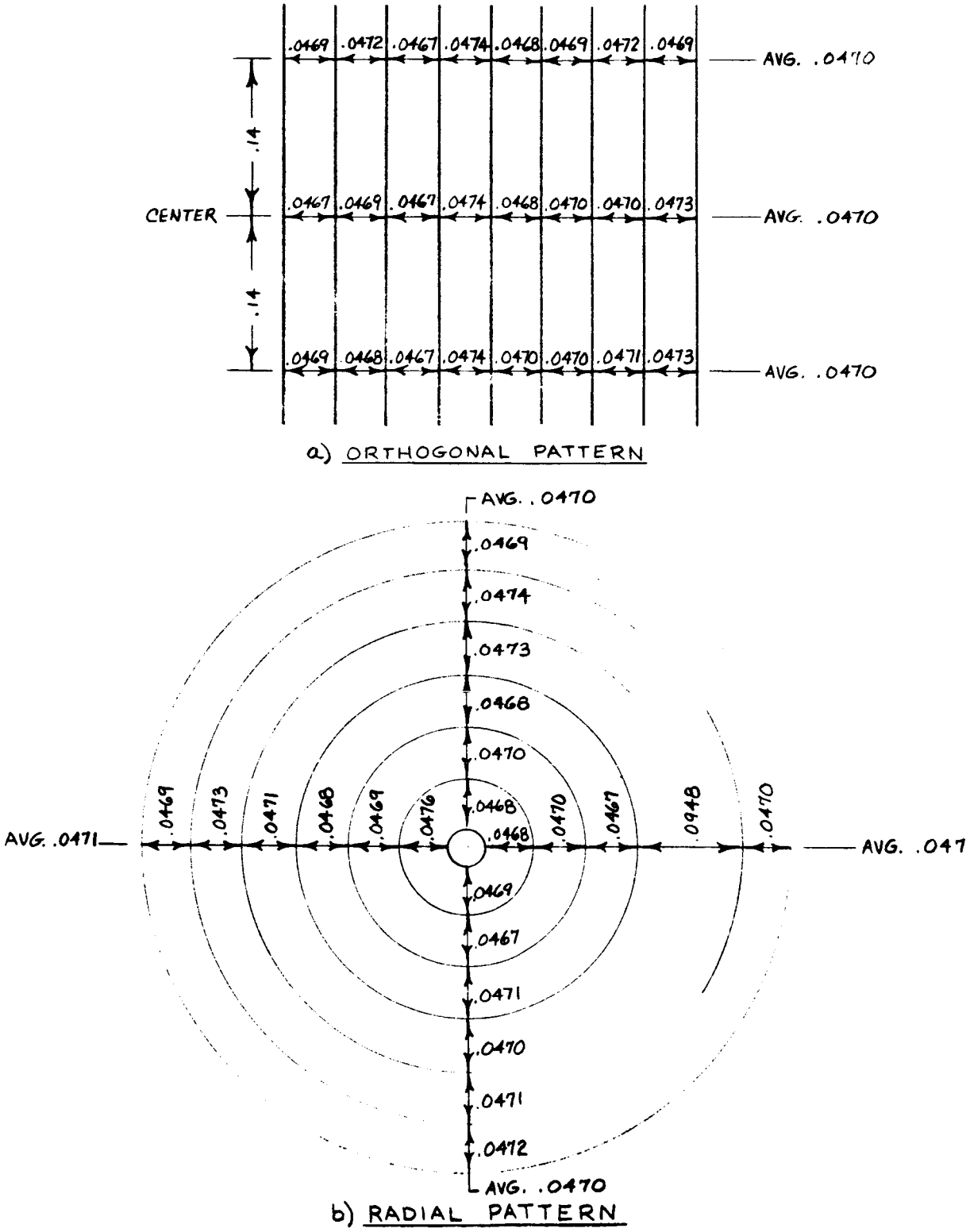

Figure 38. Dual Reticle Dimension Check

The stars used as targets were:

TABLE 11

TARGET STAR LIST

Star	Type[1]	Visual Magnitude[1]
β Orionis (Rigel)	B8	.08 to .20 Variable
α Orionis (Betelgeuse)	M2	.06 to .75 Variable
ϵ Orionis (Alnilam)	B0	1.70
ζ Orionis	09.5	1.79
δ Orionis	09.5	2.2 to 2.5 Variable

Figure 39 illustrates the video signals obtained at the input to the video processing circuits of the camera for the three dimmest stars used. The negative spikes in this figure are the reticle pulses, the star signals are the positive pulses.

Figure 40 illustrates the relationship between peak signal and visual magnitude for the targets used. The variable nature of the stars and the uncertainty about absolute viewing conditions makes it impossible to determine any precise relationships from this data. However, it is evident that:

- The camera system has adequate sensitivity to track 2.0 magnitude stars.
- The camera has sufficient dynamic range to cover a change of at least two visual magnitudes in target intensity without the need for filters or aperture changes.

SLEWING RATES

The vidicon's sensitivity depends largely on the integration of the target energy's effect on the photoconductive material between successive discharges by the electron beam. Target motion, in general, will reduce the output signal by cutting down on the integration time. Target motion also, in general, produces a non-symmetrical "smearing" or widening of the signal pulse which can detract from position determination accuracy.

A series of tests were conducted to determine the seriousness of these effects particularly at target motions up to the basic "resolution angular rate" of the data processor. This angular rate can be defined as the target motion which produces a change of 1 count in one frame time.

(1) Reference No. 10

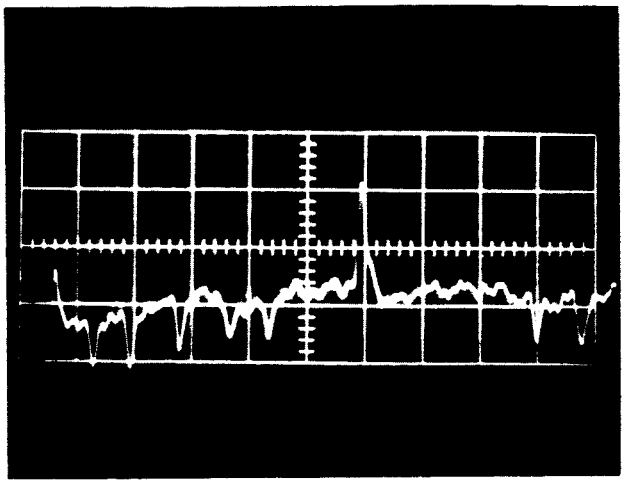

STAR: ε ORIONIS

TIME: 11:32 PM

SCALE: Y = 1V/CM
X = 20μS/CM

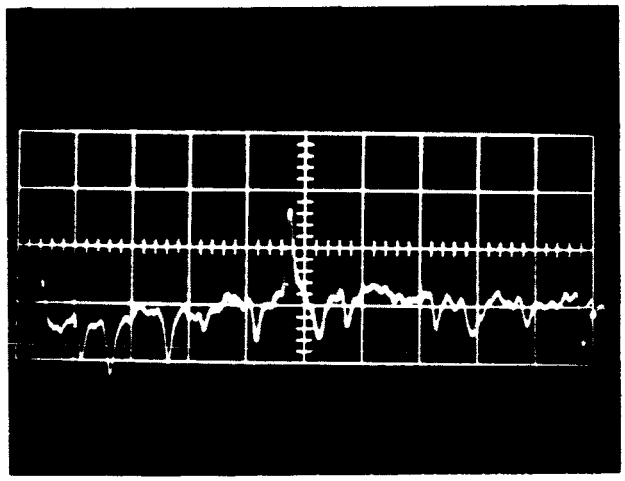

STAR: ζ ORIONIS

TIME: 11:35 PM

SCALE: Y = 1V/CM
X = 20μS/CM

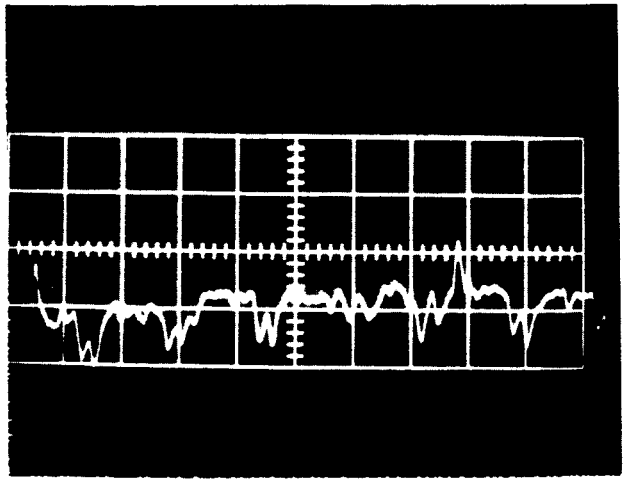

STAR: δ ORIONIS

TIME: 11:45 PM

SCALE: Y = 1V/CM
X = 20 μS/CM

Figure 39. Photometric Test Results (sheet 1 of 2)

FULL FRAME PRESENTATION
ORION'S BELT
LEFT TO RIGHT
δ (2.48 MV)
ϵ (1.75 MV)
ζ (2.05 MV)

SCALE: Y = 1V/CM
X - 20 MS/CM

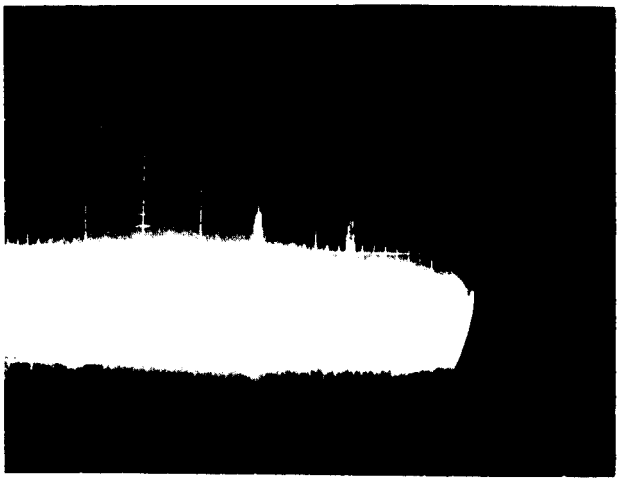

REPEAT OF ABOVE

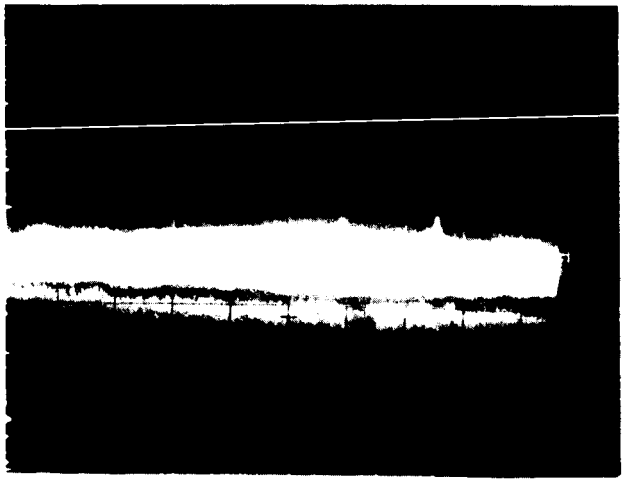

REPEAT OF ABOVE
BUT Y = 2 V/CM

Figure 39. Photometric Test Results (sheet 2 of 2)

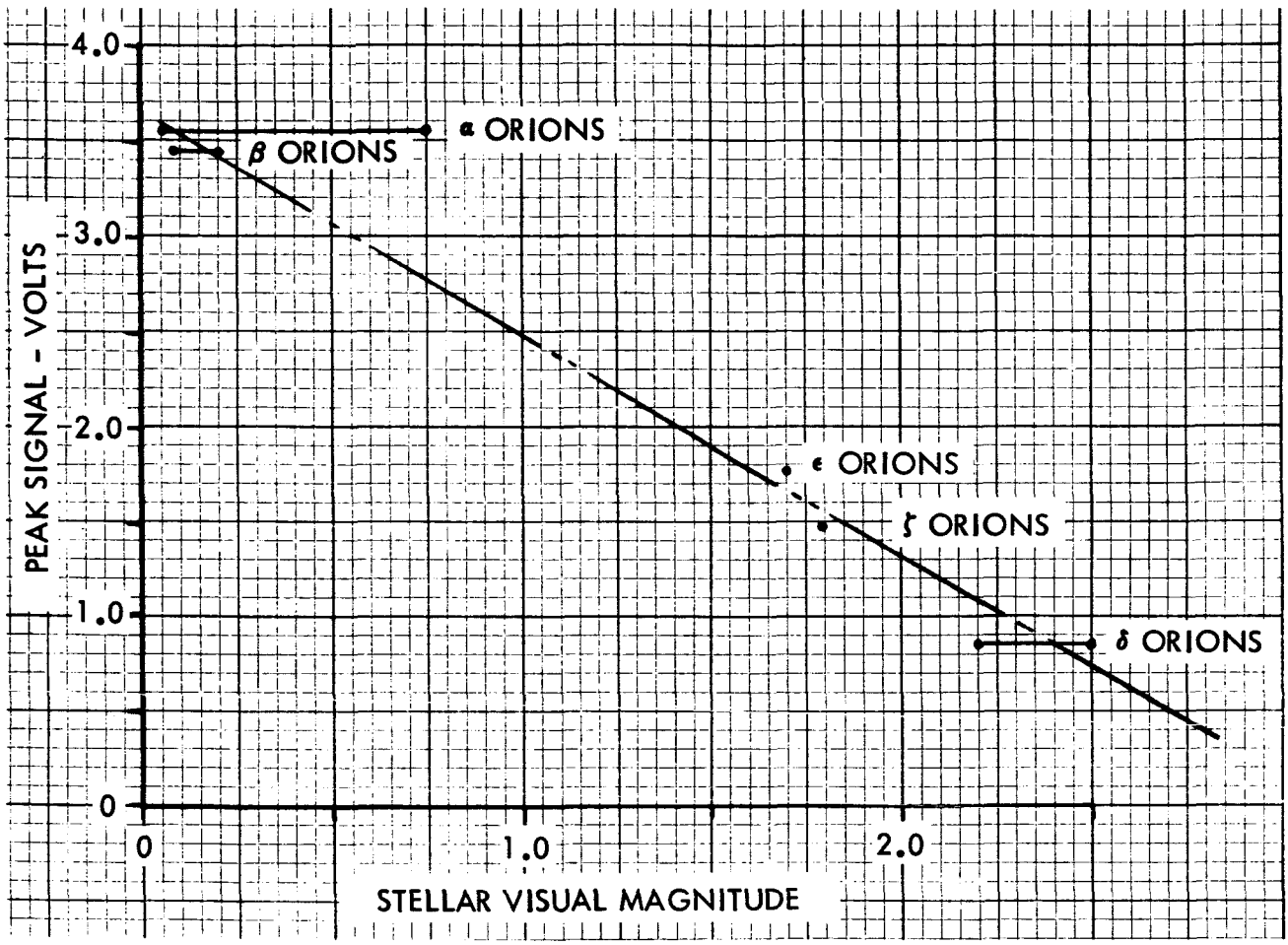

Figure 40. Peak Signal vs. Visual Magnitude

for the three optical modes this rate is given below[1]:

TABLE 12

RESOLUTION ANGULAR RATES

Optical Mode	Resolution Angular Rate
a. Narrow	0.15°/min
b. Intermediate	2.1°/min
c. Wide	13.1°/min

The tests were run with the intermediate mode optics using the collimated lab star as a target. This "star" was adjusted for +0.5 to +1.0 visual magnitude. The tracker head was mounted on a rate table which had a range of approximately 1 to 50°/min. Rate was determined by measuring the calibrated output of the rate tables' drive tachometer.

Figure 41 illustrates the results of the tests. Up to the resolution angular rate limit for these optics, the peak signal shows negligible degradation. Above 1 deg/min, about 1/2 the resolution angular rate, the signal width begins to increase. At the resolution rate of 2.1°/min, the width is increased by less than 30% and is still within the pulse center detection limits of the system. There is some degradation of symmetry, however, which would cause a lagging error in the digital readout.

The tests show that for slewing rates in excess of the resolution angular rate, system performance will be degraded.

ANGULAR ACCURACY TESTS

The angular accuracy tests were run with the Narrow Mode Optics using the collimated lab star as a target.

89 test points were run, 58 in azimuth and 31 in elevation. The azimuth and elevation tests were run separately, rotating the tracker head 90° between them to take advantage of the sensitive adjustment axis of the dividing head.

The points were chosen, in general, to be clear of reticle patterns. The azimuth points were run in 7 groups at constant elevations while the elevation points were run in 5 groups at constant azimuth. Figure 42 illustrates the locations of the test points in the image plane of the vidicon.

Using a least squares computer program, first order polynominals were fitted to the data and deviations of the individual test points from these polynominals computed.

(1) Calculations are based on a nominal frame time of 4.2 fps.

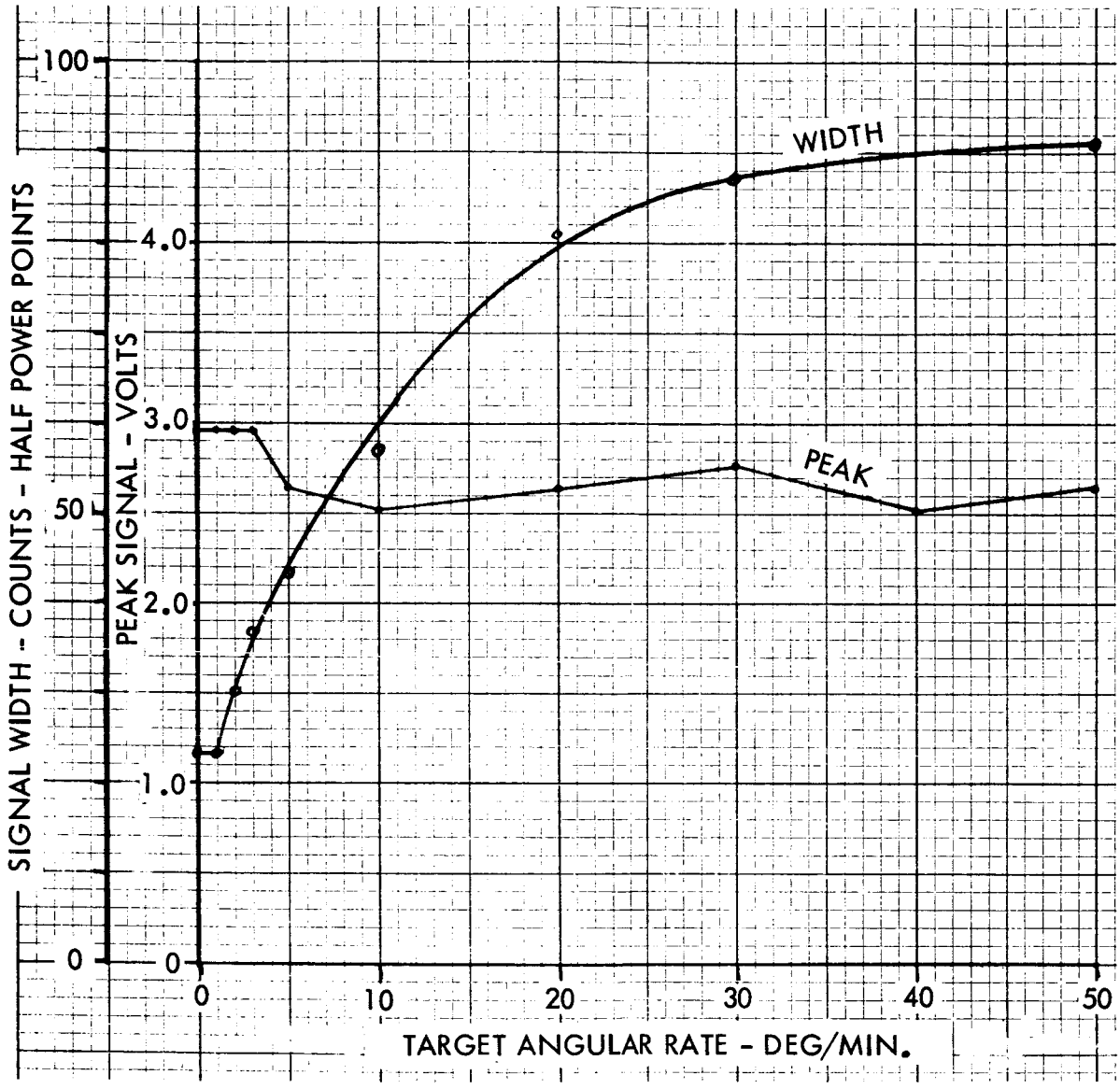

Figure 41. Signal Peak and Width vs. Angular Rate

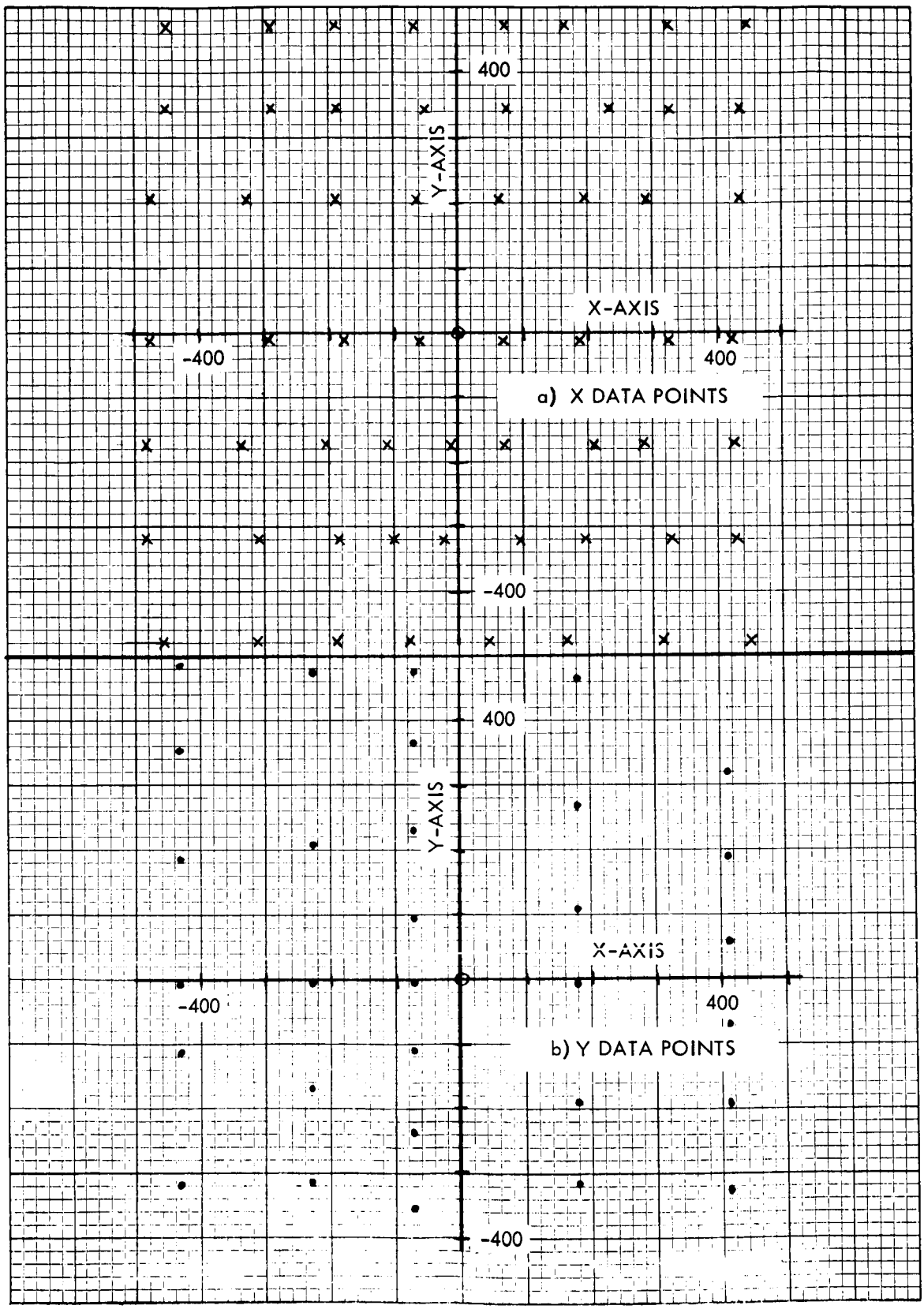

Figure 42. Linearity Test Point Locations

From the results of the elevation tests, it was apparent that there remained a residual non-linearity in the Y-axis due to geometric distortions in the vidicon not fully compensated for by the diagonal reticle and to non-linearities in the sweeps. Since the individual data points yielded steady readings and the composite data indicated an overall pattern, a Y compensation equation was determined empirically. This equation was of the form:

$$Y_c = Y_n + 64\left(\frac{Y_n}{1000}\right)^2\left[1 - \left(\frac{X_i}{1000}\right)^2\right]$$

Where

Y_c is the compensated reading

Y_n is the decimal coordinate normalized about 512

X_i is the unnormalized decimal coordinate

No such compensation was found necessary for the X data.

Applying this compensation to the Y data, the least squares program was re-applied. The composite linear coefficient relating off-axis angle to data processor counts was found to be:

$$\gamma_n = 2.2111\ (X \text{ or } Y_c) \text{ arc sec}$$

This result compares within 0.13% to the results obtained by measurements on the optics alone which were discussed in Section 2.

Figures 43 and 44 show the deviations of the X and compensated Y data from the linear fit. For convenience, the deviations are shown in counts, each count being equivalent to 2.2 arc sec.

An analysis of the deviations shows that in X there is a Gaussian distribution with a 1σ point of approximately 1.2 counts or 2.64 arc sec.

For the compensated Y data, the distribution is non-Gaussian but has a standard deviation of approximately 2.2 counts or 4.84 arc sec.[1]

MULTIPLE STAR TESTS

The systems ability to track multiple stars in a single field of view was demonstrated using the intermediate mode optics and the uncollimated star pattern simulator described earlier in this section on page 70.

(1) The uncompensated Y data had a standard deviation of 4.5 counts or 9.9 arc sec from its best linear fit.

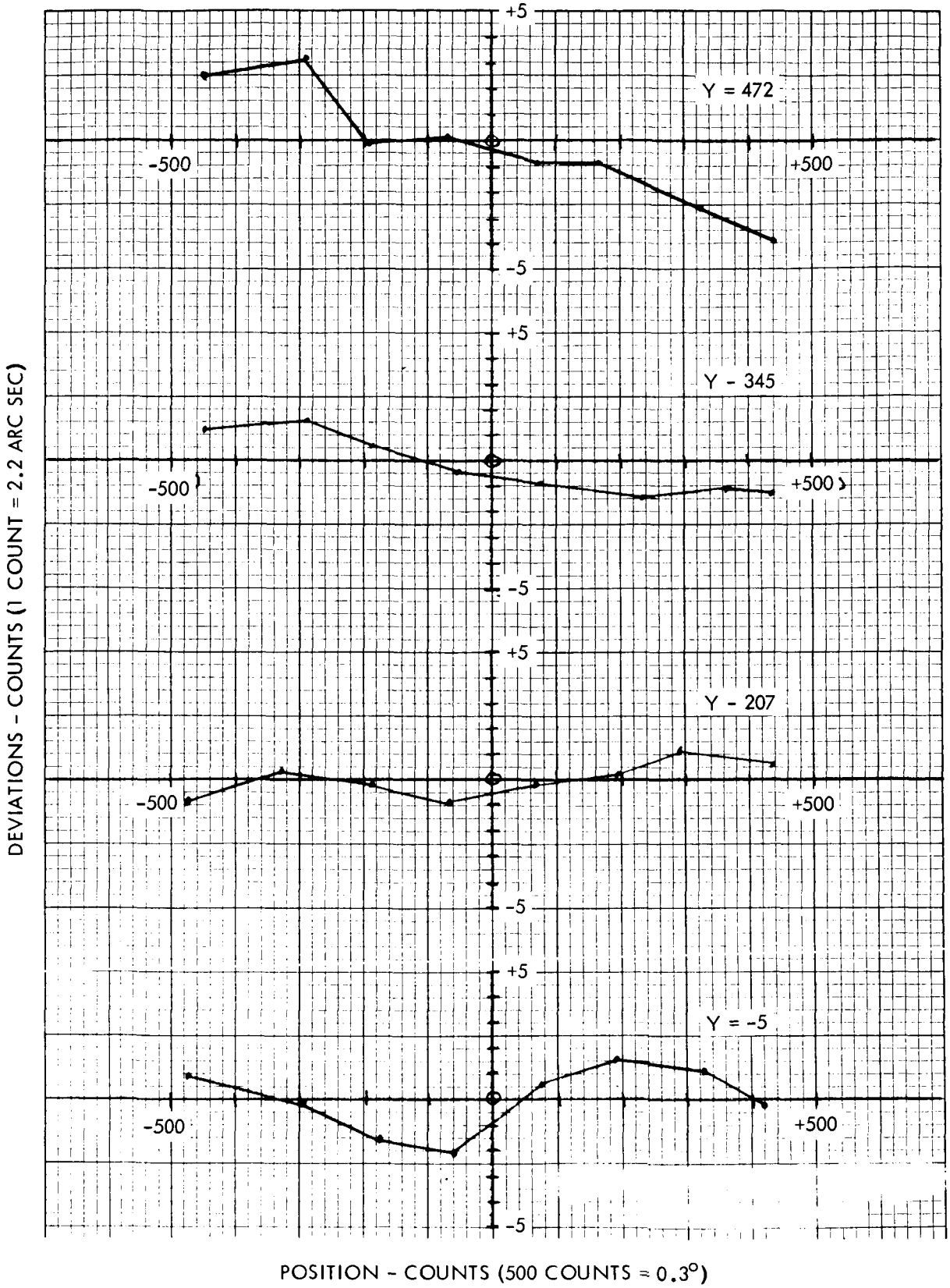

Figure 43a. Deviations Vs. Position X-Axis Test

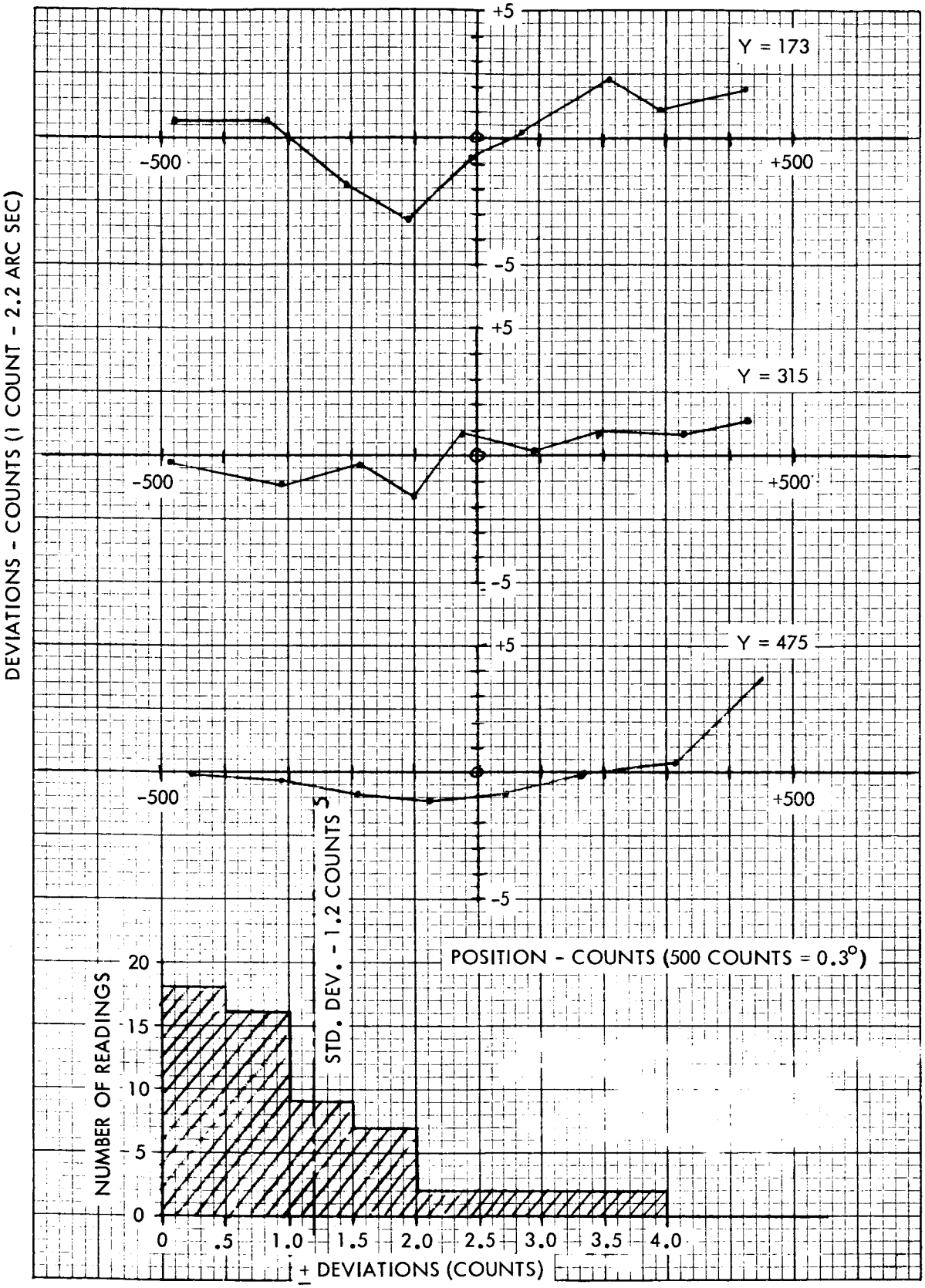

Figure 43b. Deviations vs. Position X-Axis Test

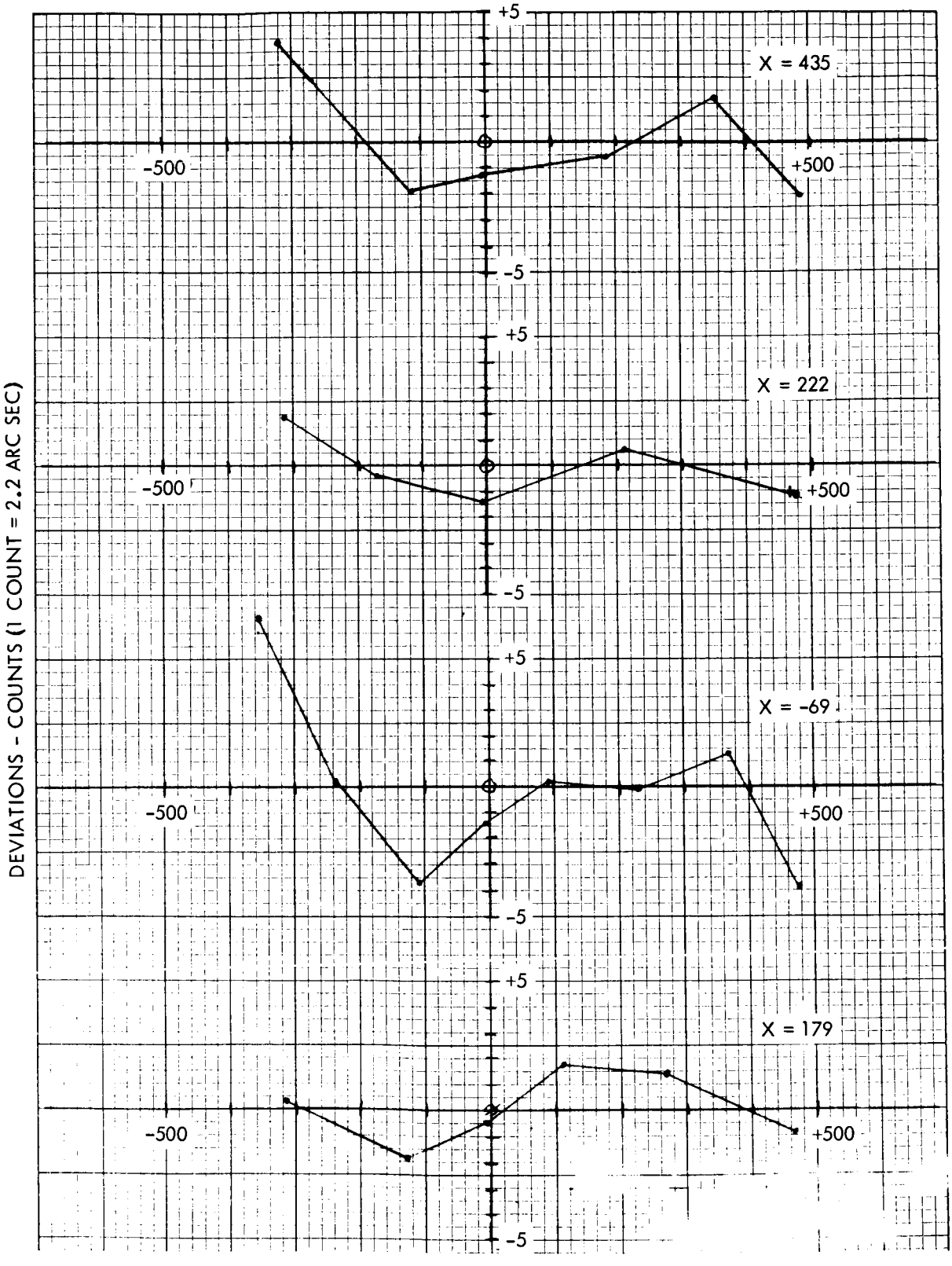

Figure 44a. Deviations Vs. Position Y-Axis Test

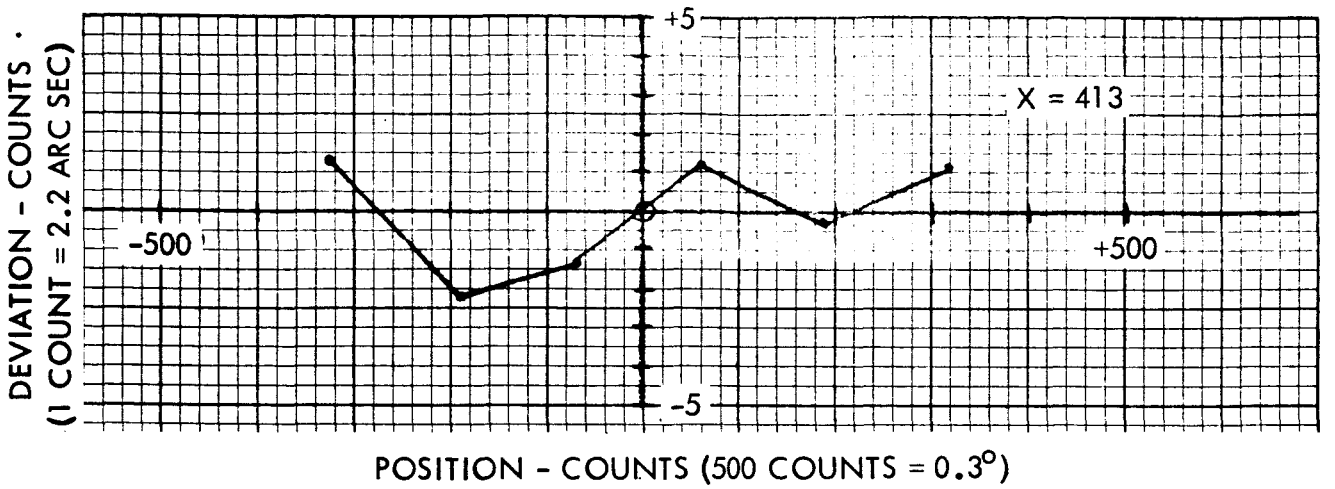

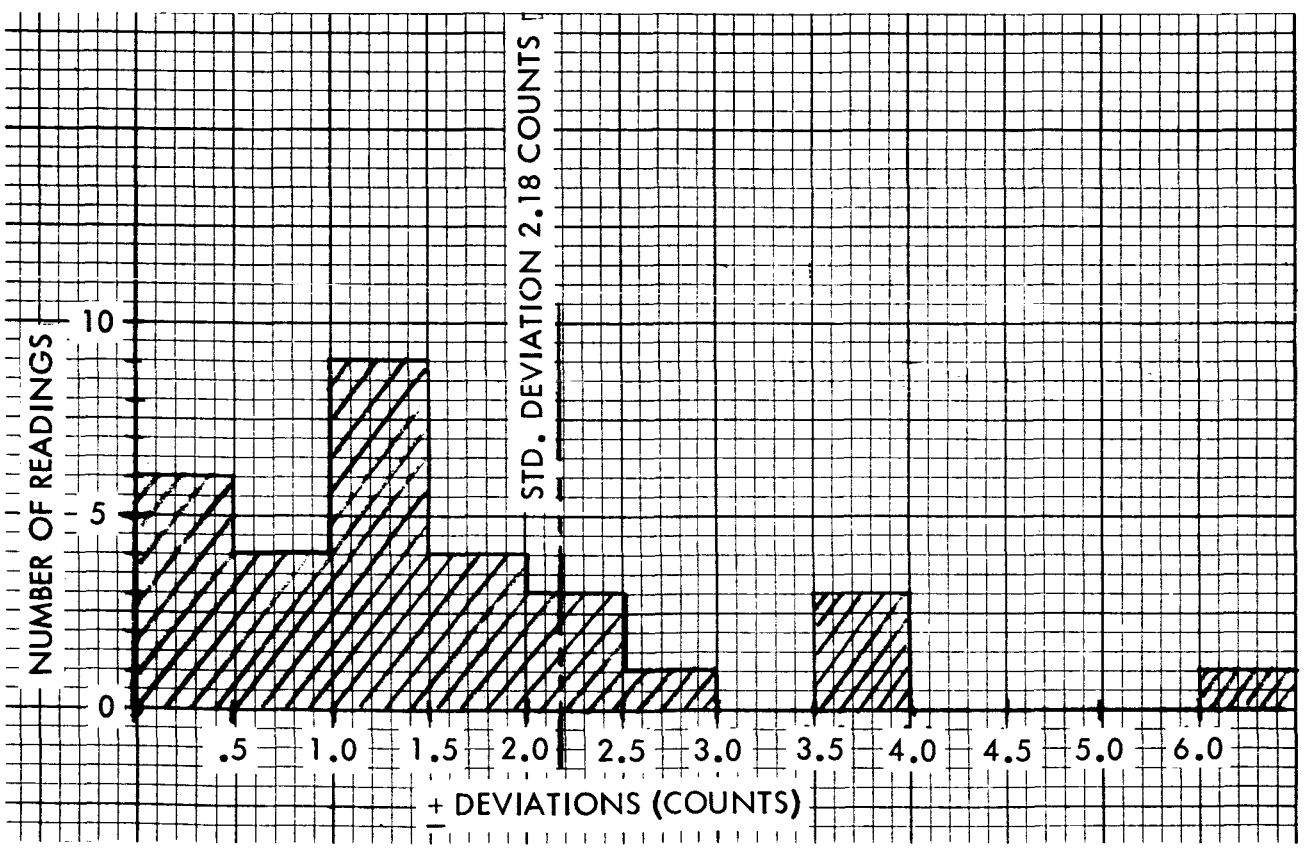

Figure 44b. Deviations vs. Position Y-Axis Test

No attempt was made here to measure the absolute angular separations of the targets, the primary purpose being to demonstrate how the multiple targets were handled in an orderly fashion.

A fixed pattern of targets was moved around in the field of view. At each position, the separations of the images, in data processor decimal counts were calculated and compared with those at other positions. Since the pattern is fixed, the separations, except for parallax error, should be invariant.

Six positions of a four star pattern were used. Plotting the outputs obtained from the data processor, these positions are shown in Figure 45. The coordinates in the figure are normalized decimal counts. Position 5 differs from position 4 in that star No. 4 was covered up and star No. 5 uncovered to change the pattern.

Table 13 gives the results of the test. All readings are in decimal counts of the data processor.

TABLE 13

MULTIPLE STAR TEST RESULTS

		IMAGE SEPARATION Decimal Counts							
	Targets →	1-2	2-3	2-4	2-5	3-4	4-1	3-5	5-1
Test Positions	1	379.8	376.5	375.6	--	537.4	532.0	--	--
	2	379.0	378.7	381.2	--	539.7	537.4	--	--
	3	383.3	378.2	381.6	--	539.3	541.9	--	--
	4	378.4	376.9	375.6	--	537.0	530.7	--	--
	5	378.4	376.9	--	388.8	--	--	539.7	541.7
	6	377.8	378.9	374.5	--	537.3	529.8	--	--
	Mean →	379.5	377.7	377.7	388.8	538.1	534.4	539.7	541.7
	Std. Dev. →	1.8	0.9	3.1	--	1.1	4.6	--	--

The observed deviations are due in part to the fact that in analyzing this data, a linear optical transfer function was assumed[1] and no compensation was applied to the Y data[2]. It is interesting to note that the largest deviations occur in those separations which have the largest Y component.

(1) Reference Section 2, Page 11
(2) Reference Section 6, Page 88

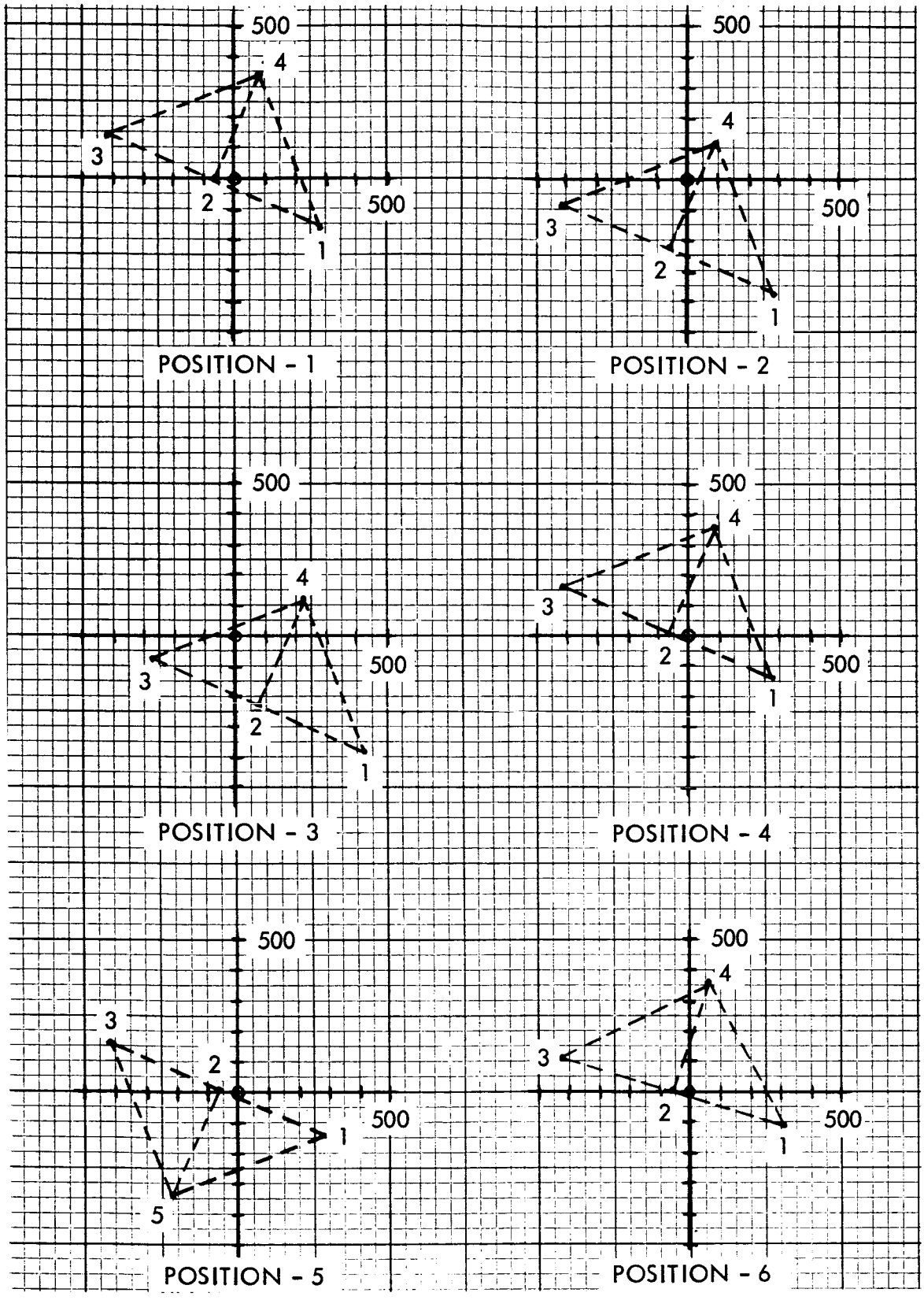

Figure 45. Multiple Star Test Positions

The test demonstrated the desired performance and pointed up one of the more interesting applications for a device of this type, star pattern recognition. Since the spacing of target images remains invariant regardless of rotation or translation, it appears feasible to use this technique to recognize the invariant spacing of actual star patterns.

As a rough check on the reasonableness of the above values, consider the fact that the target was 11' -0'' from the lens. The spacing of the ''stars'' was, as shown in Figure 34, approximately 7.05''. This corresponds to an angle, at the optics, of 3.06^{o} or 183.6 arc min. From the optics transfer function presented in Section 2, to a first approximation:

$$r = \frac{183.6}{.4941} = 372 \text{ counts}$$

However, this transfer function was developed for targets at infinity where the function is proportional to the focal length 2.56''. For a target at 11' -0'' the image is formed approximately 2.61'' behind the center of the lens and the transfer function is increased by a factor of $2.61/2.56 \approx 1.02$ so that:

$$r = 1.02 \times 372 = 379 \text{ counts}$$

This agrees very well with the observed readings.

INTERANGULAR ACCURACY TESTS

Formal acceptance tests of the system were conducted at the General Electric Company's plant in Johnson City in May 1965. As part of these tests, the ability of the system to measure the angular separation between targets was demonstrated.

Since only one collimated star source was available at the time, the tests were conducted by rotating the tracker head between readings and measuring the angle through which it moved. This angle was then compared with the angular displacement computed from the data processor's outputs.

Two series of tests were run, one using the intermediate mode optics with the readout of the dividing head as an angular measurement, and the second using the narrow mode optics with the autocollimator as the angular measurement. In both cases, the optical transfer functions described in Section 2 were used in the computations.

Figures 46 and 47 illustrate the image plane location of the test points used. In the case of the intermediate mode optics, the tracker head was rotated twice to take advantage of the sensitive axis of the dividing head. The angular separations had to be computed in specific groups since there was no measured absolute angular relationships between readings in different groups. Referring to Figure 46, the test point groups were:

Group	Test Points
1	1-2-3-4
2	5-6-7-8
3	9-10-11-12

In the case of the narrow mode optics, the autocollimator had to be moved between test groups due to its limited field of view. In addition, both normal and reverse scan was employed. Referring to Figure 47, the test point groups were:

Group	Test Points
1	1-2-3-4-5-6-7
2	8-9-10
3	11-12-13
4	14-15-16-17-18

The target coordinates for each test point were calculated using a computation procedure similar to that shown in Figure 27.

The angular separations of the test points within the various groups were then computed by taking all possible vector dot products of the individual target vectors defined by these coordinates. The results are shown in Tables 14 and 15.

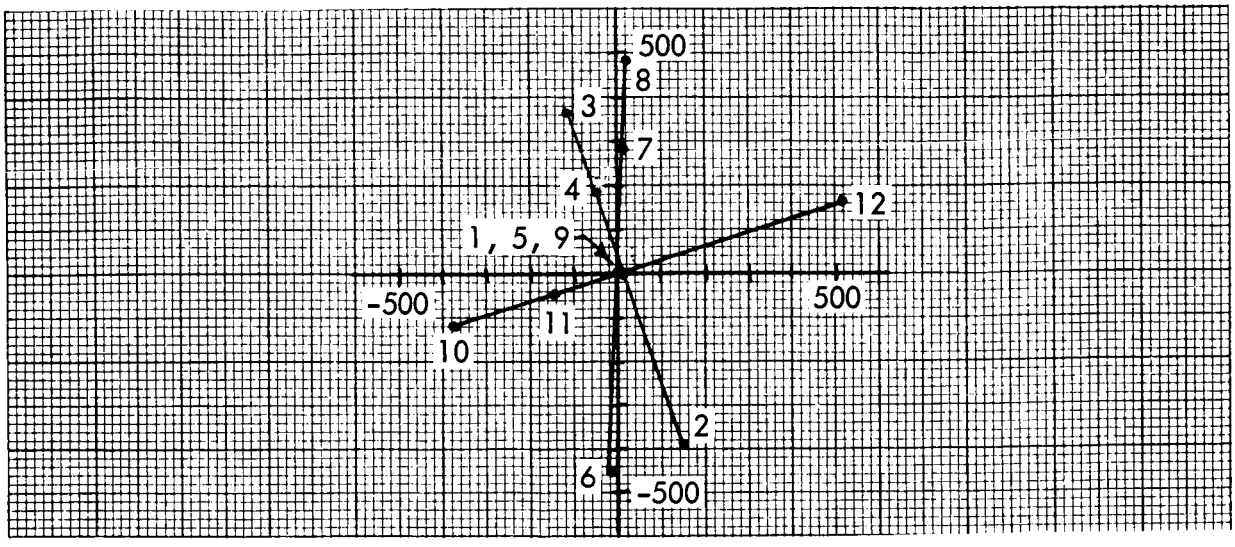

Figure 46. Test Point Locations - Intermediate Mode Optics

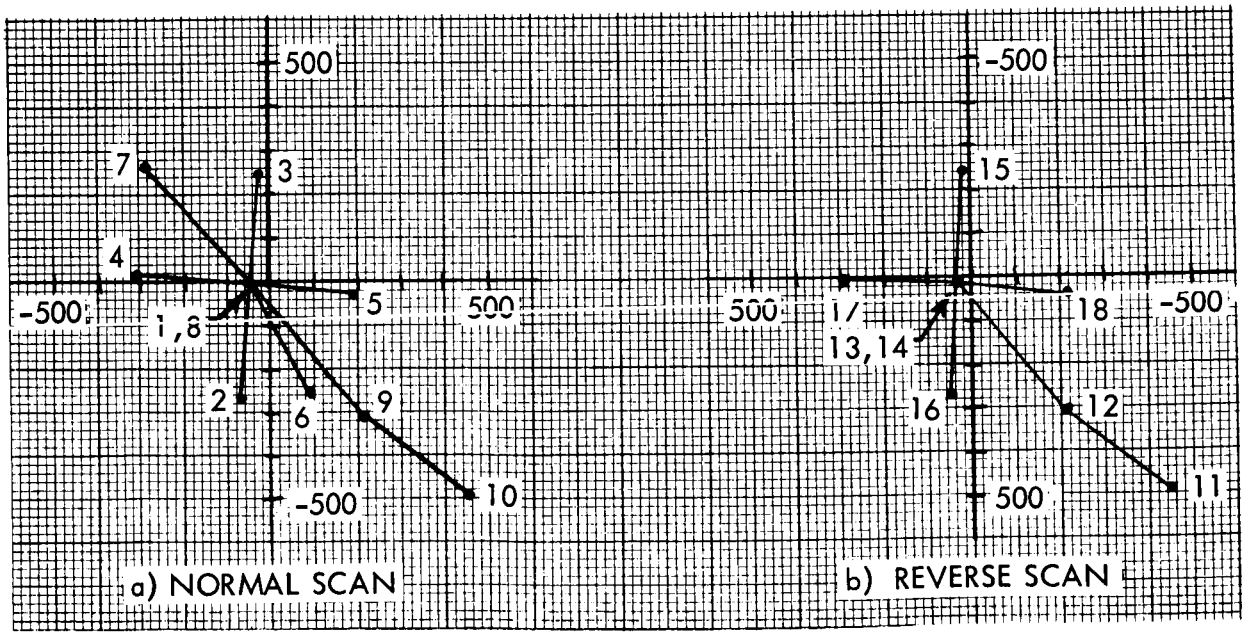

Figure 47. Test Point Locations - Narrow Mode Optics

TABLE 14

INTERMEDIATE MODE OPTICS
INTERANGULAR ACCURACY TEST DATA

Test Points	Measured Angle Radians	Computed Angle Radians	Deviations Radians
1-2	.05968056	.05937230	-.00030826
2-3	.11538565	.11469381	-.00069184
3-4	.02809495	.02769030	-.00040465
4-1	.02761013	.02763466	+.00002453
4-2	.08729070	.08700485	-.00028585
1-3	.05570509	.05532179	-.00038330
5-6	.06469838	.06426243	-.00043595
6-7	.09972617	.09962672	-.00009945
7-8	.03529443	.03508405	-.00021038
9-10	.05509907	.05549552	+.00039645
10-11	.03502778	.03517901	+.00015123
11-12	.09788388	.09936596	+.00148208
6-8	.13502061	.13471009	-.00031052
8-5	.07032222	.07044777	+.00012555
5-7	.03502778	.03536439	+.00033661
9-11	.02007128	.02031654	+.00024526
11-10	.03502778	.03517901	+.00015123
12-9	.07781259	.07905305	+.00124046
10-12	.13291167	.13454110	+.00162943

TABLE 15

NARROW MODE OPTICS
INTERANGULAR ACCURACY TEST DATA

Test Points	Measured Angle Radians	Computed Angle Radians	Deviations Radians
1- 2	.00277846	.00281264	+.00003418
2- 3	.00546870	.00556231	+.00009361
3- 4	.00394019	.00390424	-.00003595
4- 5	.00541197	.00530525	-.00010672
5- 6	.00244449	.00245224	+.00000775
6- 7	.00764780	.00757683	-.00006997
1- 3	.00269024	.00275019	+.00005995
2- 4	.00396004	.00395080	-.00000924
4- 5	.00541197	.00530525	+.00010672
5- 7	.00608298	.00598760	-.00009538
1- 4	.00284596	.00275990	-.00008606
2- 5	.00376582	.00377914	+.00001332
3- 6	.00585166	.00587898	+.00002732
1- 5	.00256621	.00254574	-.00002047
2- 6	.00281348	.00276667	-.00004681
3- 7	.00290818	.00280043	-.00010775
1- 6	.00372075	.00368748	-.00003327
2- 7	.00615411	.00619713	+.00004302
3- 5	.00372734	.00374399	+.00001665
1- 7	.00392742	.00389159	-.00003583
4- 6	.00614248	.00603573	-.00010675
4- 7	.00267571	.00271487	+.00003916
8- 9	.00423117	.00416068	-.00007049
9-10	.00332492	.00327421	-.00005071
8-10	.00751370	.00739665	-.00011705
11-12	.00339904	.00322925	-.00016979
12-13	.00414358	.00412480	-.00001878
11-13	.00750455	.00731315	-.00019140
14-15	.00274550	.00275850	+.00001300
15-16	.00539064	.00547154	+.00008090
16-17	.00389494	.00392646	+.00003152
17-18	.00565487	.00553271	-.00012216
14-16	.00264514	.00271371	+.00006857
15-17	.00401417	.00392625	-.00008792
14-17	.00288824	.00280185	-.00008639
15-18	.00392254	.00392876	+.00000622
14-18	.00276715	.00273164	-.00003551
16-18	.00379668	.00378228	-.00001440

A first order polynomial least squares fit was applied to this data with the following results:

TABLE 16

INTERANGULAR ACCURACY TEST RESULTS

Test	0 Degree Coefficient	1 Degree Coefficient	Standard Error (1) (Radians)	(Counts)
Inter Mode Optics	-1.34×10^{-4}	1.0040	6.21×10^{-4}	4.3
Narrow Mode Optics (Norm & Rev Scan)	3.17×10^{-5}	0.9845	6.46×10^{-5}	6.0
Narrow Mode Optics (Norm. Scan)	2.17×10^{-5}	0.9879	5.69×10^{-5}	5.3
Narrow Mode Optics (Rev. Scan)	6.33×10^{-5}	0.9744	7.50×10^{-5}	7.0

The 1 Degree Coefficient serves as a check on the transfer function employed. For the intermediate mode optics, the check is excellent, the results showing a difference of only 0.4%. For the narrow mode optics the difference is approximately 1.5%.

It is apparent that the reverse scan mode of operation was not calibrated as well as the normal mode, there being a difference between their standard errors of 1.7 counts.

In relating these results to those obtained with a single star (Figures 43 and 44) it must be realized that the interangular measurements include the errors

(1) The standard error, or σ of the sample populations was calculated as

$$\sigma = \left(\frac{\sum_{i=1}^{n} (\theta_m - \theta_c)^2}{n} \right)^{1/2}$$

where θ_m = measured angle

θ_c = calculated angle

n = number of samples

at two points. Based on Figures 43 and 44, the rms error at each point can be estimated as:

$$\sigma_1 = \sqrt{\overline{1.2}^2 + \overline{2.2}^2}$$

$$= 2.5 \text{ counts}$$

The rms error between points would then be approximately:

$$\sigma_2 = \sqrt{2}\ 2.5 \text{ counts}$$

$$= 3.5 \text{ counts}$$

The results achieved in normal scan are in reasonable agreement with this. It is not surprising that the narrow mode results show a larger standard error. Building vibration and air turbulence are much more critical when measuring arc sec than in measuring arc min.

EXTENDED DISC TESTS - ORTHOGONAL SCAN

These tests were performed with the intermediate mode optics utilizing the disc simulator, described on page 74, as a target.

In conducting the tests, a series of edge crossing coordinate sets were obtained from the data processor. A least squares best fit circle was then computed based on the points for each position of the tracker. The output of these computations were the radius and the center coordinates for the best fit circle.

In this mode of operation, the reticles cause a slight problem in that they tend to distort the disc edge at intersection points. These areas cause erroneous data which must be discriminated against if an accurate measurement is to be achieved.

The easiest method, and the one which was used, is to fit a circle to all the data and then eliminate those points which deviate more than $\pm$ 10 counts radially from it. A second circle is then fitted to the corrected data.

The test positions for the extended disc tests are shown in Figure 48.

The results of the tests are given in Table 17.

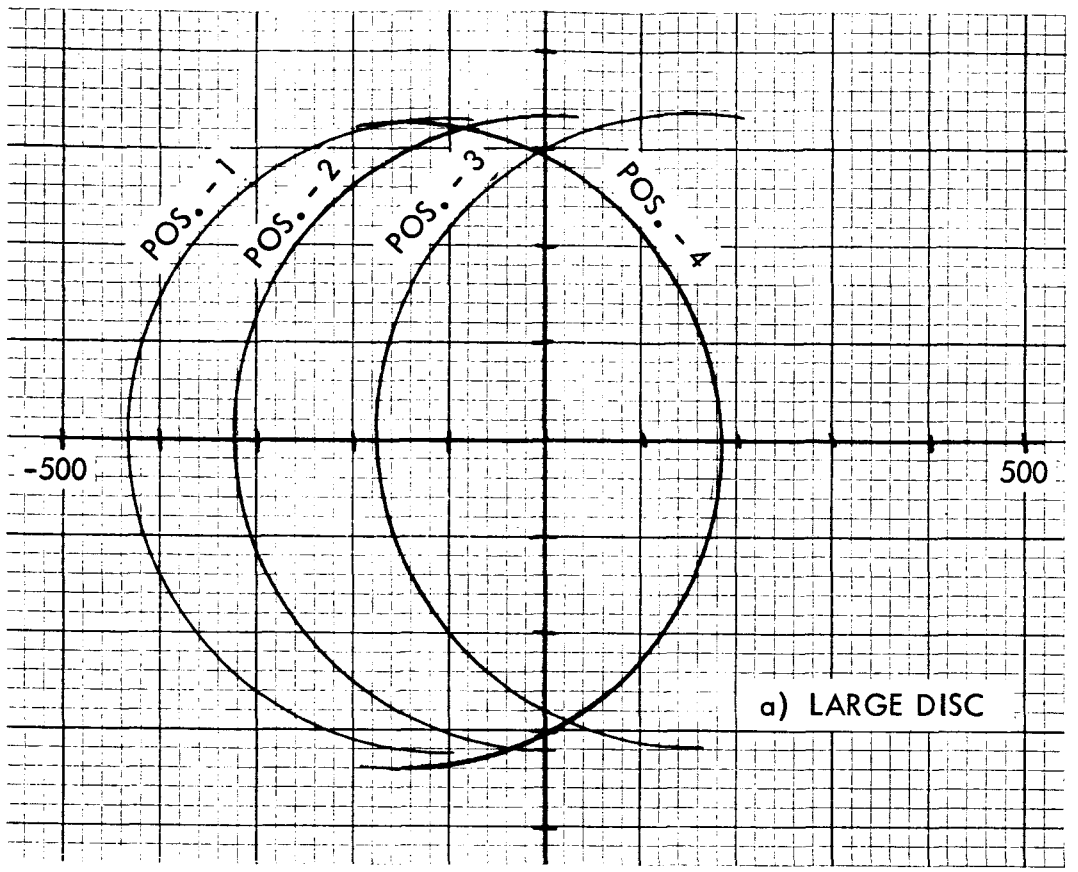

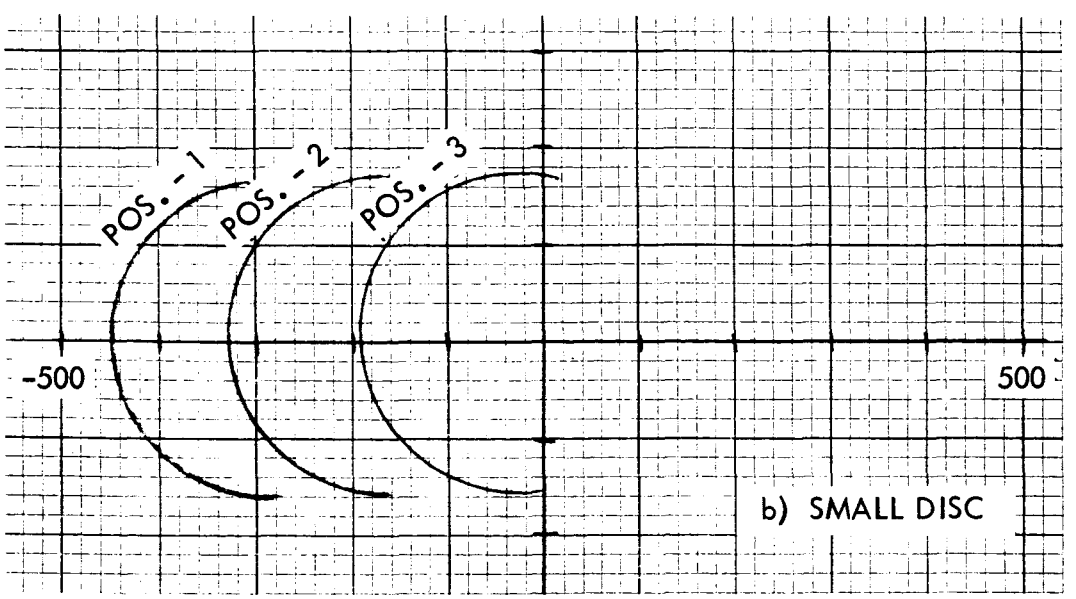

Figure 48. Extended Disc Test Locations

At the optics, the two discs subtend approximately 5.2^{o} (312') and 2.6^{o} (156'), respectively. Applying the linear term of the optics transfer function (as a first approximation) and accounting for the 2% increase in scale factor due to the uncollimated target, the measured radii should be:

$$R_L = \frac{312}{.4941} \times \frac{1.02}{2}$$

$$= 322 \text{ counts}$$

$$R_S = \frac{156}{.4941} \times \frac{1.02}{2}$$

$$= 161 \text{ counts}$$

These Figures agree very well with the results obtained. Note that the largest deviations for the large disc occurred in the reverse mode indicating a less perfect calibration of this mode.

TABLE 17

EXTENDED DISC - ORTHO SCAN
TEST RESULTS

Disc	Position	Center Coordinates o Counts	Yo Counts	Radius Counts	Radial Std. Deviation Counts
Large	1	-103.3	4.9	327.0	2.2
	2	3.1	8.8	326.2	0.7
	3	151.0	12.8	327.6	2.0
	4*	-150	- 3.8	334.1	4.6
Small	1	-283.6	3.0	160.0	4.0
	2	-164.3	8.9	163.4	6.5
	3	- 25.7	12.5	164.2	2.2

* Reverse Scan

Also to be noted is the fact that, in general, the small disc results are less accurate than the large disc results. This is due, in part, to the fact that the smaller the disc, the greater the effect the reticle distortions have on the overall computation.

No attempt was made to measure angular accuracy from one position to the other since with the uncollimated targets, the parallax error becomes excessive.

EXTENDED DISC TESTS - RADIAL SCAN

Two interesting effects were observed when the radial scan was put into operation with the complete camera system.

a. Using a radial frame rate approximately the same as the orthogonal frame rate (4.3 frames/sec) resulted in an apparent decrease in the vidicon's sensitivity. It was theorized that the much lower line density (32 radii in radial scan compared to 1024 lines in orthogonal scan) left a large percentage of the target undischarged. This undischarged area tended to "leak" over onto the discharged line reducing the signal content of the line.

   Increasing the frame rate would allow this effect less time in which to take place. The frame rate was accordingly quadrupled and a significant increase in performance was achieved. It is this higher frame rate which has been previously discussed on page 67.

b. A step like change in the dark level was encountered in those areas where the radial scan entered areas not covered by the orthogonal scan; the dark level being higher in the orthogonal scanned area. In the areas of very low dark level, reticle detection is difficult. Increasing the target voltage to increase the dark level in these areas adversely affects the higher dark level area.

   Target detection is not impaired by this phenomena. Since the radial scan is a secondary mode of operation for the tracker and since this scan will be used primarily in a nulling mode where reticle operation is not of prime importance, it was decided to run without reticles.

The tests were conducted using the intermediate mode optics with the small disc simulator (page 74) as a target.

The results from the three test positions used are plotted in Figure 49.

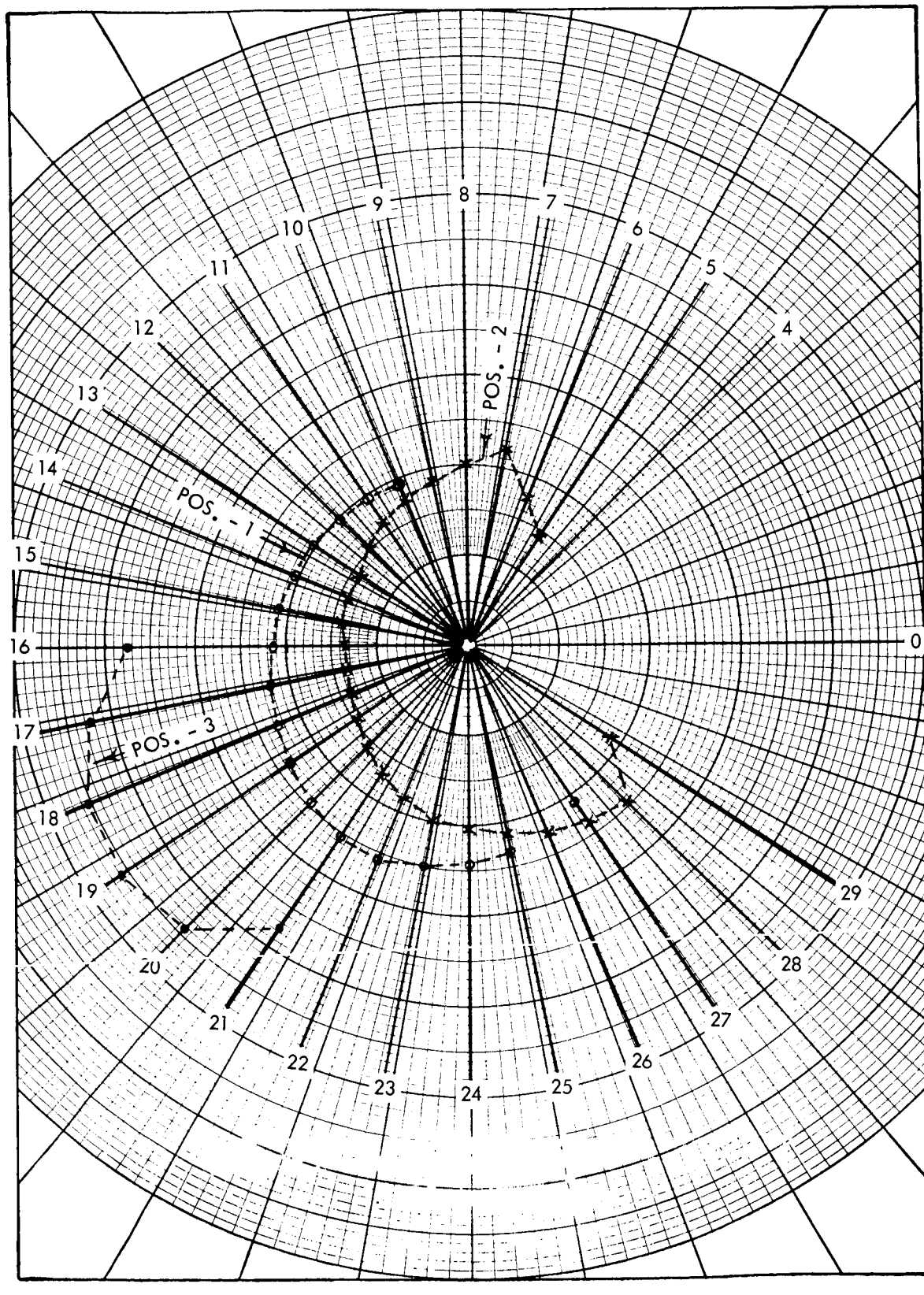

Figure 49. Radial Scan Test Positions

Nulling mode operation of the system will not require calculation of circle centers from the polar coordinate data. In this case, however, it was desirable to determine how well it tracked the circular image in off-axis positions. Therefore, the polar data was converted to orthogonal form and a least squares best fit circle was passed through the points. The results are given in Table 18.

TABLE 18

RADIAL SCAN TEST RESULTS
(Equivalent Orthogonal Form)

Position	Center Coordinates		Radius	Radial Standard Deviation
	Xo	Yo		
	Counts	Counts	Counts	Counts
1	- 7.7	- 30.8	214.8	5.8
2	70.3	- 1.7	210.7	5.3
3	-238.0	-132.7	188.3	3.5

Comparing these results with those obtained in orthogonal scan shows the effect of the lack of reticles. The scale factor relating image size to data processor is too large producing a radius reading of 210 compared to the correct value of 161. This low sweep rate was due to the fact that reticles were not used to set up the sweep rates as was done in the orthogonal mode.

The radial standard deviations are about double that in ortho scan.

The wide variation in calculated radii from Positions 1 and 2 to Position 3 is probably due to the scarcity of readings possible in Position 3.

GEC 7522 VIDICON

The GEC 7522 electrostatic focus and deflection vidicon was designed to provide a small pickup tube requiring low operating power in equipment of minimum size and weight. Deflection is accomplished by a Deflectron, a revolutionary electrostatic deflection device. Resolution of 500 lines is obtained with 300 volts beam acceleration. Power requirements and operating voltages are designed for operation with completely transistorized circuits.

DATA

GENERAL:	
Operating Position	Any
Focusing Method	Electrostatic
Deflection Method	Electrostatic
Maximum Useful Image Area Diagonal measurement of 4 x 3 aspect ratio	0.625 in.
ELECTRICAL CHARACTERISTICS:	
Heater Voltage (AC or DC)	6.3 V ± 10%
Heater Current	0.3 A
Spectral Response (See Fig. 4)	S-18
Direct Interelectrode Capacities	
Signal Electrode to all others	4 uuf
D1 to D2 (Horizontal Plates)	6 uuf
D3 to D4 (Vertical Plates)	6 uuf
ABSOLUTE MAXIMUM RATINGS:	
Grid No. 1 Voltage	
Negative Bias	300 V
Positive Bias	0 V
Heater to Cathode Peak Voltage	
Heater Negative with Respect to Cathode	125 V
Heater Positive with Respect to Cathode	10 V
Grid No. 2 Voltage	750 V

ELECTRONIC TUBE DIVISION
GENERAL ELECTRODYNAMICS CORPORATION, GARLAND, TEXAS

ABSOLUTE MAXIMUM RATINGS, Continued:

Faceplate	
Illumination	1000 ft-c
Temperature	71° C.
Signal Electrode Current	0.6 uA

TYPICAL OPERATION:

Scanned Area	0.500 x 0.375 in.
Faceplate Temperature	30° to 35° C.
Optimum Signal Output Current (Less Dark Current, with uniform 2870° K Tungsten illumination on faceplate.)	
5 ft-c and greater	0.2 uA
0.2 to 0.5 ft-c	.05 to .1 uA
Signal Electrode Voltage	20 to 100 V
Average Gamma of Transfer Characteristic over Signal Output Current Range of .05 to 0.2 uA	.55
Grid No. 5 Voltage	300 V
Focus Electrode Voltage	0 to 50 V
Grid No. 2 and Grid No. 4 Voltage	200 V
Grid No. 1 (For signal cutoff with no blanking on G1)	-45 to -100 V
Minimum Blanking Voltage (Peak to Peak)	
When applied to Grid No. 1	30 V
When applied to Cathode	10 V
Deflection Voltages (Peak to Peak)	
Horizontal (D1 to D2)	60 V
Vertical (D3 to D4)	50 V
Horizontal Plates DC Voltage	200 V to 250 V
Vertical Plates DC Voltage	200 V to 250 V

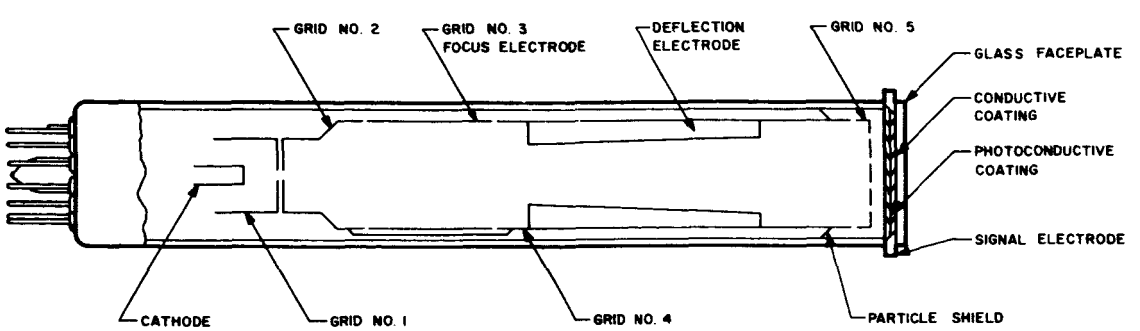

FIG. 1

PRINCIPLES OF OPERATION

Basic Vidicon Operation

The GEC 7522 vidicon is a photoconductive imaging device using electrostatic focus and deflection. The vidicon faceplate inside surface is coated with a transparent conductive coating as shown in Figure 1. Over this a layer of photoconductive material is deposited. This material when dark is a reasonably good insulator but increases in electrical conductivity when exposed to light. The electron beam scans the back surface of this photoconductor.

In operation, the photoconductor front surface is held at a positive potential with respect to the cathode, by applying voltage to the transparent conductive coating. The scanning electron beam deposits a negative charge on the photoconductor back surface. Where the photoconductor is dark and its resistance high, a negative charge accumulates until the back surface reaches cathode potential.

Where light from the scene falls on the photoconductor, conductivity increases, reducing negative charge at the illuminated point. Negative charge reduction at any point is proportional to the illumination on that point. The photoconductor therefore becomes charged much like a capacitor in a pattern conforming to the scene image. As the electron beam scans the photoconductor, it will release electrons into the less negatively charged areas and the resultant varying electron flow through a load resistor constitutes the video signal.

The vidicon has the ability to store the image for an entire scanning cycle. The image is "photographed" in a pattern of varying charge on the photoconductor back surface and is accumulated there for one complete frame. By this process the vidicon produces usable signal output from dimly lighted scenes.

Field Correction

A special mesh electrode, G5, is incorporated in the 7522 to assure flat field output and to compensate for beam landing error and optical lens distortion. The potential of this mesh can be varied independently of the other electrodes.

Focus

Electrostatic focus is accomplished in a saddle field lens arrangement composed of G2, G3, and G4, with G3 as the variable focusing electrode.

Deflection

Electrostatic deflection in the 7522 is accomplished through the use of a specially designed deflection plate configuration called the Deflectron. The conventional crossed pair deflection plates causes the electron beam to be deflected sequentially; that is,

PRINCIPLES OF OPERATION, Continued:

in passing between the first set of plates it is deflected in one plane and then when reaching the second set of plates is deflected in the other plane. The Deflectron causes the beam to be deflected both horizontally and vertically simultaneously as in magnetic deflection. This common center of deflection reduces the undesirable effects of fringe fields, defocusing and other distortion found in conventional deflection plate scanning.

Physically the Deflectron is a tube of insulating material, the inside of which contains the printed deflection plate pattern. The pattern of the Deflectron is illustrated laid out on a flat plane in Fig. 2. If the pattern is rolled to connect Side A to Side B, four individual electrical paths can be traced.

OPERATING CONSIDERATIONS

Installation

The GEC 7522 may be operated in any position, however, it must be oriented to place the horizontal deflection axis parallel to the horizontal image plane. The horizontal deflection axis is essentially parallel to a line through base pins 2 and 9. (See Fig. 7) The 13 pin socket for the 7522 is Type GEC 52-01 or equivalent.

Shielding

The 7522 should be shielded during operation from the effects of stray magnetic or electrostatic fields by the use of a suitable magnetic shield.

Deflection Circuits

The 7522 may be driven by standard electrostatic deflection circuits incorporating DC centering. The Deflectron elements are operated at a variable DC potential of from 200 to 250 volts positive with respect to cathode that will permit critical adjustment for minimum astigmatism.

Video Amplifier

The video amplifier design for use with the 7522 should incorporate all of the characteristics of an amplifier for a standard vidicon - low noise, high gain, aperture correction and high peaking. A typical transistor video preamplifier is shown in Fig. 3.

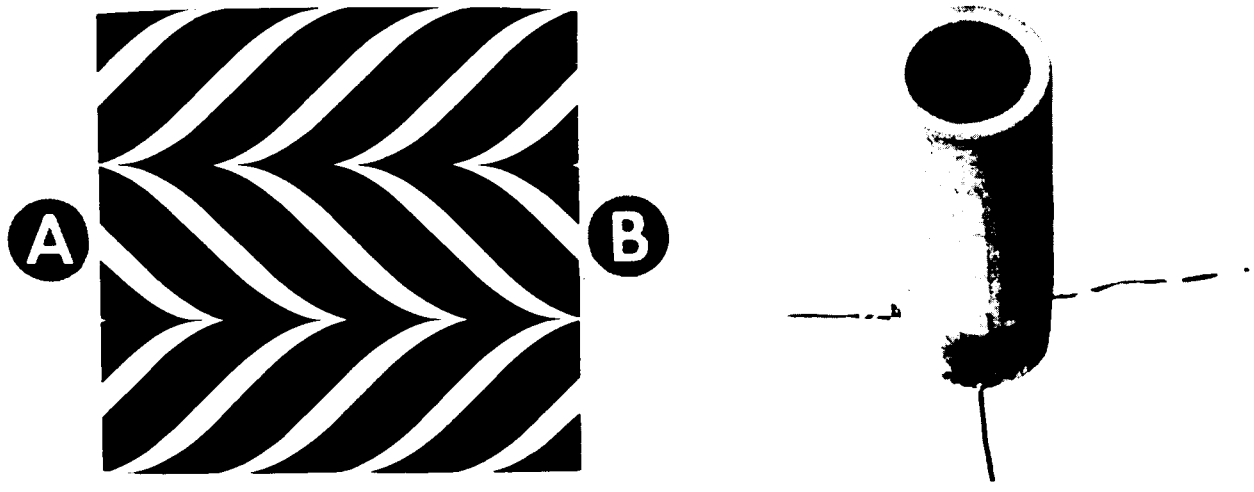

FIG. 2

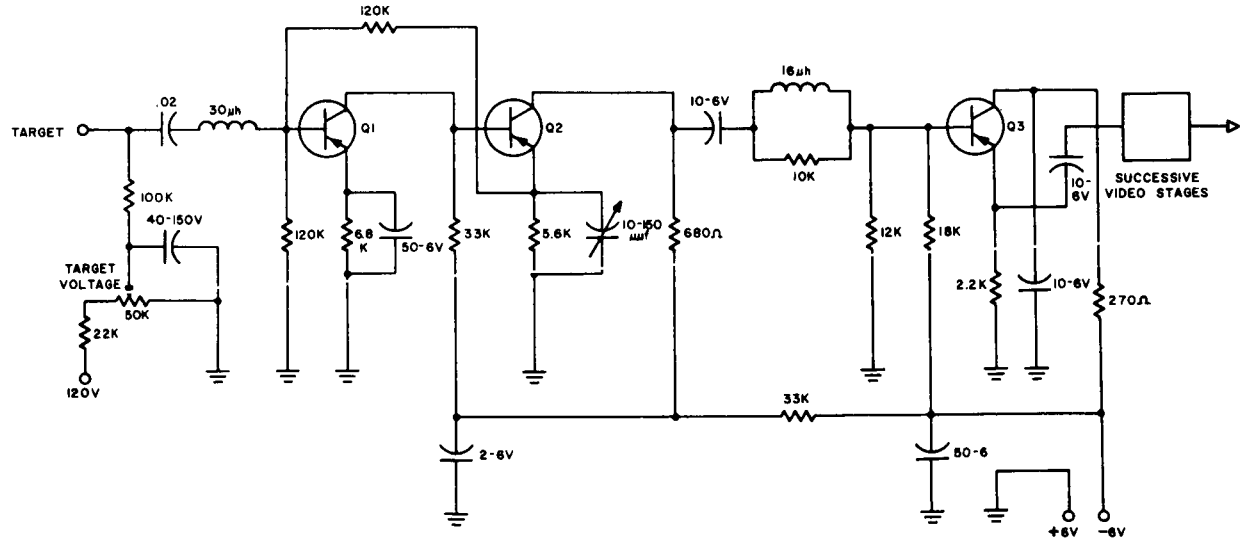

FIG. 3 TYPICAL TRANSISTOR VIDEO PRE-AMPLIFIER

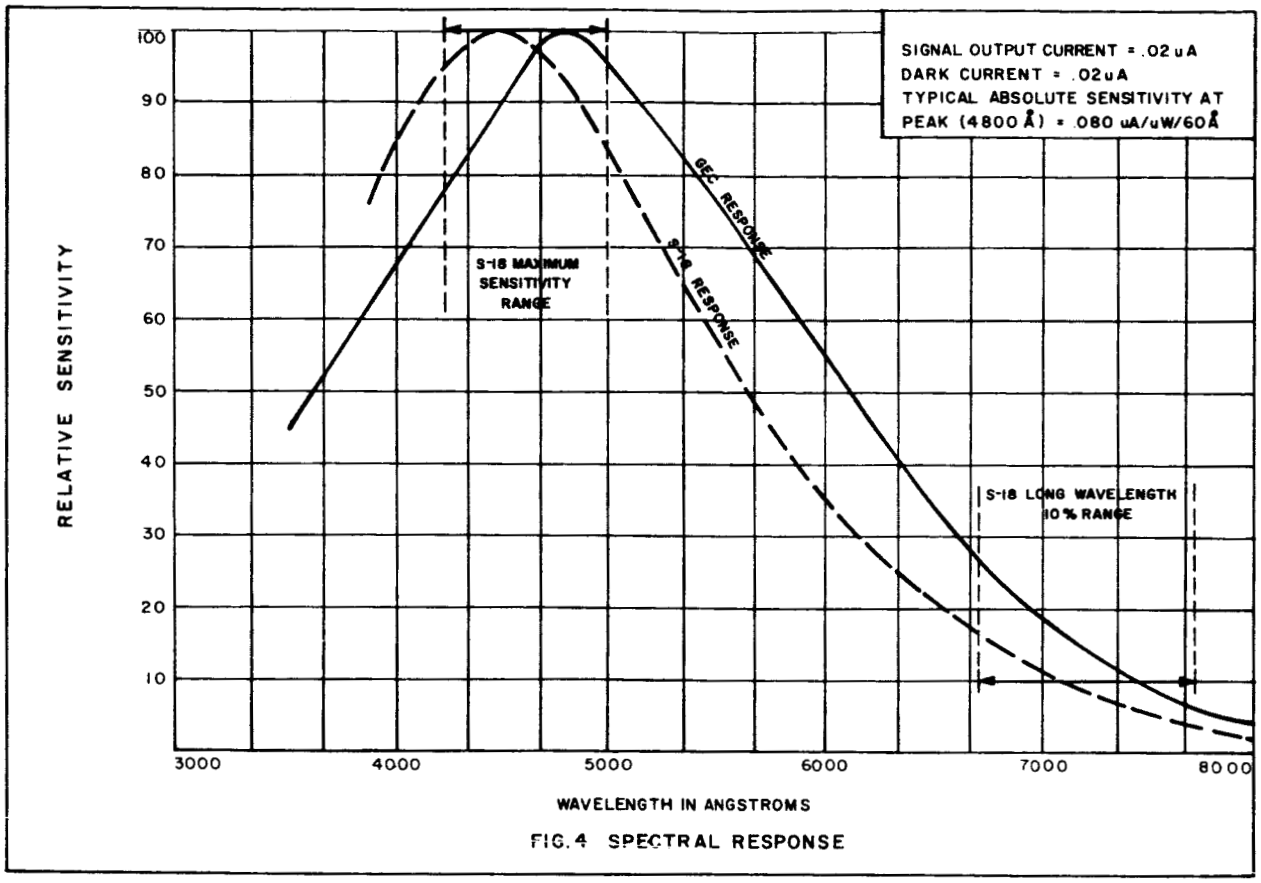

FIG. 4 SPECTRAL RESPONSE

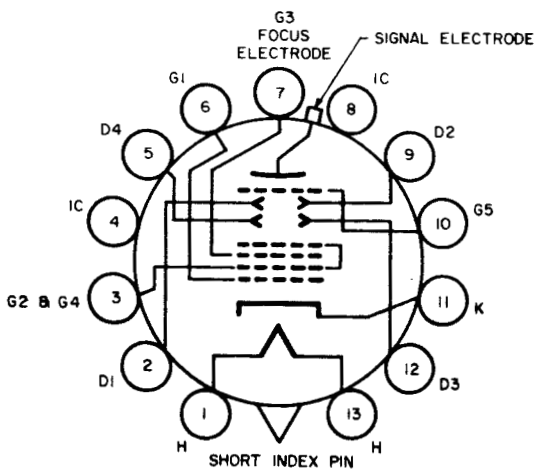

DIRECTION OF LIGHT:
INTO FACEPLATE OF TUBE

PIN 1: HEATER
PIN 2: D1 HORIZONTAL DEFLECTION PLATE
PIN 3: GRID NO. 2 & 4
PIN 4: INTERNAL CONNECTION--DO NOT USE
PIN 5: D4 VERTICAL DEFLECTION PLATE
PIN 6: GRID NO. 1
PIN 7: G3 FOCUS ELECTRODE
PIN 8: INTERNAL CONNECTION--DO NOT USE
PIN 9: D2 HORIZONTAL DEFLECTION PLATE
PIN 10: GRID NO. 5
PIN 11: CATHODE
PIN 12: D3 VERTICAL DEFLECTION PLATE
PIN 13: HEATER
SHORT INDEX PIN: INTERNAL CONNECTION--DO NOT USE
FLANGE: SIGNAL ELECTRODE

FIG. 5

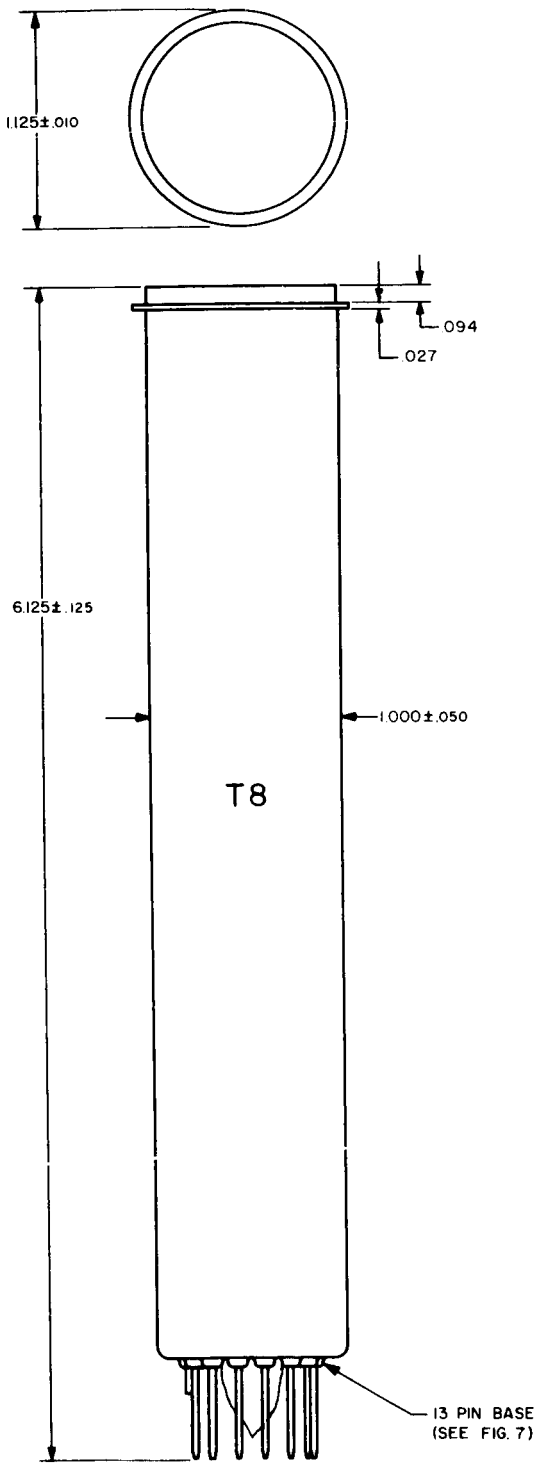

FIG. 6

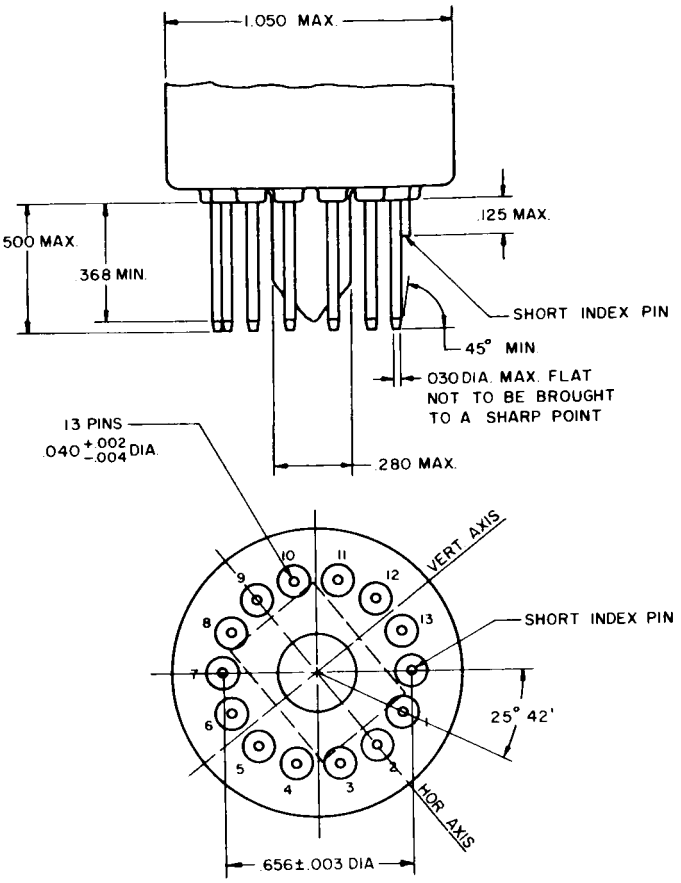

FIG. 7

NOTES

1. ALL DIMENSIONS ARE SHOWN IN INCHES.

APPENDIX B

GENERAL COORDINATE RELATIONSHIPS

The optics coordinate system will be as defined in Figure B-1.

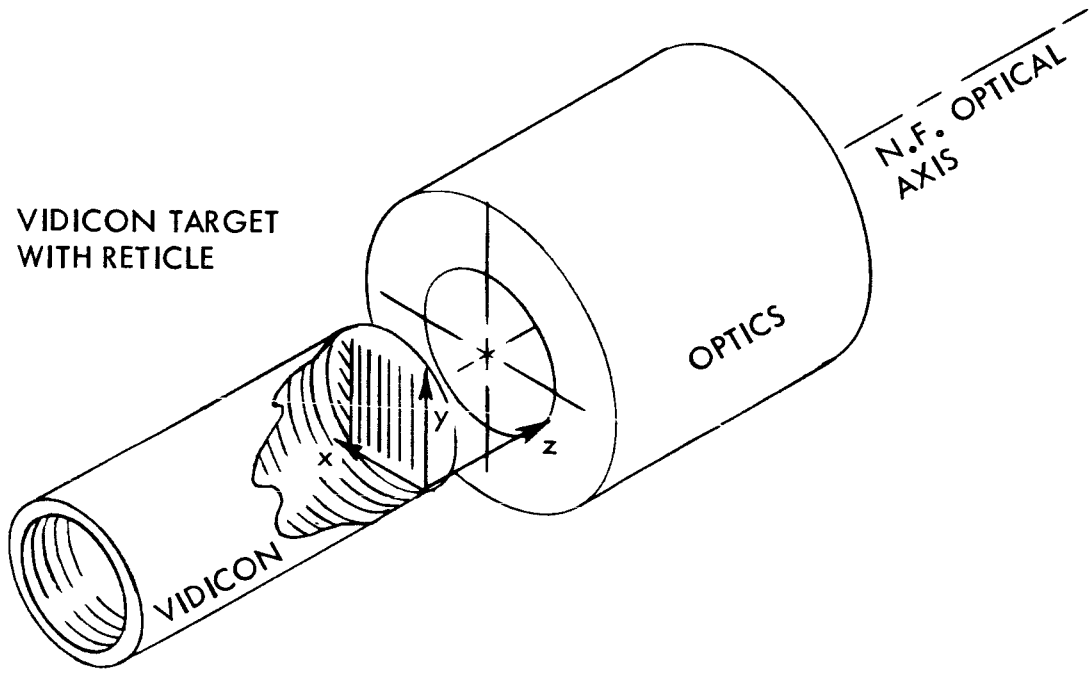

Figure B-1. Optics Coordinate System

The direction of the target ray can be related to this coordinate system as shown in Figure B-2. In this figure $\bar{a}$ is a unit vector along the target ray pointing from the optics to the target.

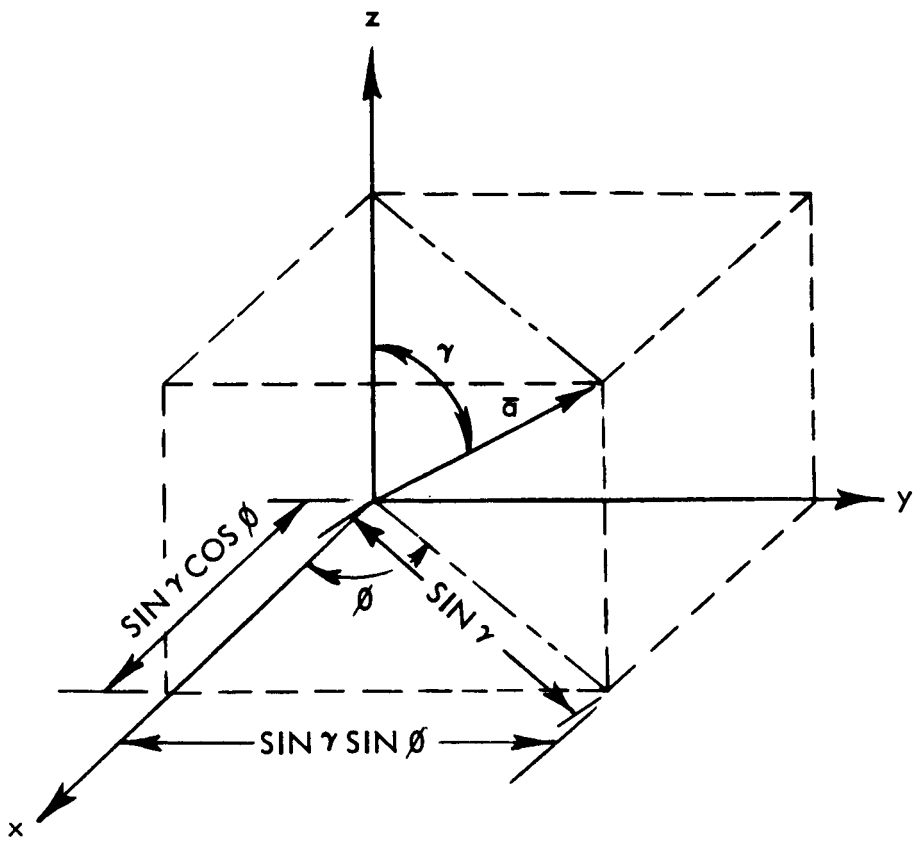

Figure B-2. Target Ray Geometry

Defining a_x, a_y and a_z as the direction cosines of the target ray, in the x, y, z optics frame, from Figure B-2, the following relationships can be developed:

$$a_x = \sin\gamma \cos\phi$$

$$a_y = \sin\gamma \sin\phi$$

$$a_z = \cos\gamma$$

Corresponding to Figure B-2, the image plane presentation is as shown in Figure B-3. The displacement of the target image from boresight is indicated by the image plane coordinates x_1 and y_1.

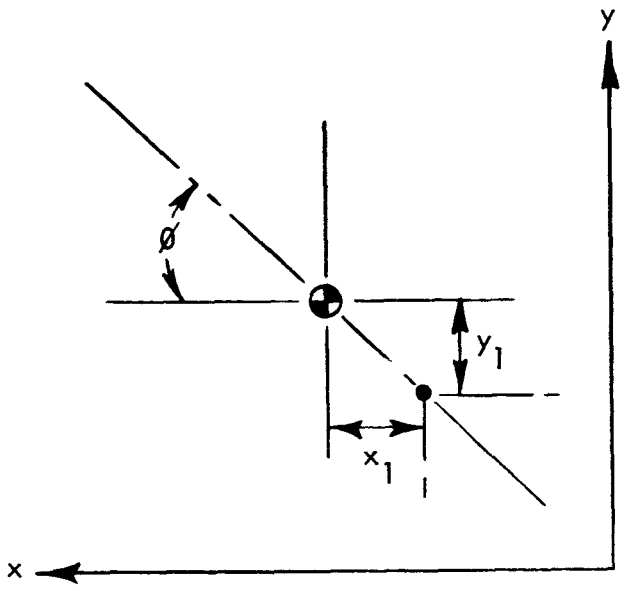

● = TARGET IMAGE
◕ = CENTER OF RETICLE CORRESPONDING TO $\gamma = 0$, WITH COORDINATES x_o, y_o.

Figure B-3. Vidicon Target Presentation Corresponding to Figure B-2.

From Figures B-2 and B-3, relationships can be developed for cos ϕ and sin ϕ in terms of x, and y so that the expressions for the direction cosines become:

$$a_x = \sin\gamma \frac{(-x_1)}{-\sqrt{x_1^2 + y_1^2}}$$

$$a_y = \sin\gamma \frac{(-y_1)}{-\sqrt{x_1^2 + y_1^2}}$$

$$a_z = \cos\gamma$$

REFERENCES

1. Optical Inertial Space Sextant for an Advanced Space Navigation System, NASA Contractor Report No. CR-133, Dec. 1964 (General Electric Armament & Control Products Section Report No. LMEJ 6914 2/64)

2. Auclair, G. F., 15^{o} Lens Linearity Measurements, Project Memo No. 2, 28 October 1964

3. Auclair, G. F., Timing Circuit, Project Memo No. 3, 18 November 1964

4. Auclair, G. F., Star Pattern Simulator for Space Sextant, Project Memo No. 4, 18 January 1965

5. Auclair, G. F., 15^{o} Lens Diaphragm Stops, Project Memo No. 5, 20 January 1965

6. Auclair, G. F., Vidicon Dual-Reticle Pattern Measurements, Project Memo No. 6, 29 January 1965

7. Foley, W. D., Dual Mode Reticle Design, Project Memo No. 7, 5 February 1965

8. Foley, W. D., Orthogonal & Radial Frame Rates, Project Memo No. 8, 10 February 1965

9. Auclair, G. F., Simulated Extended Discs for Space Sextant Testing, Project Memo No. 9, 5 March 1965

10. The Observers Handbook 1965, Ruth J. Northcott Editor, The Royal Astronomical Society of Canada

11. Hicken, C.W.R., Pulse Center Detector, Patent Document No. 35-19D-962, General Electric Company, LMED, A&CPS, Johnson City, N. Y.

12. Welch, J. D., An Advanced Optical Inertial Space Navigation System, Paper presented at the annual summer meeting of the American Institute of Aeronautics & Astronautics, Los Angeles, Calif., June 17, 1963

13. Derby, R. M., Stellar Tracking Devices, Patent Document 35-19D-954, General Electric Company, LMED, A&CPS, Johnson City, N.Y.